NASA CR 112097

GASL TR-759

NONUNIFORM FLOW FIELD GENERATION FOR SUPERSONIC COMPRESSOR STATOR DEVELOPMENT: DESIGN AND PRELIMINARY RESULTS

By Frederick W. Lipfert
Irving Fruchtman

Prepared under Contract No. NAS1-10004 by
GENERAL APPLIED SCIENCE LABORATORIES, INC.
Westbury, New York 11590

for

NATIONAL AERONAUTICS AND SPACE ADMINISTRATION

For sale by the Office of Technical Services, Department of Commerce: Washington, D. C. 20230, Price $

Report No.	2. Government Accession No.	3. Recipient's Catalog No.
NASA CR 112097		

Title and Subtitle	5. Report Date
NONUNIFORM FLOW FIELD GENERATION FOR SUPERSONIC COMPRESSOR STATOR DEVELOPMENT: DESIGN AND PRELIMINARY RESULTS	May 1972
	6. Performing Organization Code

Author(s)	8. Performing Organization Report No.
FREDERICK W. LIPFERT AND IRVING FRUCHTMAN	GASL TR-759
	10. Work Unit No.

Performing Organization Name and Address	11. Contract or Grant No.
GENERAL APPLIED SCIENCE LABORATORIES, INC. MERRICK AND STEWART AVENUES WESTBURY, L.I., NEW YORK 11590	NAS1-10004
	13. Type of Report and Period Covered
Sponsoring Agency Name and Address NATIONAL AERONAUTICS & SPACE ADMINISTRATION LANGLEY RESEARCH CENTER HAMPTON, VIRGINIA	Final Report
	14. Sponsoring Agency Code

Supplementary Notes

Abstract

Design and preliminary results are given for a technique which can generate a nonuniform flow similar to the discharge of an impulse supersonic compressor rotor. The technique utilizes a carefully contoured, two-dimensional blunt body in a conventional hypersonic wind tunnel to generate the required flow field. To show the effects of the flow vorticity, a cascade of impulse-type blades was tested in this test stream. Some preliminary performance data are given along with comparison with previously determined uniform flow results.

17. Key Words (Suggested by Author(s))	18. Distribution Statement
Supersonic compressor, wind tunnel testing, cascade testing, nonuniform flow, flow field prediction.	

19. Security Classif. (of this report)	20. Security Classif. (of this page)	21. No. of Pages	22. Price*
		72	

TABLE OF CONTENTS

LIST OF ILLUSTRATIONS

LIST OF ILLUSTRATIONS (continued)

LIST OF ILLUSTRATIONS (continued)

LIST OF ILLUSTRATIONS (concluded)

LIST OF SYMBOLS

M	Mach number
P	static pressure
P_p	pitot pressure
P_o	upstream (tunnel) stagnation pressure
P_t	downstream (isentropic) stagnation pressure
R	blunt body radius (half thickness)
x	blunt body axial coordinate
y	blunt body normal coordinate (Figure 16)
z	blunt body span wise coordinate
z'	
θ	cascade coordinates (Figure 7)
y	

Subscript

∞	theoretical wind tunnel nozzle discharge value

NONUNIFORM FLOW FIELD GENERATION FOR SUPERSONIC COMPRESSOR STATOR DEVELOPMENT: DESIGN AND PRELIMINARY RESULTS

By Frederick W. Lipfert and Irving Fruchtman
General Applied Science Laboratories, Inc.

ABSTRACT

Design and preliminary results are given for a technique which can generate a nonuniform flow similar to the discharge of an impulse supersonic compressor rotor. The technique utilizes a carefully contoured, two-dimensional blunt body in a conventional hypersonic wind tunnel to generate the required flow field. To show the effects of the flow vorticity, a cascade of impulse-type blades was tested in this test stream. Some preliminary performance data are given along with comparison with previously determined uniform flow results.

I. INTRODUCTION

It has long been recognized that significant gains in compressor performance could be achieved by increasing the relative velocity of the working fluid to supersonic values. To generate the highest performance, e.g., stage pressure ratios greater than 10, a high-turning rotor is required in which the static pressure rise is realized in downstream diffusing stators. The experimentally-observed performance of such impulse rotors has been quite good, with adiabatic efficiencies as high as 90%. However, the addition of diffusing stators severely degraded overall stage performance. The history of successful rotor development and unsuccessful stator design is responsible for the conspicuous lack of operational systems using supersonic compressors in spite of 30 years of effort and identification of attractive applications.

There are, to be sure, many problems which make the design of the diffusing stator almost an empirical art. Some of these problems such as shock-boundary layer interaction, starting criteria, radial equilibrium, etc., have received a great deal of attention, while others, such as the highly nonuniform character of the rotor discharge flow, have hardly been examined. The purpose of the present work was to experimentally examine the effect of nonuniform inlet flow on the performance of a 2-D impulse-type supersonic cascade and ultimately to create a testing device with which the stators for the supersonic compressor could be developed.

The background of this problem is discussed in Section II; the method used to generate the nonuniform flow field is described in Section III; the experimental setup in Section IV, and testing in Section V.

Uniform inlet flow performance of the test cascade used for this work was previously reported in Reference 1. Comparison between these data and the information measured in the present test program was intended to delineate the effects due to flow nonuniformity.

However, the present test program was limited by the presence of high test-cabin pressure. This situation resulted from interference of the model shock system with the tunnel boundary layers in combination with a limiting facility exhaust system, and allowed taking only preliminary cascade test data.

II. PROBLEM BACKGROUND

Nonuniform flow is a consequence of the radial variations which occur in an impulse compressor wheel due to both design factors and loss variations. To highlight the magnitude of these gradients, design and actual performance data taken from Reference 2 are shown in the table below. Although separation regions were experienced at both hub and tip, the experimentally determined adiabatic efficiency of this rotor was 0.88.

TABLE I. - ROTOR DISCHARGE CONDITIONS OF SUPERSONIC, IMPULSE ROTOR

[From Ref. 2]

Radial Station	Design			Actual		
	P_{t_2}/P_{t_1}	P_2/P_1	M_2	P_{t_2}/P_{t_1}	P_2/P_1	M_2
Tip	19.1	1.14	2.58	8.	1.5	1.9
Mid	16.7	1.0	2.60	11.	0.8	2.1
Hub	14.7	0.87	2.64	2.	0.75	1.2

and where the subscript 1 is the reference upstream condition

2 is the rotor discharge condition.

Problems associated with the different diffusion of nonuniform streams have been discussed in References 3 and 4 and blamed by the authors of Reference 5 for the disappointing efficiency of their supersonic compressor. The thrust of the argument is that when a nonuniform stream is diffused, separation and recirculation of the low momentum regions can occur. Consider, for example, the case in which the back pressure is greater than the total pressure of the low momentum portions of the stream. The resulting flow exhibits large separation in the low momentum region and multiple shocks in the high momentum region, so that finally the average total pressure level in the stream would be close to the lowest value. It has been suggested that the dual functions of a diffusing stator

(to turn the flow back to the axial direction and to convert the kinetic energy of the flow into static pressure) are almost impossible to realize efficiently in a single blade row. Thus the diffusing stator should be a tandem system, similar to that proposed in Reference 6, to turn the flow by means of impulsive blades and then diffuse in an annular diffuser passage. For this reason, the effect of nonuniform entrance flow on the stator problem can be divided into two parts; the effect on impulsive turning and the effect on the diffusion process.

Although impulse-type turning blades have been thoroughly tested in stationary coordinates and also in wheels, performance with a known radial inlet flow gradient has not been documented, aside from that obtained naturally from rotor tests. It is to be expected that the effect of this stator inlet distortion will be to modify the secondary flow picture in the stator from that generated by an irrotational inlet flow, since the downstream vorticity is proportional to the turning angle and the inlet velocity gradient, c.f., Reference 7 . Because of the many unknowns and simplifications in such secondary flow analyses, the magnitude of these effects must be understood, not only to determine performance of the turning blades, but also to properly design the diffuser element (of a tandem stator).

III. BLUNT BODY FLOW FIELD COMPUTATION

This section presents the method for generating an appropriate nonuniform flow and the computed results. The flow field is produced by placing a blunt, two-dimensional body upstream of the test cascade in a conventional wind tunnel, as shown schematically in Figure 1. Generally speaking, a blunt body with a highly curved bow shock is required to produce the desired simultaneous flow field variations in stagnation pressure, static pressure, and Mach number. Accurate computation of both the subsonic and supersonic portions of the flow field is required, with the final output consisting of body coordinates that result in a specified flow field with a given upstream (uniform) Mach number.

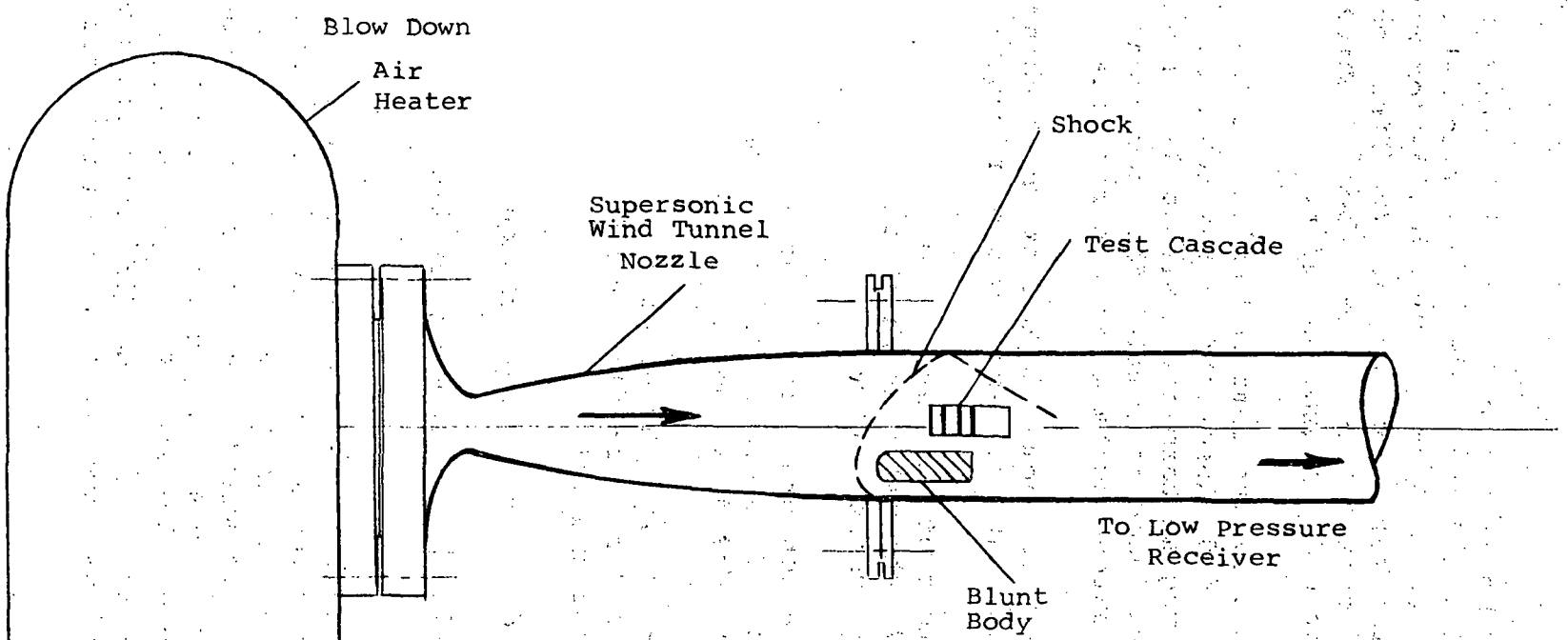

Figure 1. - Schematic of Test Arrangement

It was recognized that computation of the required body shape from the specified flow field would not be practical (the solution may not even be unique), and thus a direct blunt body method was chosen which was fast and relatively inexpensive. The final body shape was then selected from several trial shapes each of which had been supplied to the blunt body program as input.

The flow about the blunt body was computed using a time-dependent finite-difference method, described in Reference 8. The flow field computed by this program terminated with a data line in the supersonic region which was used as initial data for a characteristics network solution extending back and out from the body.

The following properties were deemed important in choosing the nonuniform flow distribution at the test cascade entrance:

1. The average Mach number of the test region should be around 2.7, the value at which the cascade was tested in uniform flow.

2. The static and stagnation pressure ratios - from hub to tip - should be comparable to those indicated in Table I (design values).

3. The flow angle variation from hub-to-tip should be small, in order to preclude shock waves from the cascade end walls.

4. No shock waves should enter the test region.

5. The longitudinal variation in flow properties should be small.

An elliptical contour was chosen as the basic blunt body shape, with the minor axis parallel to the upstream flow direction, based on prior estimates of the flow distribution. By adjusting the fineness ratio (the ratio of major to minor axes) and/or the upstream Mach number, the downstream flow properties could be changed in a relatively predictable manner until the desired cascade entrance conditions were realized. Table II lists the different cases which were examined and the conclusions drawn from the resulting data.

TABLE II. - COMPUTED BLUNT BODY FLOW FIELDS

Fineness Ratio	Supersonic Wind Tunnel Mach Number M_∞	Results
2.0:1	5.5	Average Mach number in cascade region too low.
2.0:1	6.0	Shock wave extended into test region due to over-expansion around corner.
1.5:1	5.5	Acceptable flow properties.

The computed flow field results and the coordinate system used are given in Figures 2 to 6.

The results of the selected flow field calculations can be seen in Figures 3 to 6, where the Mach number, static pressure, flow angle, and total pressure (streamlines) are, respectively, shown overlaying the characteristic net. Only the region of interest along the afterbody is indicated in these figures, between the nose shock and the Mach-wave coalescence. (The coalescence results in a very weak shock with pressure jump around 5%.) The origin ($x = 0$, $y = 0$) is located at a distance of one minor axis from the leading edge. The blade height of the test cascade is 2 inches, the pitch is 2.13 inches, and the stagger is 45°. It is composed of three blade passageways. With these dimensions in mind, the value of R is taken as 2 inches; thus the blades extend an axial length $\Delta x/R = 2.6$ and a height of $\Delta y/R = 1.15$. By positioning the cascade as shown in Figure 6, the average Mach number of the flow entering the center blade passage is 2.70, while the average Mach number gradient from hub-to-tip (in the y direction) is

$$\frac{\partial M}{\partial y_{\mathbb{C}}} = \frac{2.84 - 2.57}{1.15} = 0.235$$

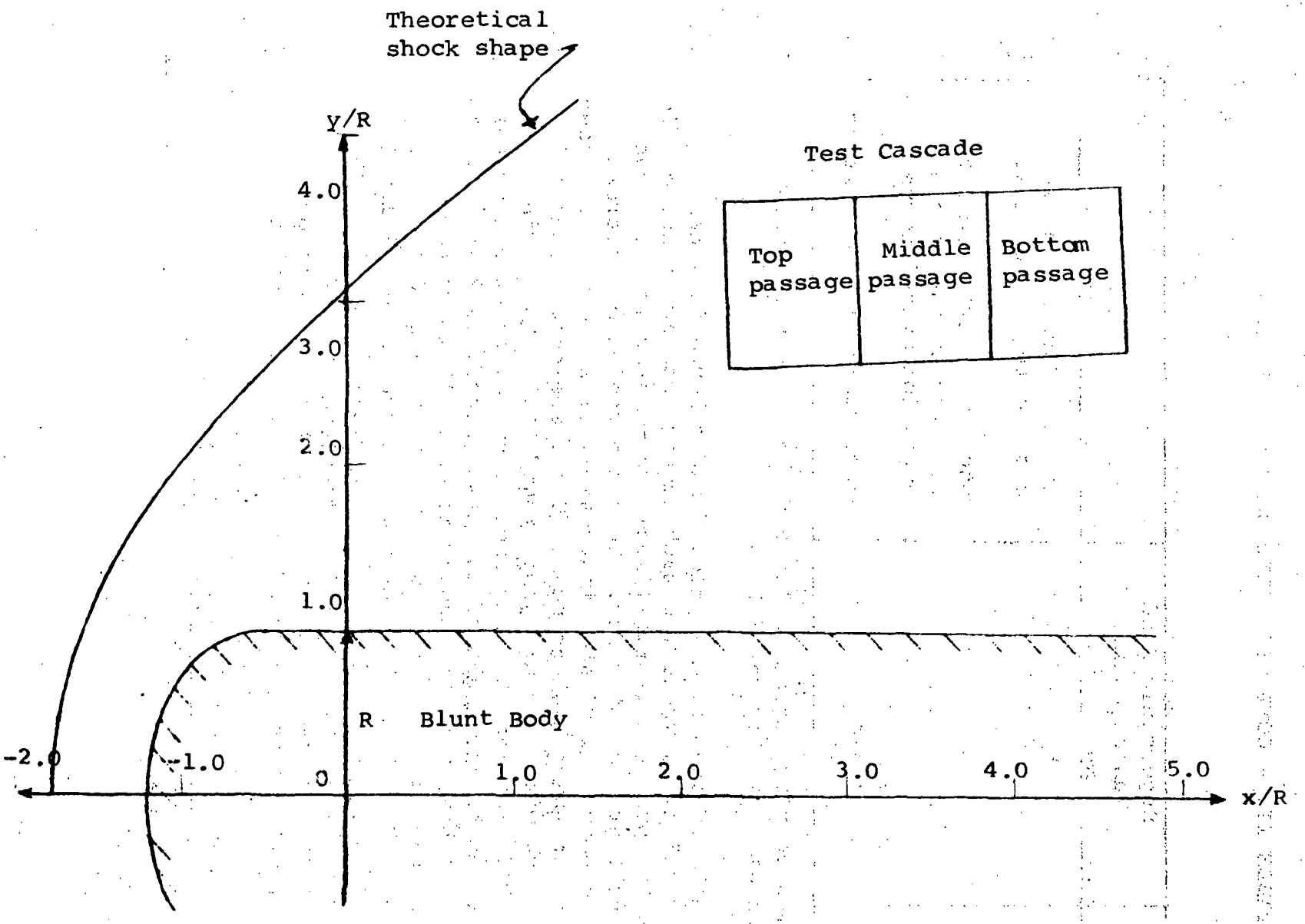

Figure 2. - Coordinate System, Cascade and Shock Location

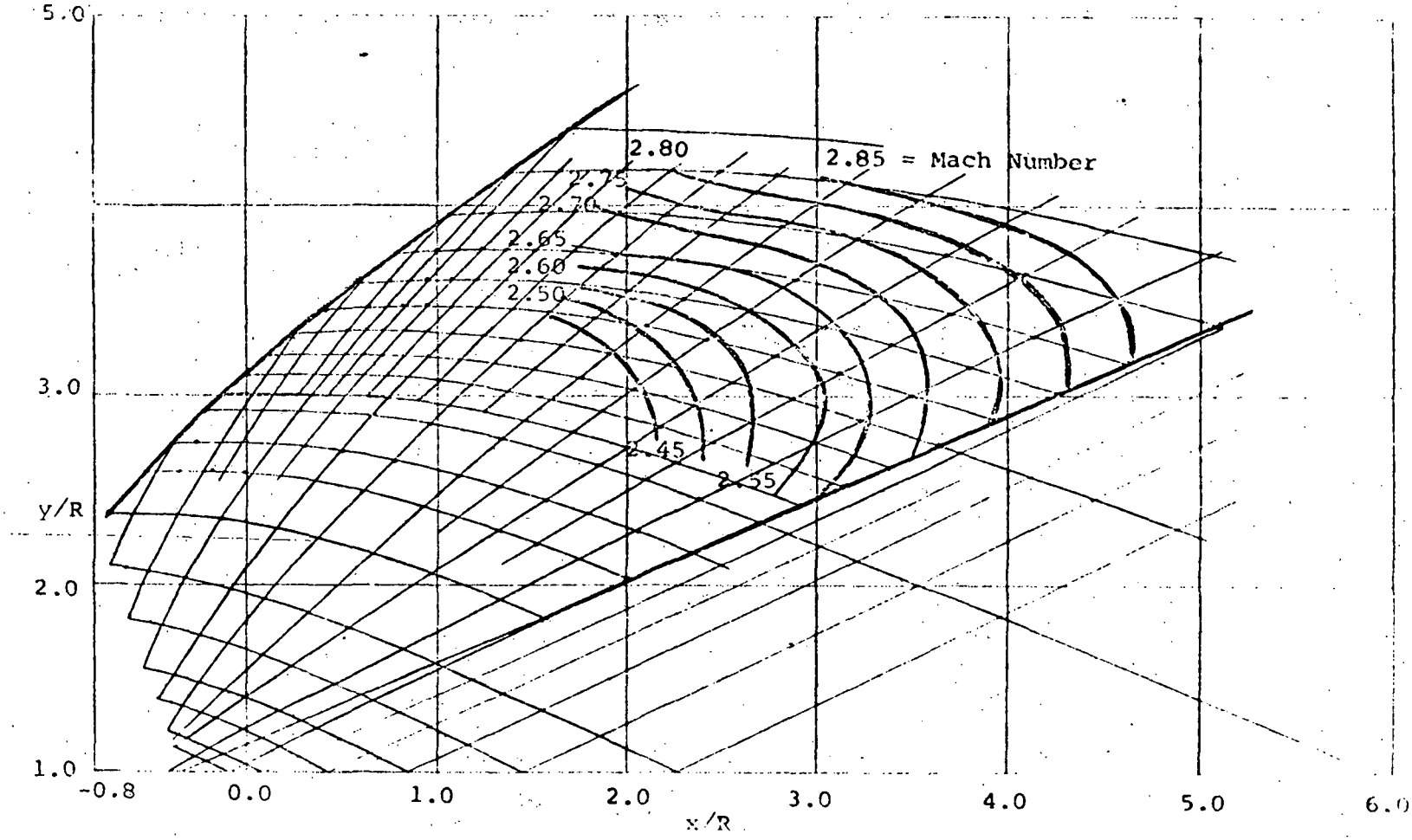

Figure 3. - Mach Number Distribution 1.5:1 Elliptical Forebody, M_∞ = 5.5

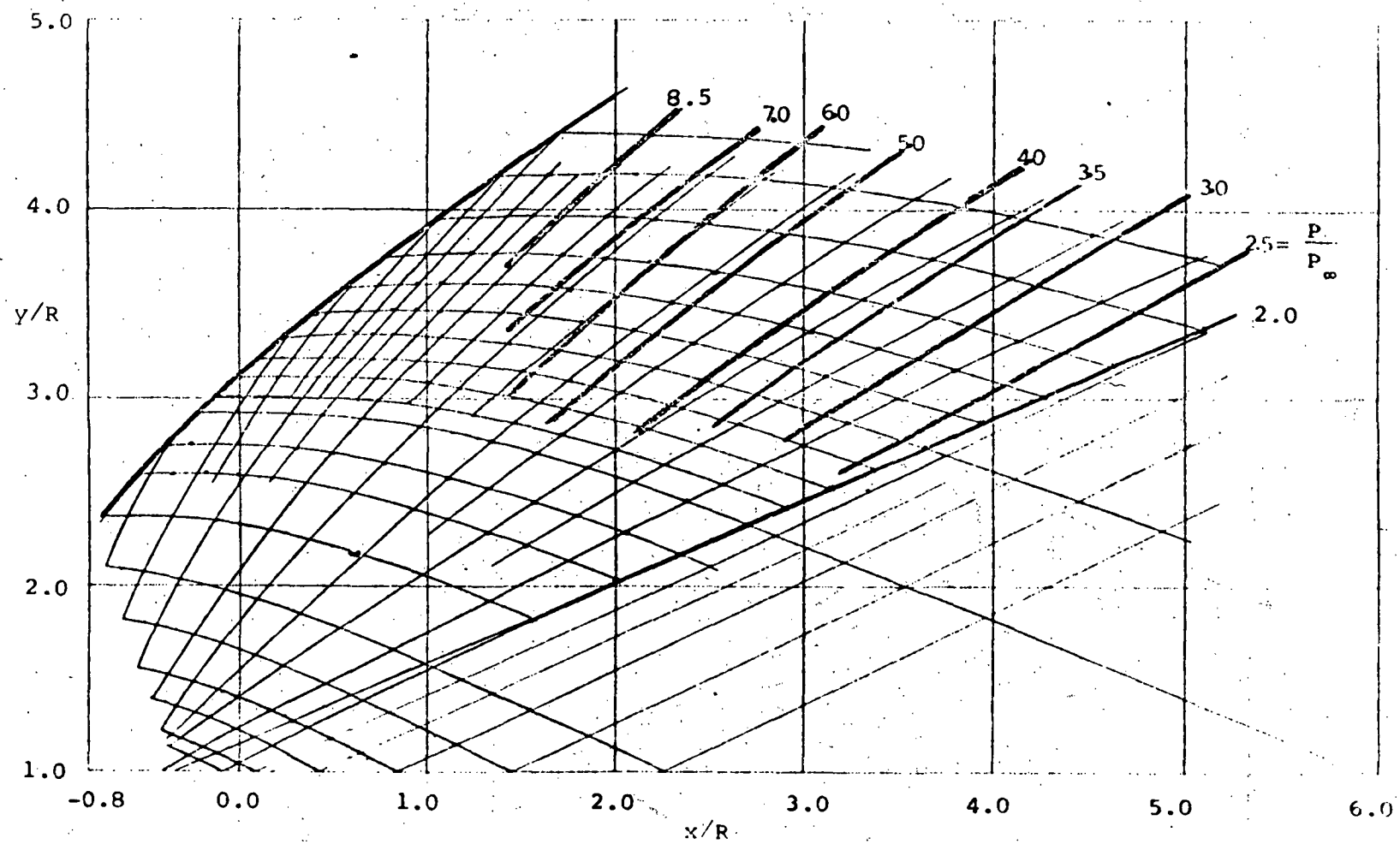

Figure 4. - Static Pressure Distribution (P/P_∞) 1.5:1 Elliptical Forebody, $M_\infty = 5.5$

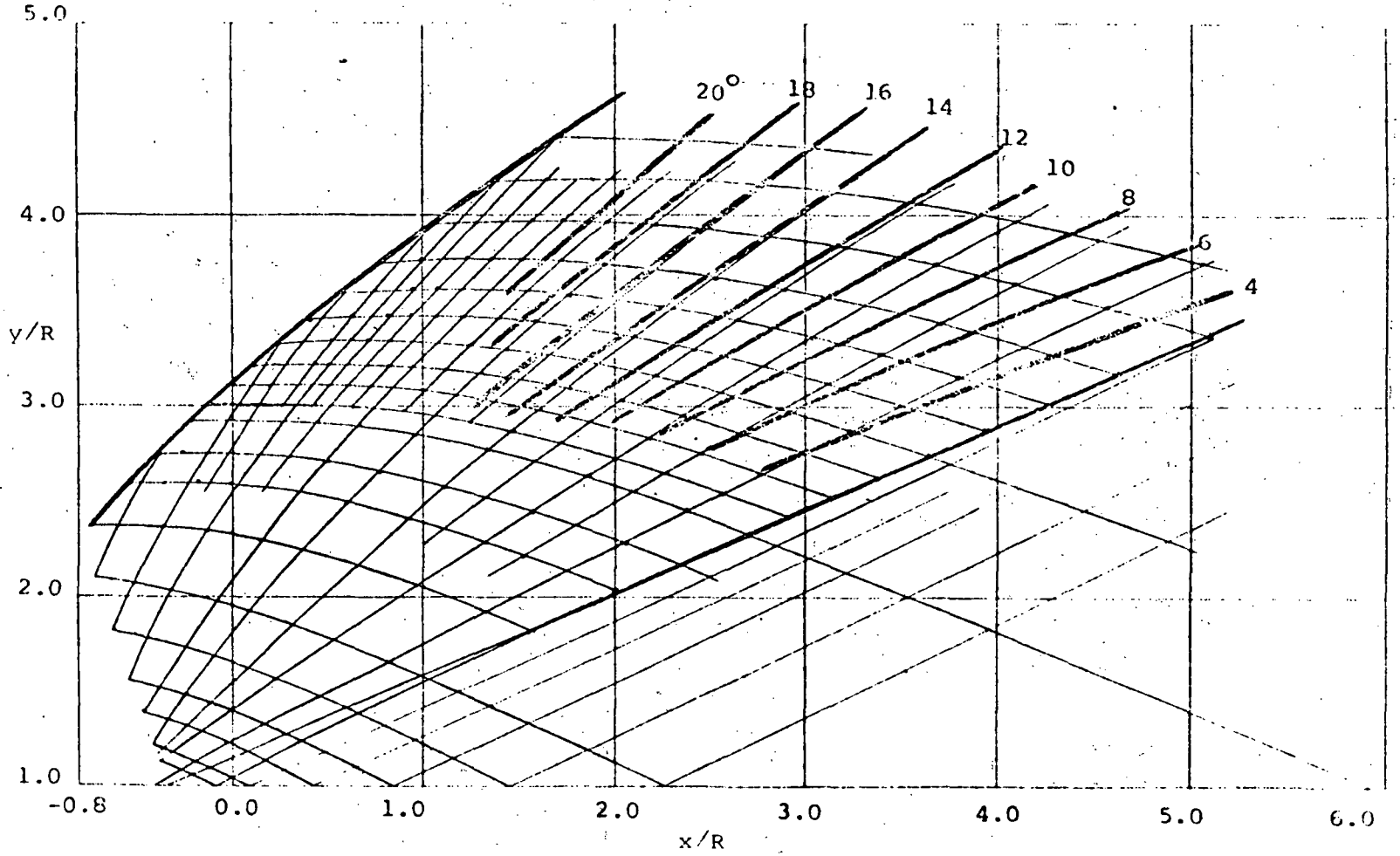

Figure 5. - Flow Angle Distribution (Degrees), 1.5:1 Elliptical Forebody, M_∞ = 5.5

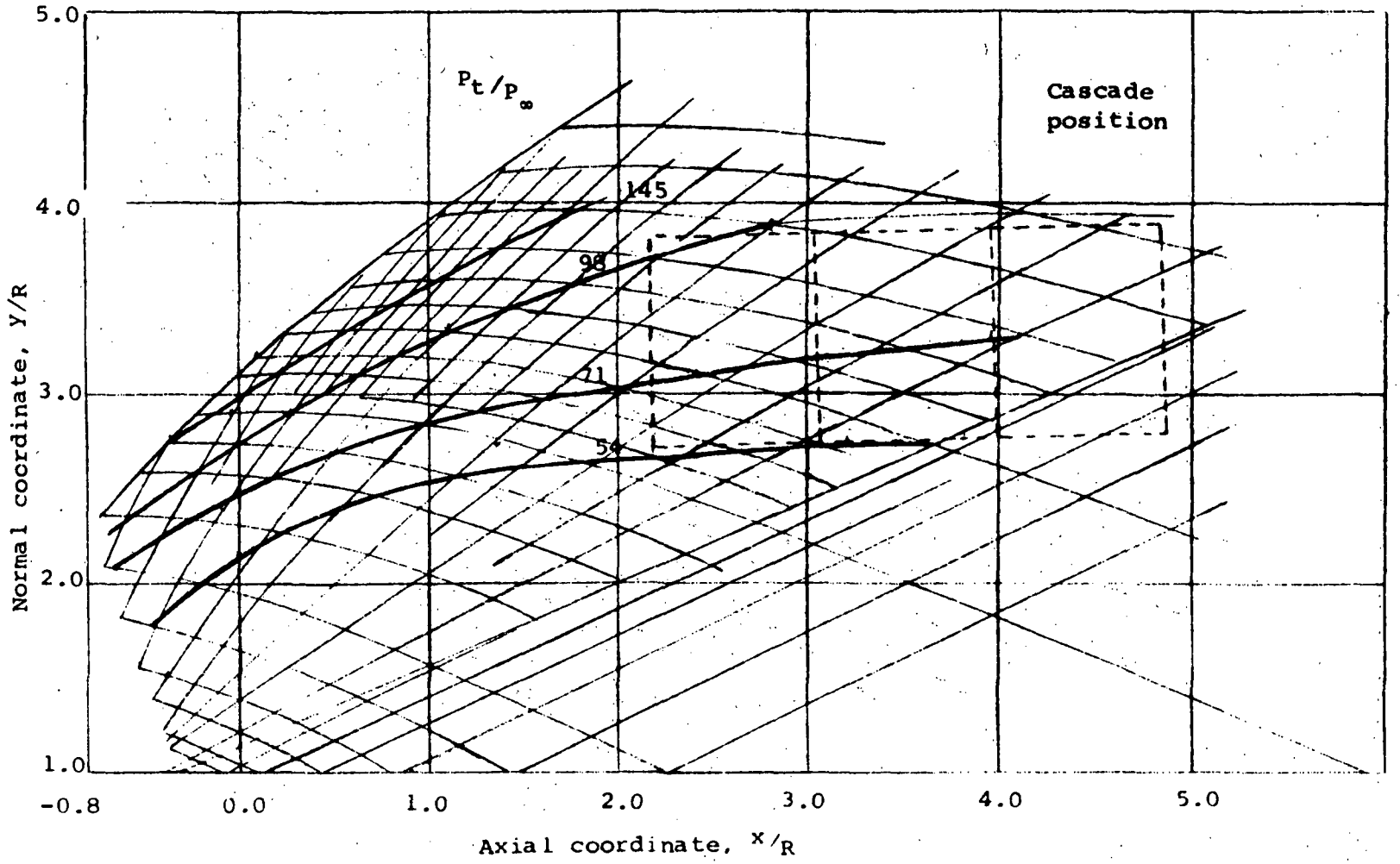

Figure 6. - Stagnation Pressure Distribution (Streamlines)
1.5:1 Elliptical Forebody, $M_\infty = 5.5$

Because the flow properties vary in the longitudinal direction, there is also some change in flow conditions from passage-to-passage. For instance, the average Mach number gradient in the swirl direction, θ (parallel to the blade entrance plane) is

$$\frac{\partial M}{\partial \theta} = \frac{2.74 - 2.67}{1.07} = .066$$

However, it is felt that since $\partial M/\partial y$ is about four times greater than $\partial M/\partial \theta$ and since $\partial M/\partial \theta$ is relatively small, the swirl variation would be unimportant compared to the hub-tip variation.

From Figures 4 and 6, the ratios of static and total pressure from hub-to-tip (in the y-direction) are seen to be 1.6 and 1.8, which is a good compromise between the theoretical and actual rotor values of Table I.

IV. - DESCRIPTION OF THE EXPERIMENTAL FACILITY

The test arrangement consisted of a storage-type air heater directly connected to a Mach 5.5, 14.2 in. square, contoured wind tunnel nozzle. The test-cabin with the blade-cascade and blunt body was attached to the nozzle exit. A 20 in. diameter 25 ft long exhaust pipe, ducted the airflow into a 40,000 ft^3 vacuum sphere receiver. At the entrance of the sphere was a 20 in. butterfly-type valve which was used to isolate the vacuum sphere from the test cabin between tests.

Air for these tests was stored in a large capacity bottle filled at 2000 psi and dried by passing through a silica gel dryer. Blowdown-type testing was performed with the air pressure controlled by a preset regulator with manual fine adjustment. Because of the limited vacuum capacity the test time was about 10 to 15 seconds. During this test perior there were negligible variations in either supply air pressure or temperature which were nominally 450 psi and 1000^{o}R.

Drawings of the test arrangement are shown in Figures 7 and 8. As indicated, the airflow captured by the cascade is ducted out of the test cabin through a flexible pipe and rejoins the main portion of the airflow, just downstream of the test cabin. A

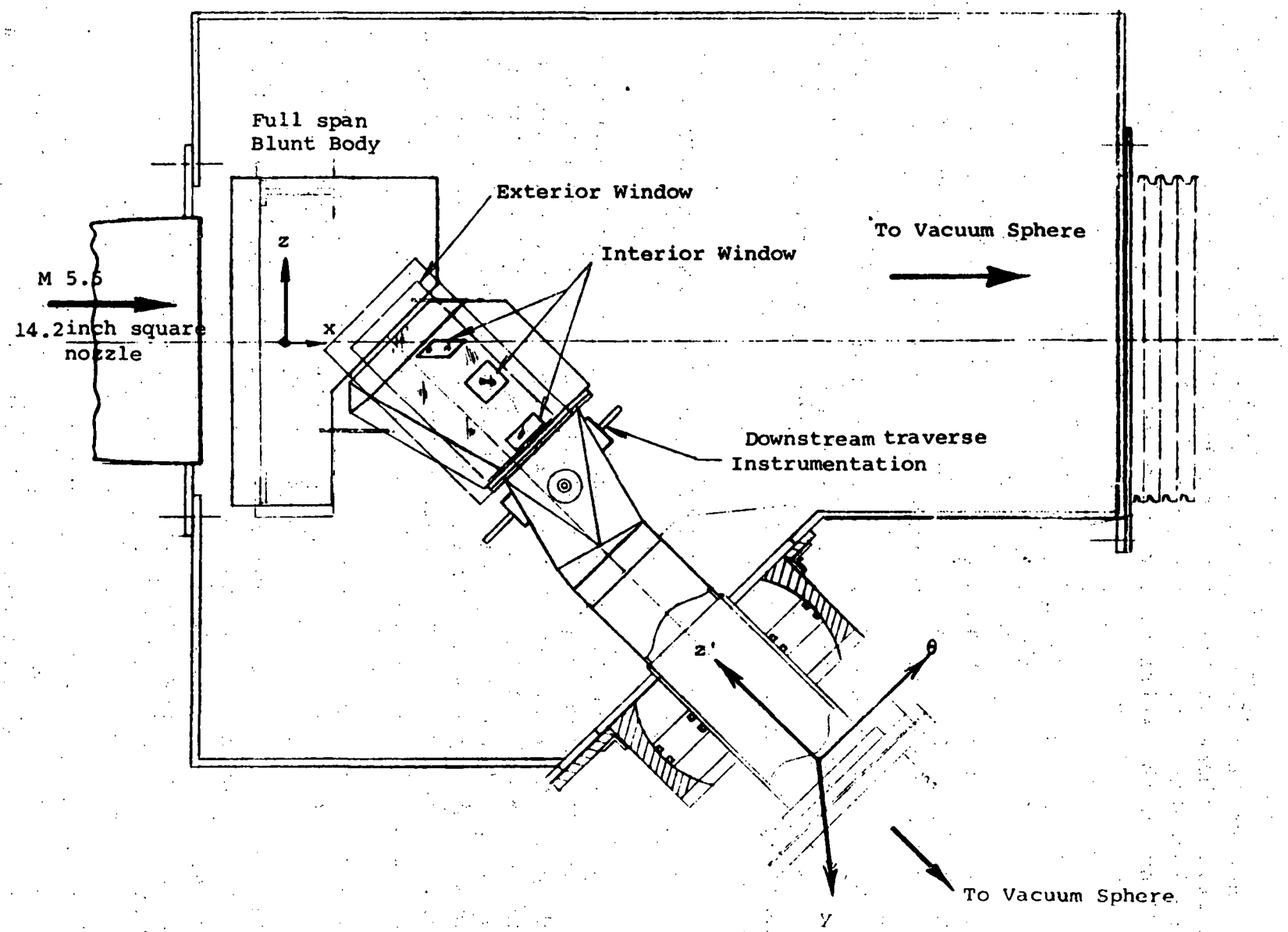

Figure 7. - Elevation of Test Facility - Original Configuration
(No Fairings)

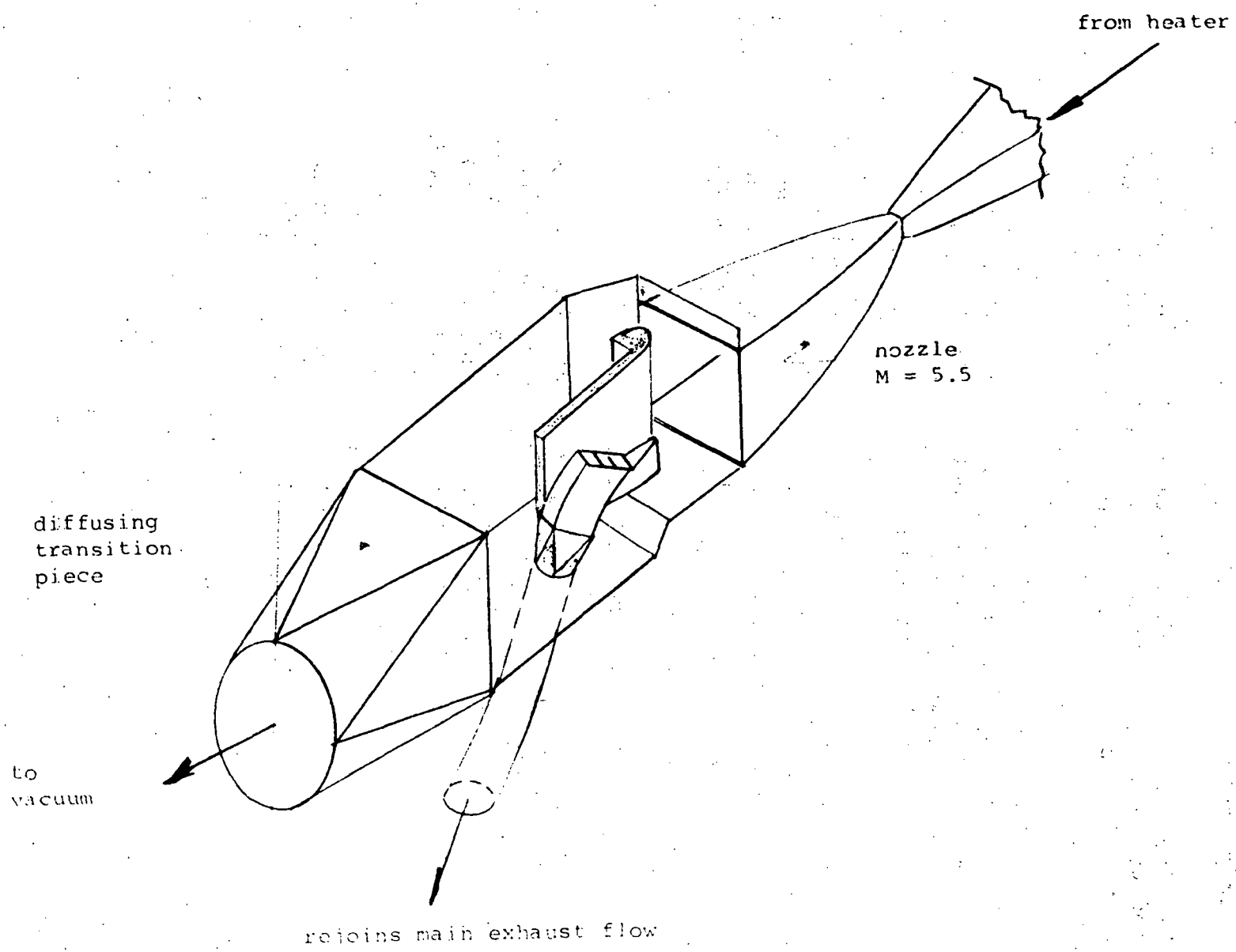

Figure 8. - View of Test Facility with Top and Side Test Cabin Walls Removed Showing Internal Flow Path

throttle valve was located at this juncture which was to be used to apply back pressure to the blade flow.

Positioning of the cascade relative to the blunt body was accomplished by means of a gimbal arrangement, allowing translation in the θ and z' planes and rotations about θ, z' and y axes (see Figure 7).

The blunt body and flat plate afterbody were made of aluminum and bolted together. The blunt leading edge was milled from a block of aluminum using a tool which had the required contour as its cutting edge. The flow generator assembly was attached to the test cabin by two thin, diamond-shaped steel struts.

A drawing of the blading is shown in Figure 9, taken from Reference 1. Two complete blades, and a pressure and suction surface making a total of 3 interblade passageways, comprised the test cascade. End walls were flat plate inner surfaces with 15° wedge (external) angle leading edges. The blades were of cast stainless steel.

Instrumentation

Measurements were taken in both the flow field generated by the blunt body and by the blade cascade. The basic probes used included both wedge and cone types so that flow Mach numbers and direction could be determined. Blade surface, end wall, flow generator and wind tunnel static pressures were also monitored.

The instrumentation used for the cascade exit flow field is described in detail in Reference 1 and shown in Figures 10 and 11, included a 15° half-angle wedge probe which extended the height of a blade, and 6 pitot pressure probes. By traversing parallel to the blade outlet plane, all of the central passage could be mapped and portions of the inner and outer passageways. A change was made in the method of probe movement, however, from that indicated in Reference 1. For the present tests, a pneumatic-hydraulic actuator assembly was used in place of the motor-driven gear mechanism. This had the advantage of better traverse speed control. By mounting the actuator outside the test cabin and using four universal joints, alignment problems were avoided and traversing was smooth and trouble-free.

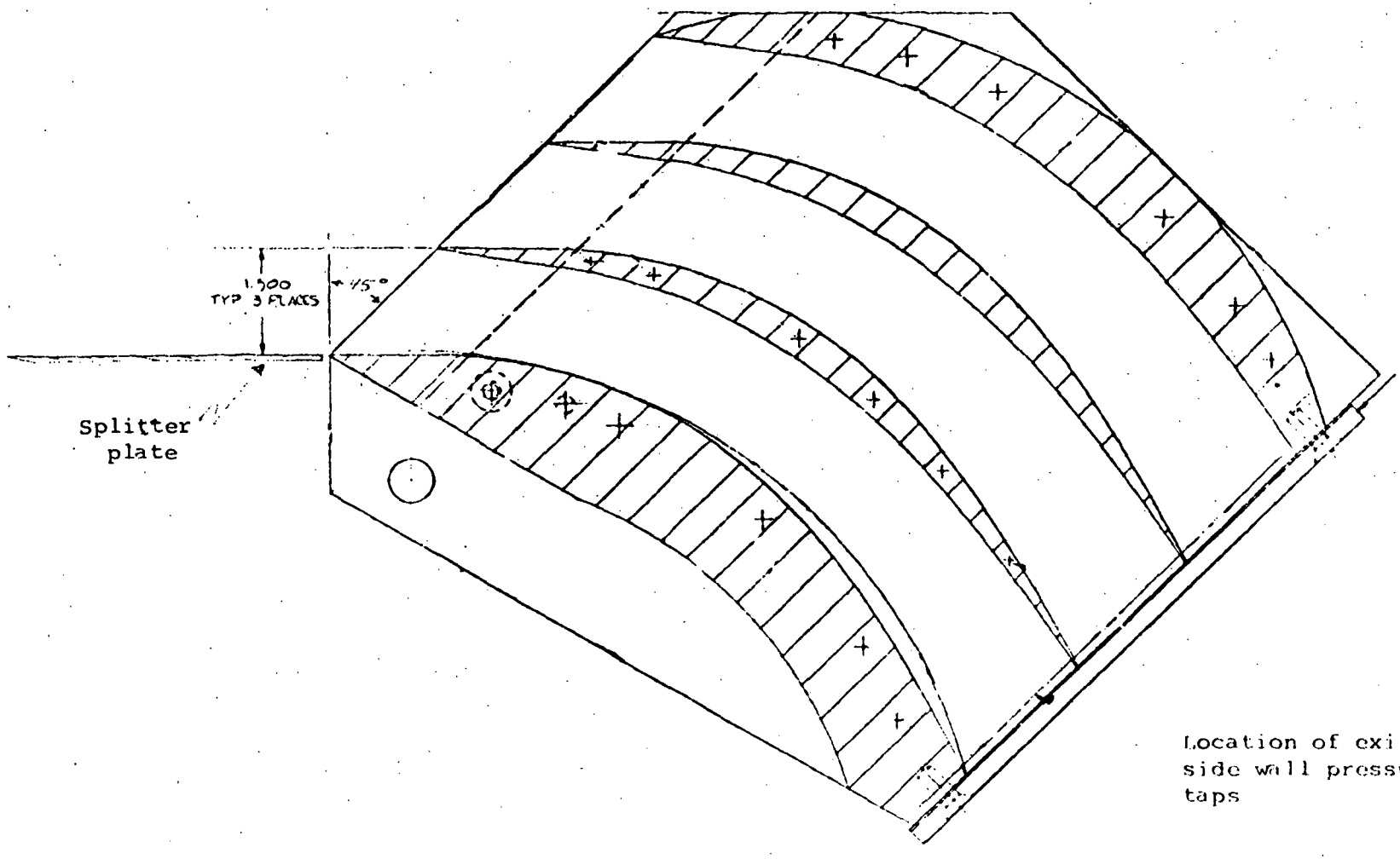

Figure 9. - Section Through Two-Dimensional Cascade

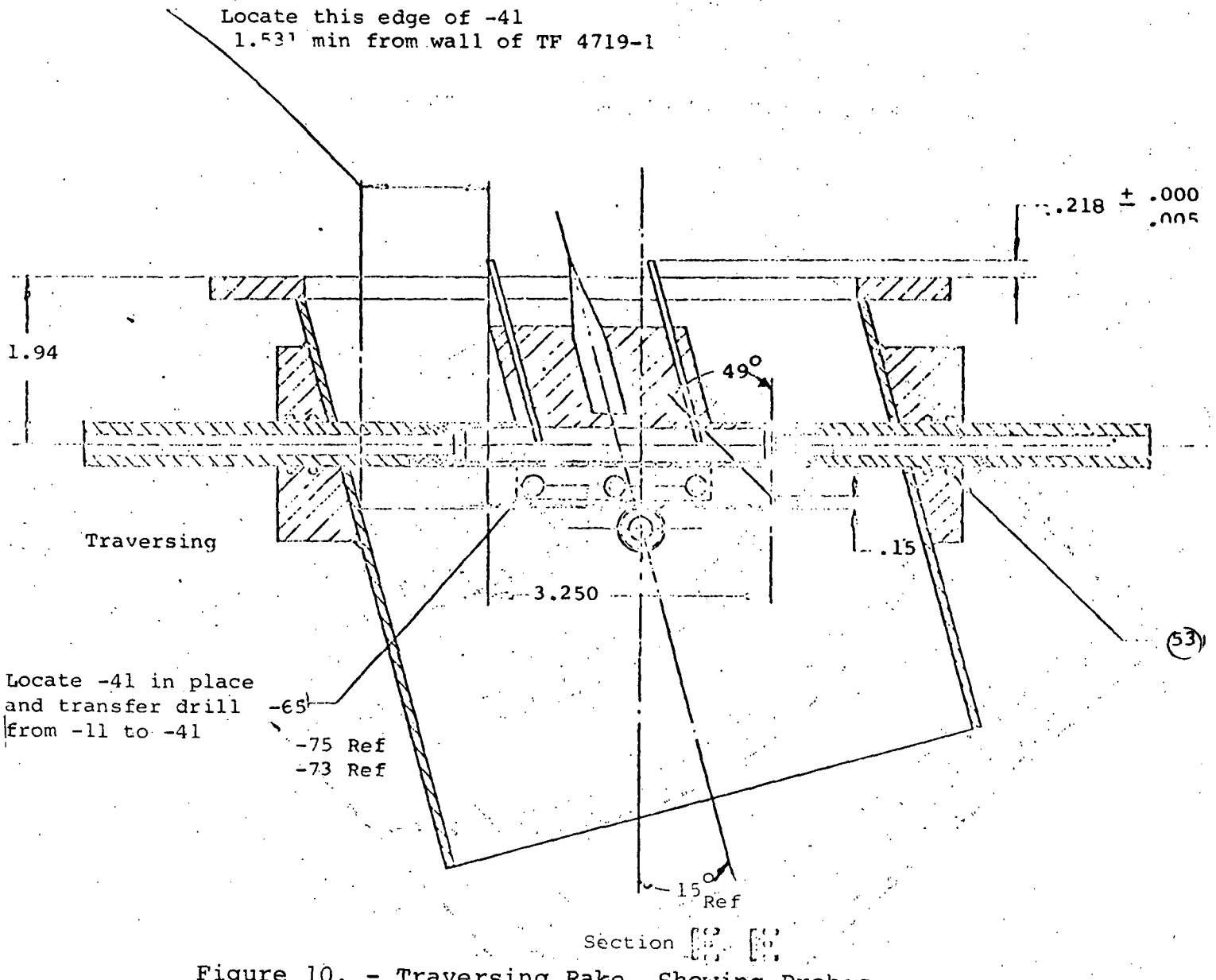

Figure 10. - Traversing Rake, Showing Probes

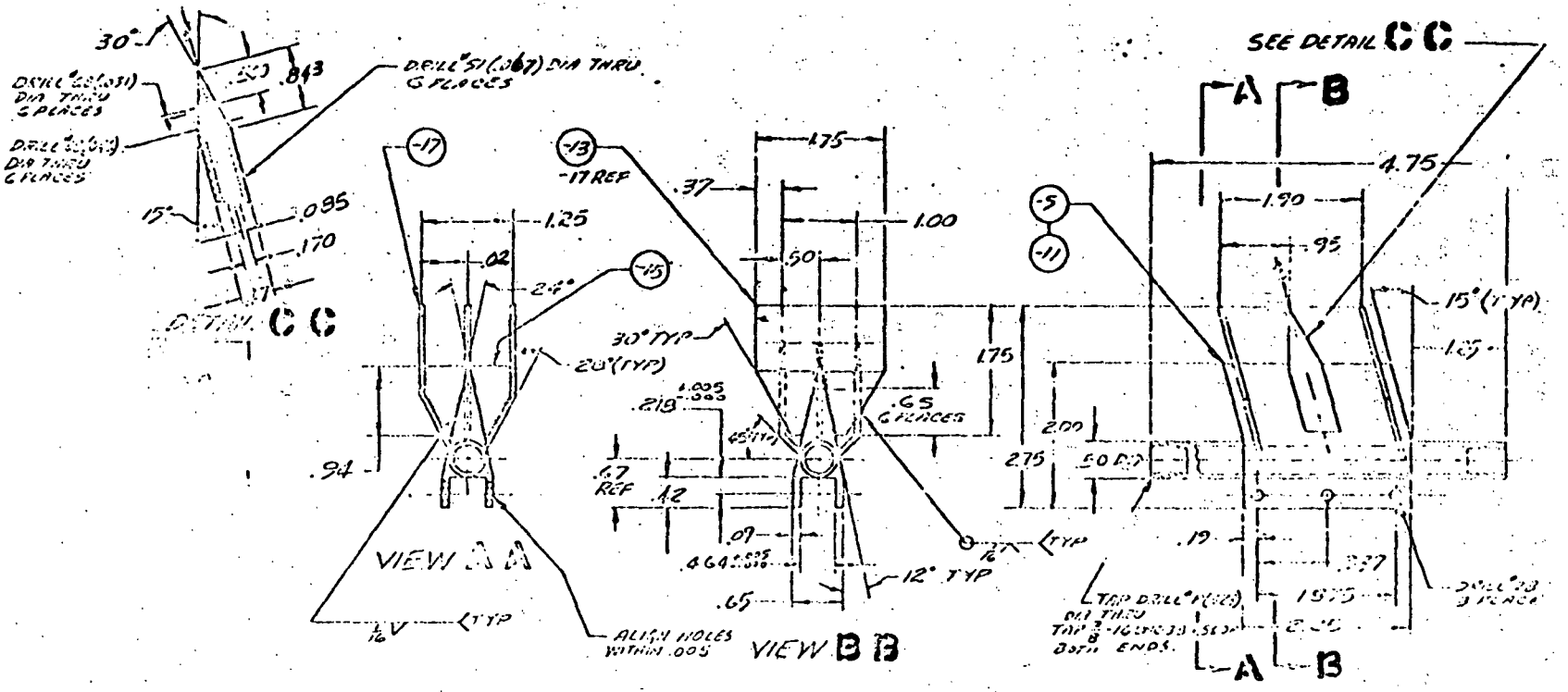

Figure 11. - Rake, Wedge, and Pitot Probe Details

To determine the flow field generated by the blunt body, three probes, each consisting of a 5° half angle wedge, and two pitots were mounted on a platform and driven by the same pneumatic-hydraulic actuator. The traverse path was now normal to the plate surface and extended from 1/2 in. to a maximum of 7 in. Traverse speed was controllable independently in either direction.

V. TEST RESULTS

The original test plan was as follows: First, map the flow field produced by the blunt body, and verify the proper position for the cascade. Second, install the cascade and determine its performance with nonuniform inlet flow. Third, determine the effects of back pressure on the cascade performance.

During Phase I testing (blunt body alone), it was found that severe interactions existed between the blunt body shock and the tunnel boundary layer and test cabin environment. The following sections describe the efforts expended to deal with these problems and detailed results for both blunt body and cascade flow fields for some of the configurations that were tested. These interactions were found to influence the test section flow to the point where it was deemed essential to maintain the cascade in place for proper back pressure during cascade inlet flow field mapping measurements. As a result, only very limited data could be obtained on the cascade inlet flow because of physical restrictions to probe access. Useful tunnel test times were also severely restricted because of the model/tunnel interactions and premature flow breakdown.

A. Facility Model Improvements

The original facility was equipped with a full-span model, an open-jet test section with $L/D = 3.4$, and an isolation butterfly valve to allow access to the test cabin without loss of vacuum in the sphere. This system suffered from excessive model blockage, even though the open jet arrangement was intended to provide geometric relief from this blockage. The inability of the flow to

utilize this relief was traced to the excessive exhaust line blockage, due to the isolation valve (nearly 30% in the fully open position) as follows:

The exhaust flow is choked near the position of the isolation valve, providing the vacuum receiver pressure is sufficiently low, which it is during the initial portion of a test. This allows estimation of the pressure at the entrance to the exhaust pipe, based on 1-D frictional flow relations. If the flow in the pipe is subsonic throughout, the pressure at the entrance to the pipe (downstream end of test cabin) will be of the order of 12 times free stream (nozzle exit). On the other hand, if the flow is supersonic at the pipe entrance, the pressure will be of the order of 6 times free stream (or less). With 30% blockage by the valve, these pressure ratios were 30% higher.

The state of flow at the entrance to the exhaust pipe obviously depends upon conditions in the test cabin. Subsonic flow is likely if any of the following conditions occur:

(a) Excessive free-jet length, causing dissipative mising and spreading of the jet to a diameter greater than that of the exhaust pipe entrance;

(b) Excessive model blockage, causing strong shocks and separation of the tunnel boundary layers;

(c) Extensive separation of the tunnel boundary layers due either to adverse pressure gradients or the geometry of the test section (steps, cavities, etc.)

Note also that a supersonic stream will be able to utilize expansions in the test section, intended to relieve blockage and locally cancel impinging shocks, only if the downstream pressure permits. As shown in the sketch below, if the downstream pressure is high, a step will cause a shock to exist because of the upstream propagation of the high pressure through the separated region. These separated regions will allow three-dimensional spreading of the high pressure zones so that the entire test cabin may be affected.

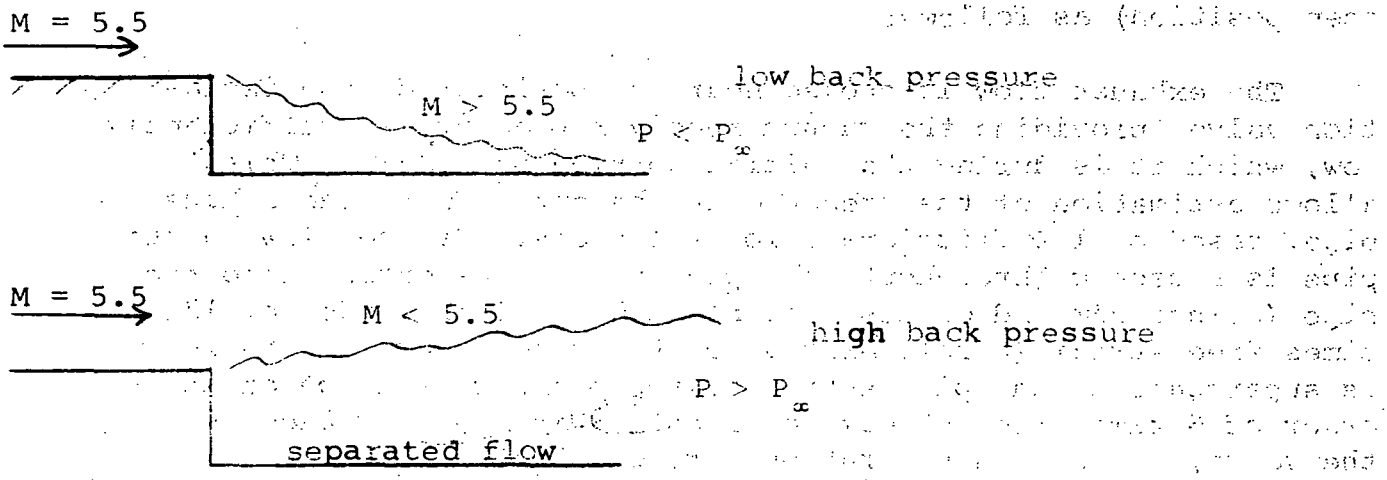

Note also that at a Mach number of 5.5, a turbulent boundary layer can experience a pressure ratio jump of no more than 2.5-3 without separating. Thus the back-pressure ratio of about 6 must be spread over some distance to prevent separation and any model shocks stronger than that will surely have an adverse effect.

At the beginning of the test program, the main problems were (a) and (b). Factor (a) was eliminated by the use of a 20 in. square-to-round transition piece, closing down the free jet length to L/D = 2.0. With no model in the test section, the tunnel boundary layer was able to negotiate a pressure ratio (increase) of 6, without extensive separation. Factor (b) was eliminated by reducing the blunt body span from in. (completely spanning the flow), to 10 in. and by cutting the blunt nose in half, reducing the blockage to 10% from the original value of 28%, based on nozzle exit area. This agrees with other supersonic-hypersonic wind tunnel data (Reference 9). The tunnel had also been fitted with a number of fairings which tended to approximate a closed=jet configuration (with several large cavities), thus improving the situation with regard to factor (a) and (c) as well. The final configuration was shown schematically in Figure 8.

Now the back pressure has an effect on the cascade as well, since it exhausts into the system at a point near the main exhaust pipe entrance. Since the cascade duct is a poor diffusor, this pressure is felt more-or-less all the way back

to the cascade exit. Thus the case of low cabin (cascade entry) pressure and high back pressure, may cause the cascade flow to break down or even unstart.

B. Blunt Body Test Results

1. Half-body results. -The 2 x 10 half-blunt body model shown below did not interfere with the tunnel flow, but did not attain the desired full blunt body flow pattern. The lower splitter plate was intended to replace the stagnation streamline of the full body, and thus its protruding length was that of the calculated shock stand-off distance, 1.2 inches. This plate isolated the top and bottom regions of the nose, which normally communicate in blunt body flow. However, this particular configuration has another stable flow pattern, that of an oblique (straight) shock attached to the splitter plate leading edge, as shown in the sketch below. The expansion around the blunt body shoulder weakens this shock much more rapidly than in the design case, so that low pressures are felt over most of the afterbody. This flow pattern hypothesis corresponds fairly well to the actual measurements, Figure 12. The low pressures at the blunt plate trailing edge may be due to end effects, since end plates were not used on this configuration.

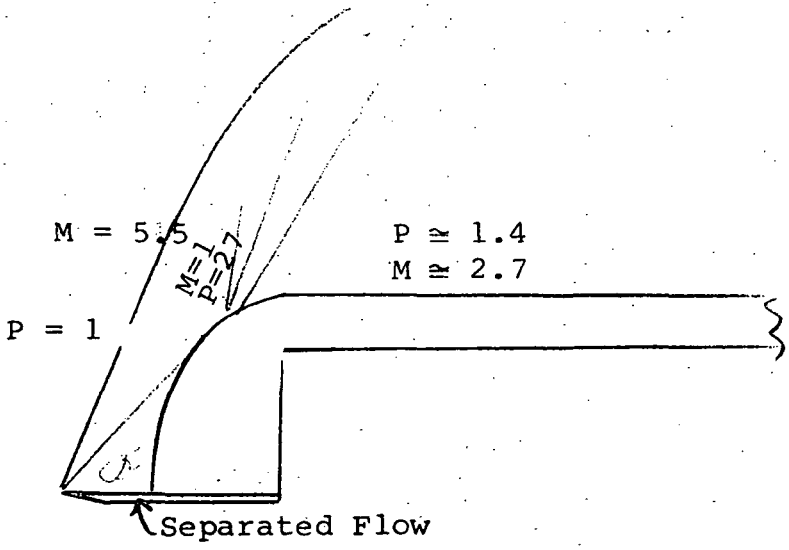

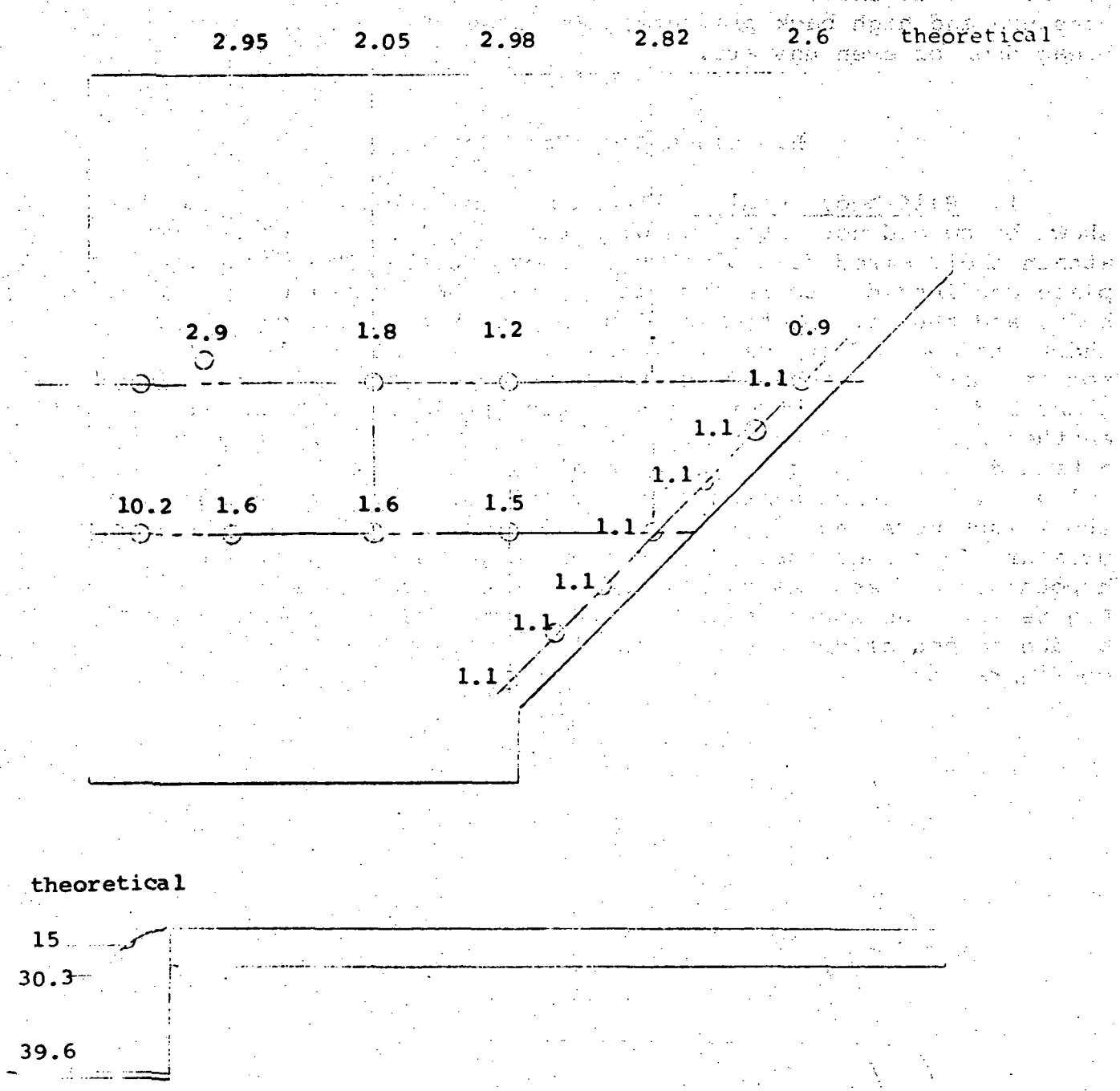

Figure 12. - Blunt Plate Pressure Distribution (P/P_∞)
Half Body (Isolation Valve Out)

These results also display practically no interaction between the blunt body shock and the opposite tunnel wall boundary layer, further evidence that the oblique shock flow pattern was established. Also, detailed traverses of the flow field (discussed below) revealed peak Mach numbers of about the level expected.

The effects of high cabin pressure may be seen by comparing Figure 12 (exhaust isolation value out) to Figure 13, (exhaust isolation value in). Note that the pressure distribution near the leading edge is essentially the same, and that a small region of low pressure exists on Figure 13. The remainder of the flow pattern displays an increase with downstream distance, which may be attributed to end effects. The larger extent of end effects is directly related to the pressure rise, i.e., a Mach wave at M = 2.7 lies at 21.7° (a) in the sketch below, and a shock with pressure ratio of 4 has an angle of 44° (b) in the sketch below.

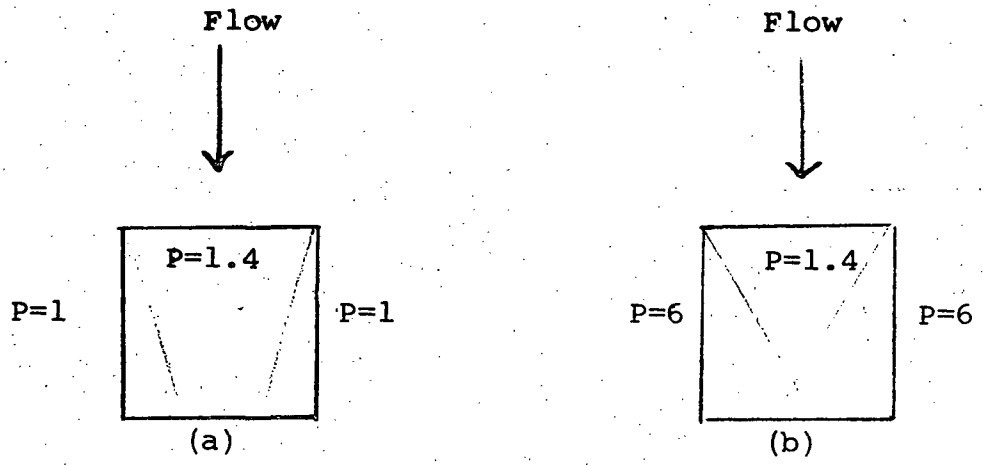

2. Full body results. - Because of the unsuitability of the half-body flow field, the blunt body model was restored to its full 4 in. thickness (symmetrical nose) and reinstalled in the wind tunnel. With the isolation valve removed, and the 8 in. cascade back-pressure valve removed as well, the flow in the wind tunnel was improved to the point where useful measurements could be obtained, even though the exhaust flow was completely subsonic. The (10 in. span) model with no end plates revealed a similar flow pattern (Figure 14) to that of Figure 13; pressure increasing with distance back along the afterbody rather

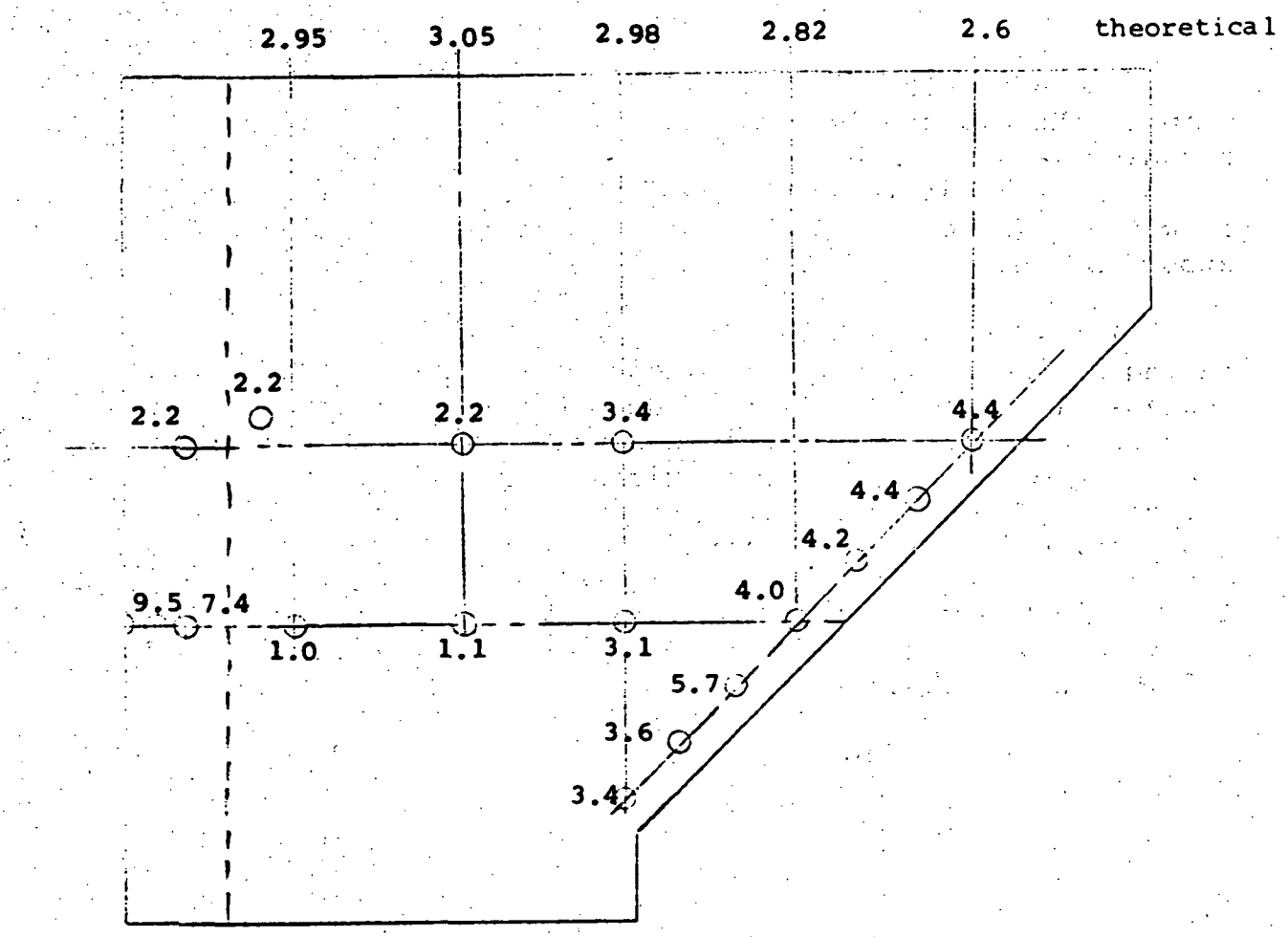

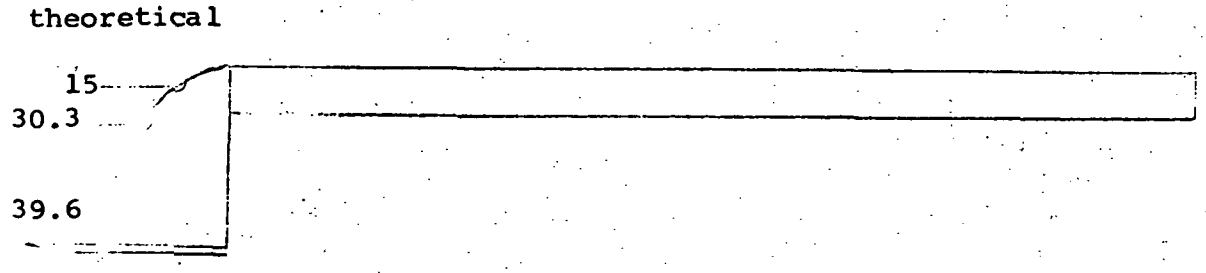

Figure 13. - Blunt Plate Pressure Distribution (P/P_∞)
Half Body (Isolation Valve In)

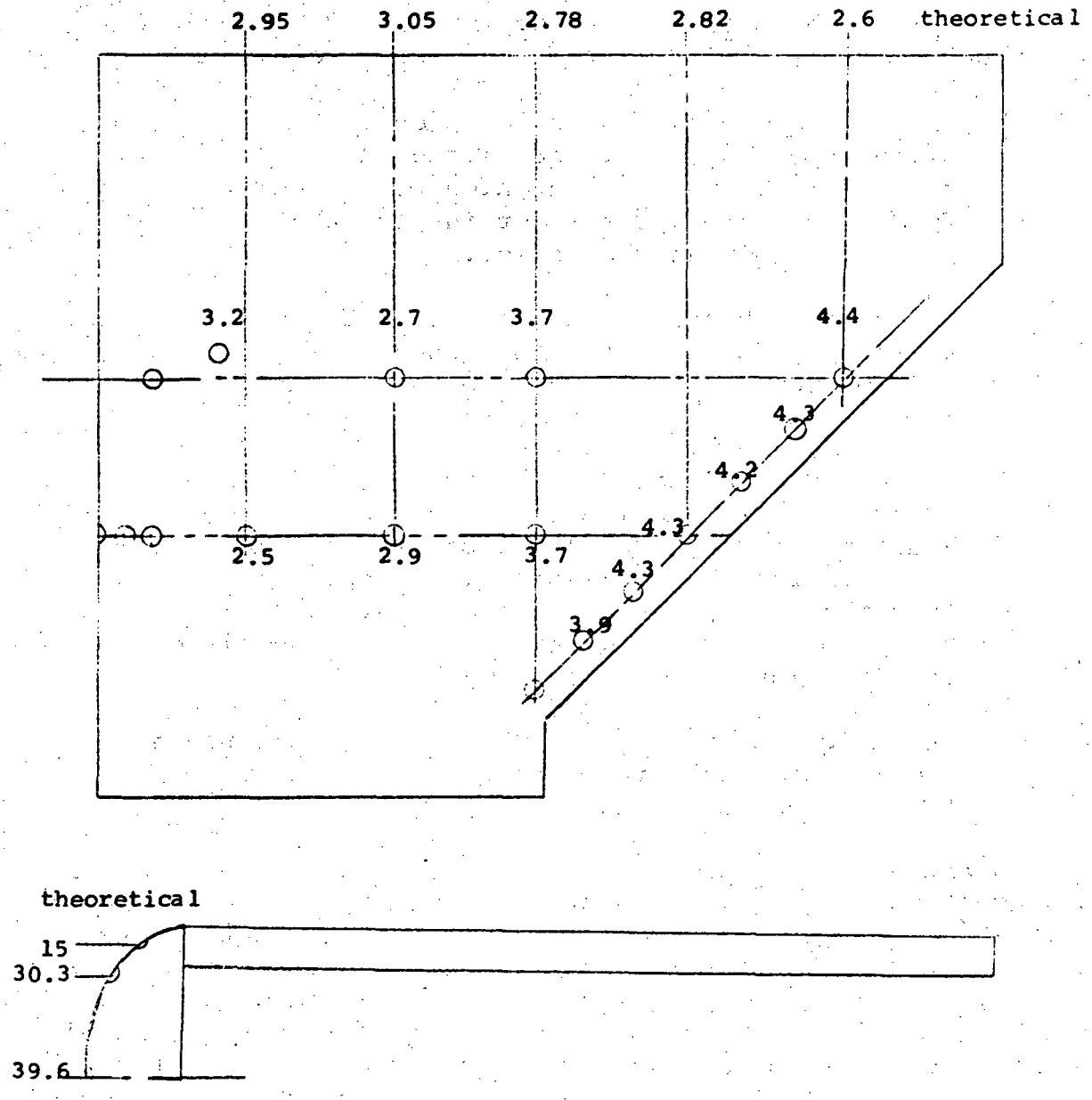

Figure 14. - Blunt Plate Pressure Distribution (P/P_∞): Full Body, No End Plates, Original Cascade Position

than decreasing, as predicted. This was also attributed to end effects, and the following effort was initiated to deal with them.

An analysis of the blunt plate and cascade flow field results thus far was made, with the following conclusions:

1) The pressure distribution on the blunt plate appears to be as predicted out to $x/R = 1.3$, at which point high pressures feeding up from the rear or in from the sides are felt at the center.

2) These disturbances on the plate surface apparently do not enter the cascade, but side effects off the plate surface ($y/R > 1.0$) may enter.

3) These side and rear disturbances can be circumvented by installing an extension on the blunt plate and side plates or fences. However, there may be disturbances propagated from the side plates due to the interaction of the blunt body bow wave with the side plate boundary layer.

4) The height of a side plate (off the blunt plate surface) may have to be considerable because of the cascade position.

An extension was thus installed on the blunt plate afterbody, creating a rectangular shape and making the overall model length about 16 inches. The previous length and shape of the afterbody had been dictated by cascade flow visualization constraints, which were now relaxed in favor of obtaining an improved flow field. This change, as seen in Figure 15, resulted in a nonuniform pressure distribution of the taps along the 45° line formerly the trailing edge, apparently due to side effects feeding in (from the top).

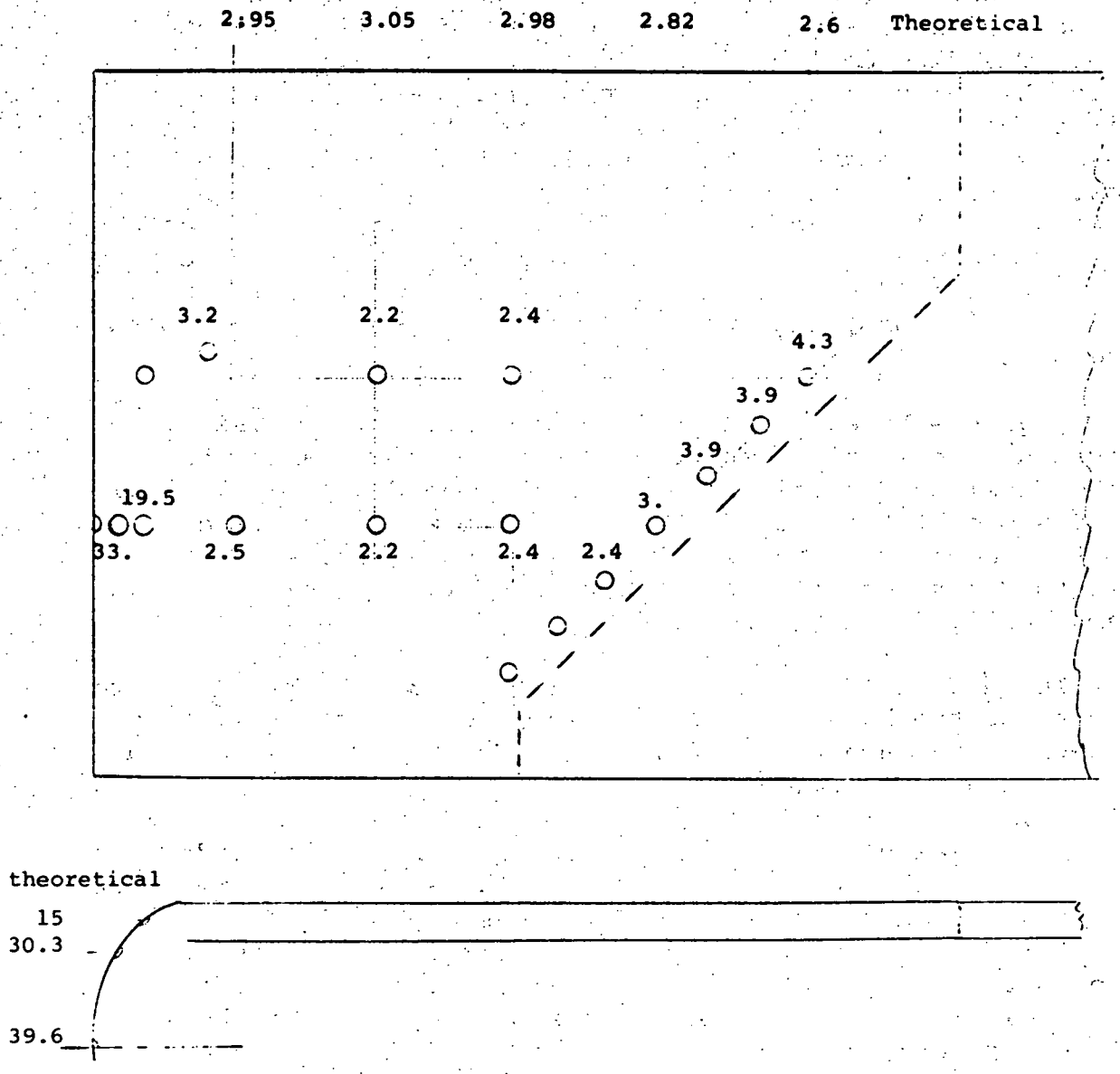

Figure 15. - Blunt Plate Pressure Distribution (P/P_∞): Full Body, No End Plates, with Aft Addition Original Cascade Position

The blunt body span (z dimension in Figure 7) had previously been reduced in order to lessen its blockage effect, an effort which was successful. Of course, since the nose region of the body has subsonic flow, there would be some end (side) effect no matter what the span. However, the pressure created in the test cabin on the lower side of the (full thickness) body is so high that it feeds around and creates a high pressure zone along the sides of the blunt plate. The flow deflection and shock angle (in the x-z plane) due to this high pressure could be significant, and it is believed to be this effect which creates the "reverse" axial gradients experienced in the cascade which are discussed below. Of course, the steeper the wave angle, the larger the required end plate becomes in order to prevent these waves from entering the cascade. If the high pressure zone could be physically shielded from this region, then an end plate would have to handle only Mach waves signalling the end of the blunt plate span.

A quasi-three-dimensional characteristics analysis was conducted by computing Mach cone locations (in planes normal to the flow) to determine the forward three-dimensional domain of influence of the cascade. This region was then projected onto the two (x-y) planes of the blunt body plate sides in order to determine the required shape of the end plate, shown schematically in Figure 16.

The end plate leading edges (labeled 3 in Figure16) were tailored to the blunt plate shock shape in order to minimize shock-boundary layer interaction here (blunt plate shock-end plate boundary layer).

A partial end plate was already present on one side of the cascade - this was the triangular splitter plate (6) which had been mounted on top of the first cascade blade flow deflector (5) serving as an extension of the first cascade blade suction surface (see below). These two plates combine aerodynamically to make a continuous shield from the shock on back to the cascade entrance, preventing side disturbances from being felt in the cascade (as long as the side flow does not break down).

On the opposite side, a very extensive end plate would be needed if its function were to prevent a higher pressure region from being felt in the cascade. This is because the high pressure at the termination of the plate would feed upstream through the boundary layer on the "good" side, and the resulting separation shock would likely enter the cascade. This phenomenon was experienced to some extent on the blunt plate extension.

For this reason the blunt plate top surface (x-y plane) was extended in the z direction all the way to the tunnel boundary wall.[4] However, a sharp leading edge was used instead of an extension of the blunt plate contour in order to reduce blockage. The end plate was then placed between the two (in the x-y plane) in order to keep the lower surface pressures that were expected on the side extension from being felt. The complete assembly is depicted schematically in Figure 16. A wedge-shaped fairing[5] was used in front of the cascade in order to guide the flow (not entering the first passage) around the cascade. To prevent high pressures from the side of this wedge from being felt inside the cascade, the triangular spitter plate[6] was installed parallel and in line with the first passage suction surface entry.

3. Test results with end plates. - The chief results from the use of the end plates and blunt plate extension were:

- Many of the nozzle and test cabin pressures were reduced
- The aft portion of the blunt plate showed pressures lower than theoretically predicted vs higher than predicted without the end plate (Figure 17)
- The cascade entry pressures were still higher than theoretically predicted

Thus, in general, the flow field was quite improved, but there was considerable evidence that the cascade entry conditions were other than predicted, including limited traverse data as discussed below.

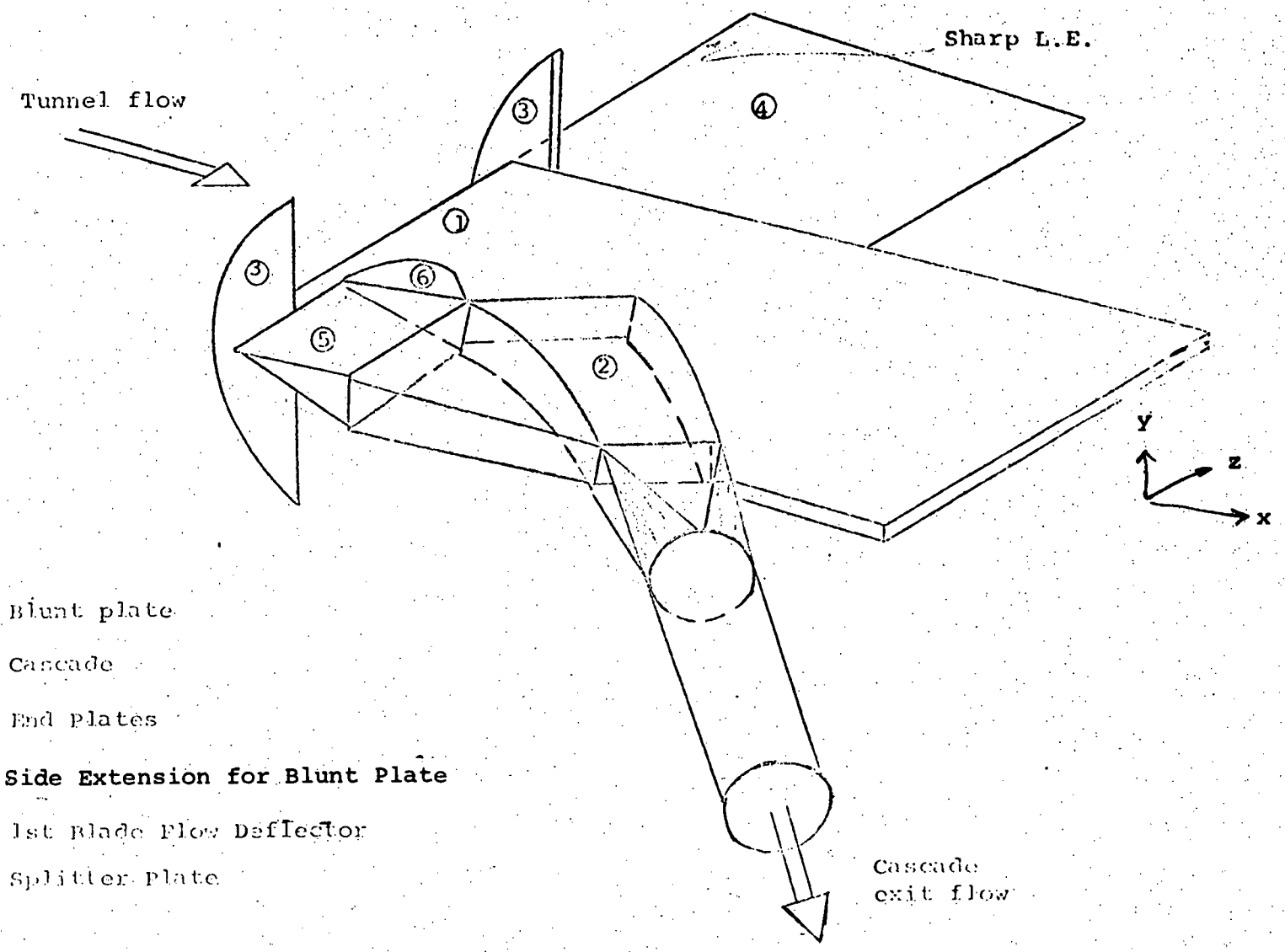

Figure 16. - Final Test Model Configuration

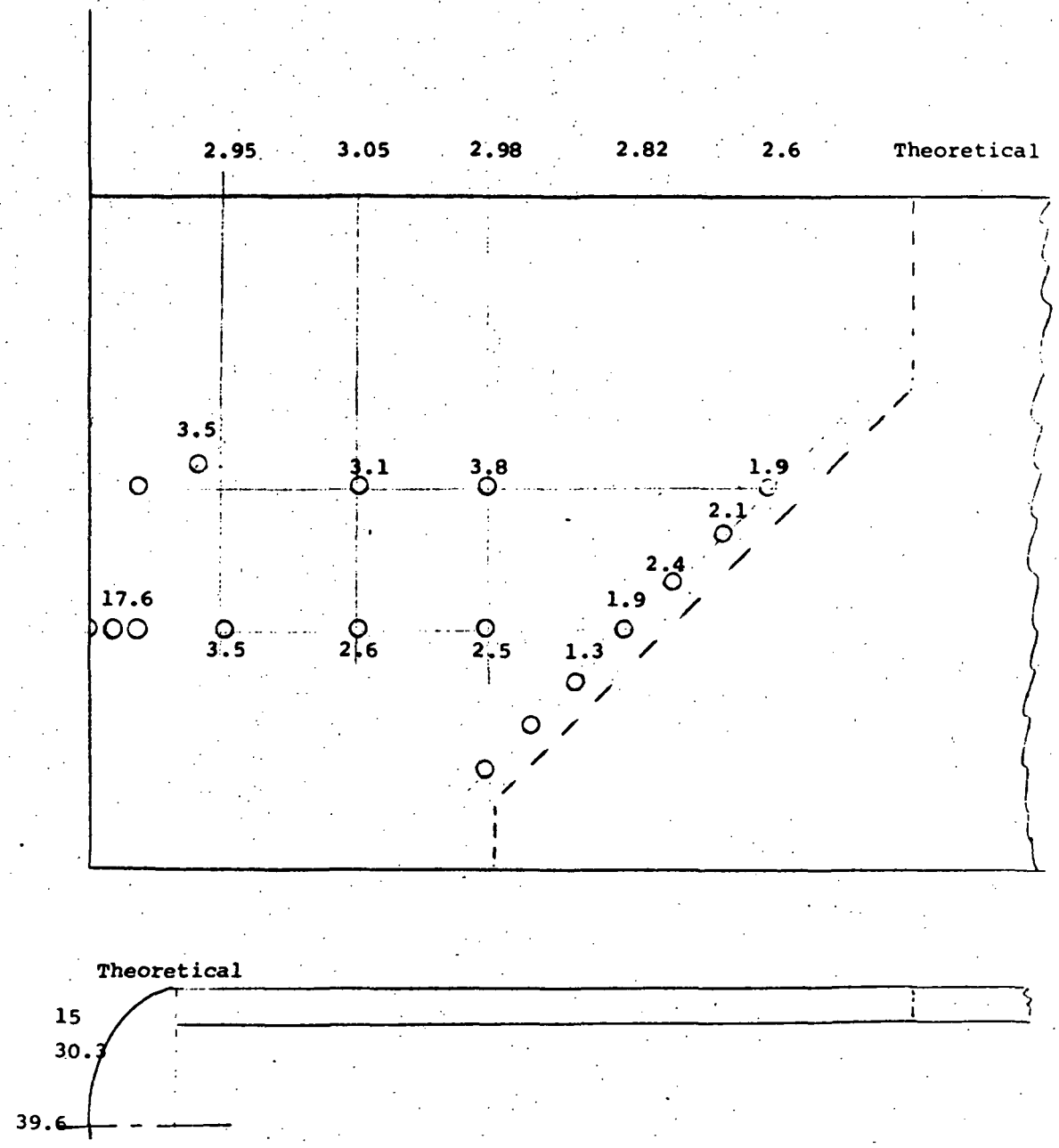

Figure 17. - Blunt Plate Pressure Distribution (P/P_∞): Full Body, with End Plates, Original Cascade Position

The hypothesis evolved from these results was that the blunt body was interacting with the adjacent tunnel boundary layer, causing an oblique shock to be generated upstream of the blunt body and preventing the establishment of the desired flow pattern. This hypothesis was based in part on the tunnel wall pressure distribution, and on the afterbody pressure distribution with the half-body configuration.

Accordingly, the blunt body model was moved one inch further away from the closest tunnel wall, with the cascade held fixed, resulting in the cascade centerline being positioned at $y/R = 2.6$. This resulted in generally higher pressures throughout the test section, but some improvement in the flow properties near the cascade. The blunt plate pressure distribution exhibited some three-dimensionality as shown in Figure 18. This failure of the end plate was attributed to an upstream flow different than the design values on which the end plate shapes were based.

No further configurations were attempted, since it appeared unlikely that the basic facility size limitations could be overcome.

C. Flow Field Traverse Results

Extensive traversing of the blunt body flow field was accomplished early in the test program, with the half-blunt body configuration and without the cascade installed. However, the exhaust system isolation value was in place at this time and the tunnel had subsonic flow at the test section exit. The results are believed to be similar to the full-body configuration without the blocing isolation valve.

The mapping was accomplished by traversing three wedge/pitot combinations through the flow field in the y-direction. The three probes were each located at different values of z and x, staggered along a 45° line similar to the cascade. This procedure was designed with a two-dimensional flow field in mind; in the present situation with a 10 in. span model, end effects (z variations) would be indistinguishable from x variations.

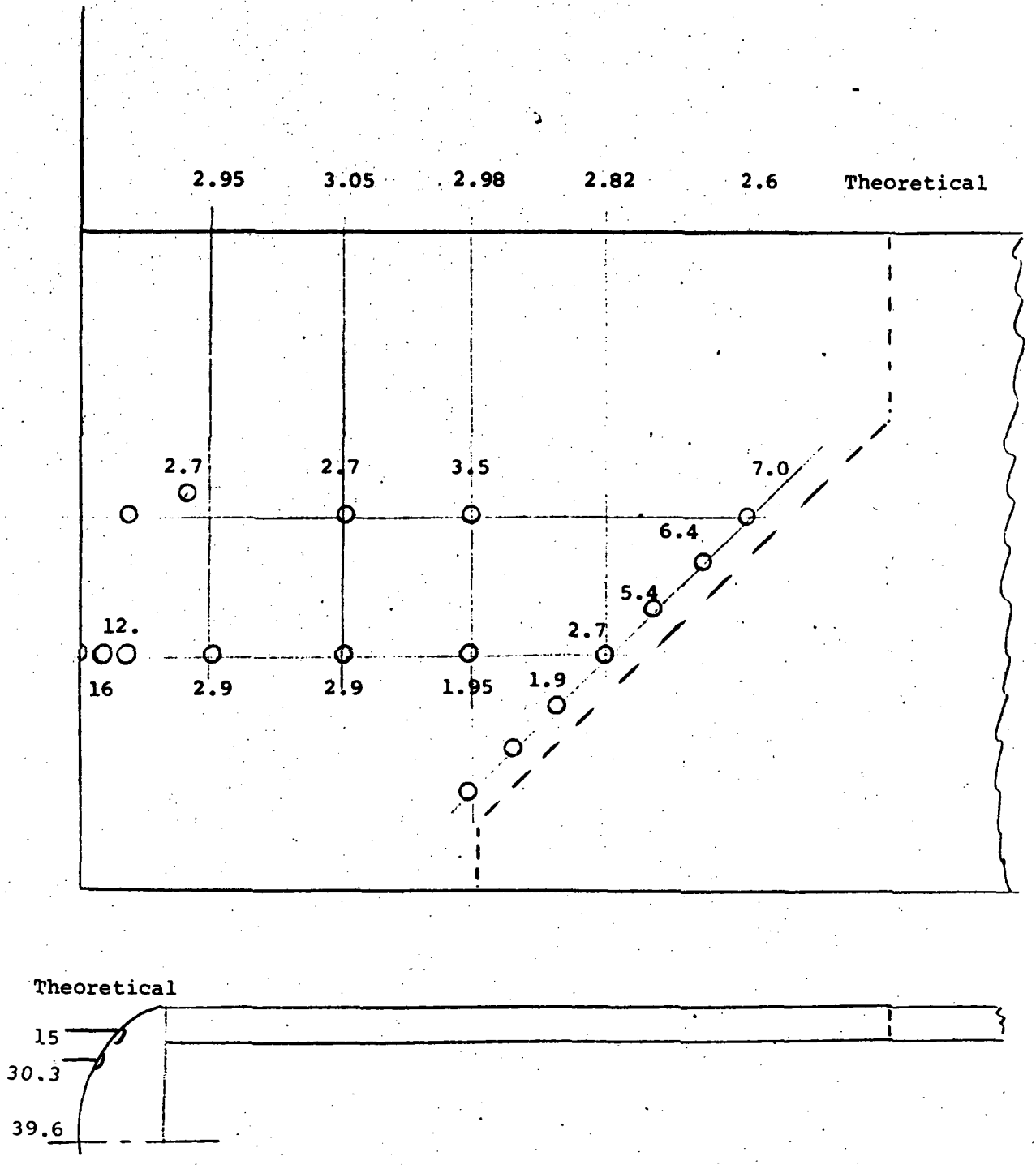

Figure 18. - Blunt Plate Pressure Distribution (P/P_∞): Full Body, with End Plates, Cascade 1 in., Closer to Blunt Plate

The results are presented in Figures 19 - 22, in terms of iso maps of each flow property, drawn from the detail distributions. It is clear that the generated flow field is quite irregular; shocks and expansions from the tunnel walls and afterbody are quite apparent as are end effects due to the accelerated flow around the corners of the blunt model.

Reducing the blunt body thickess created a flow field more representative of a slender body which indicated the ineffectiveness of the half-body underplate. Instead of a quasi-normal shock standing on the leading edge of the underplate, there was, more likely, an oblique shock system caused by flow separation on the plate.

However, portions of this flow field were deemed acceptable from the standpoint of determining inlet gradient effects on cascade performance, and so the test cascade was installed as previously described.

After installation of the blunt body end plates and achievement of what appeared to be an acceptable flow field, cascade inlet flow surveying was continued, using a fixed 5-hole conical probe mounted near the cascade. The probe was maintained at constant y and z coordinates (z corresponding to the center of the middle cascade passage), and moved in the x direction. Two sets of data were obtained; one with the cascade in the original position, and one with the cascade moved 1 in. closer to the blunt body. The results are shown in Figures 23 and 24, corrected for the axial gradient along the probe between static and stagnation orifices.

The data with the cascade in the original position (probe at $y/R = 4.2$) displayed a wide variance from the predicted flow field; the data for the cascade 1 in. closer (probe at $y/R = 3.7$) was nearly acceptable. However, the cascade inlet flow data at $y/R = 2.6$, as estimated from suction-surface mid-span taps,* did not corroborate the proper theoretical gradient with respect to y. Thus the near agreement ay $y/R=3.7$ may be fortuitous.

---

* The data of Ref. 1 were used as a guide to account for inlet angle of attack effects.

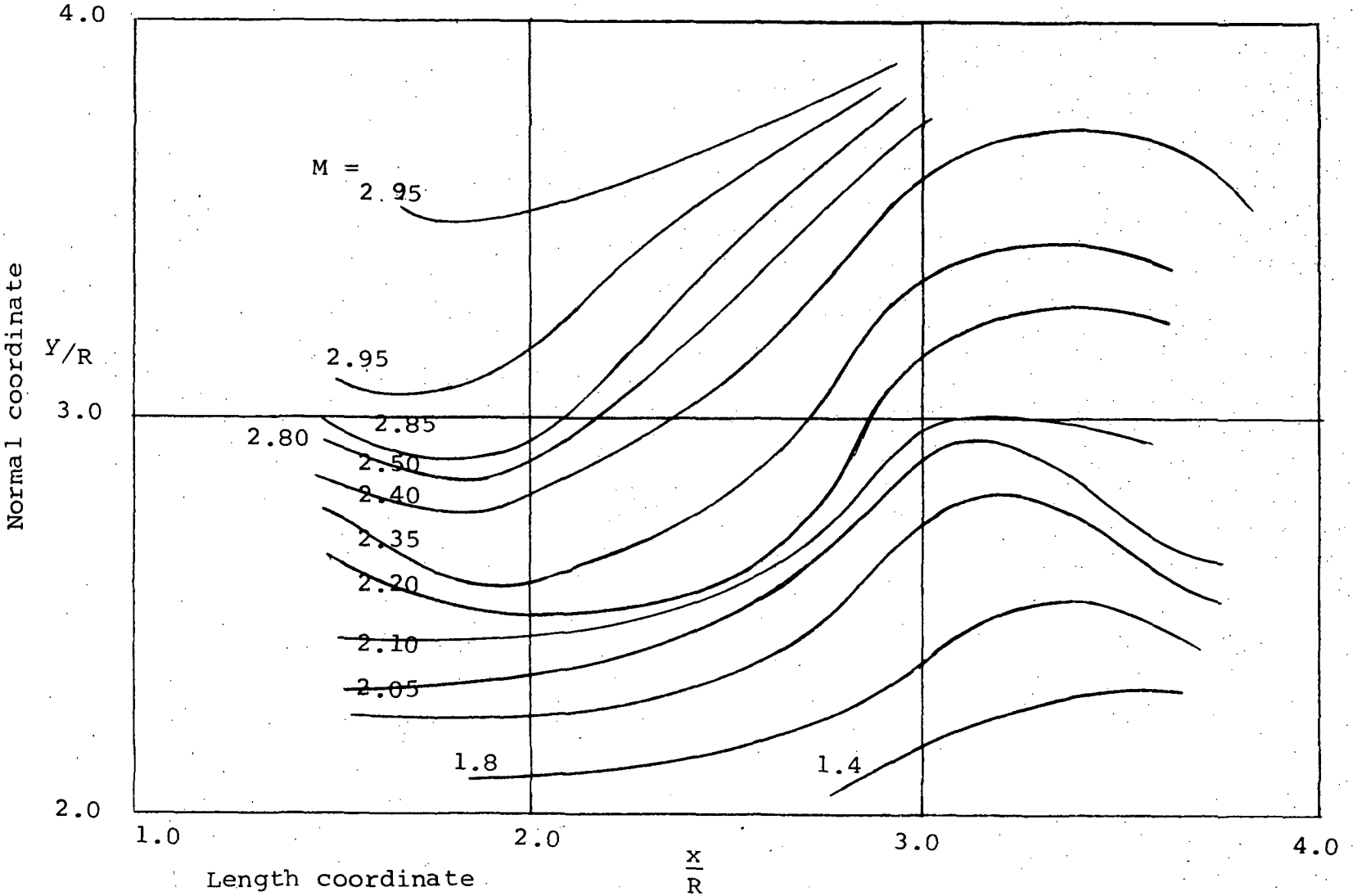

Figure 19. - Map of Mach Number at Cascade Inlet

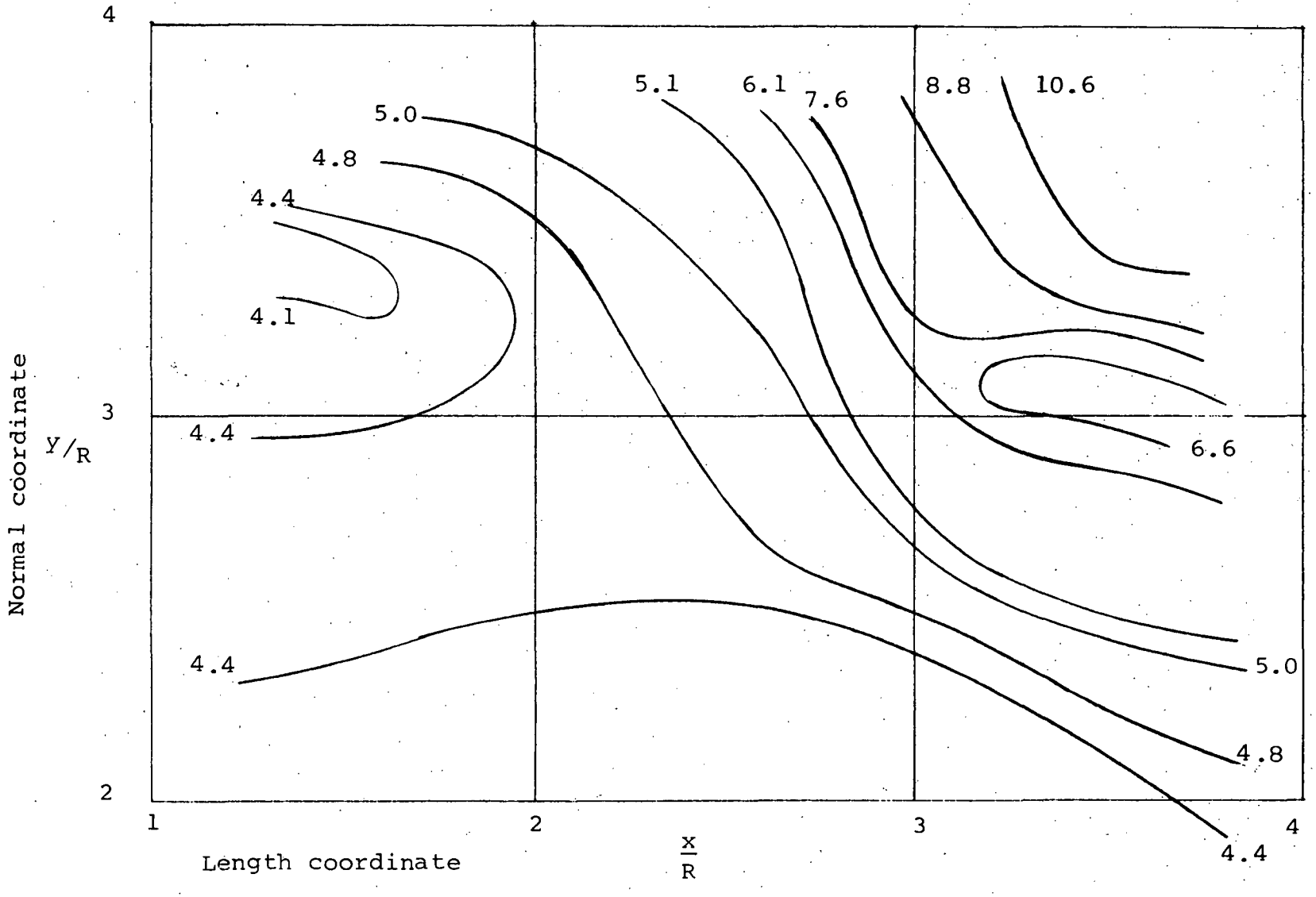

Figure 20. - Map of Static Pressure, $(P/P_o \times 10^3)$ at Cascade Inlet

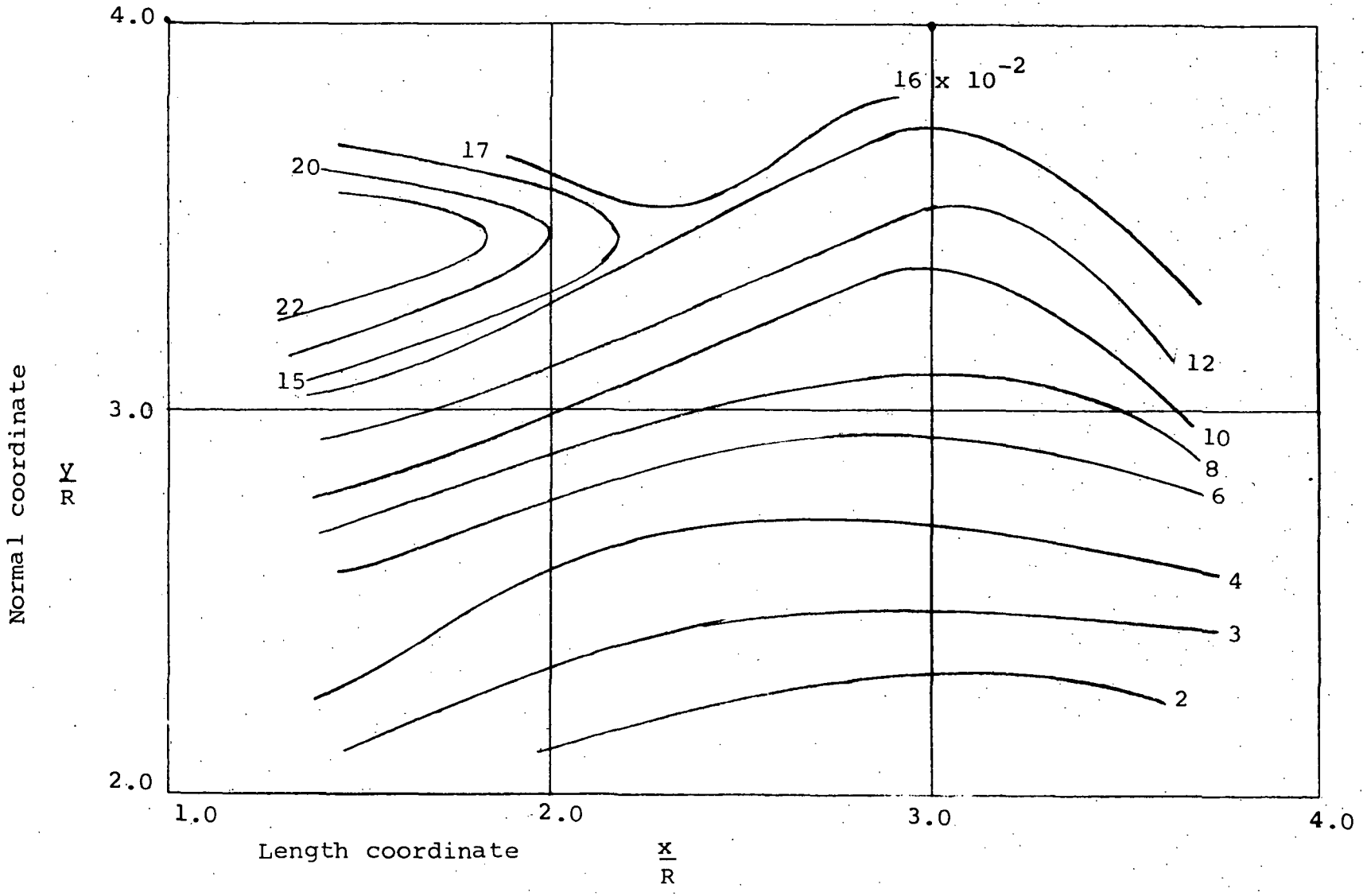

Figure 21. - Stagnation Pressure ($P_t/P_o \times 10^2$) at Cascade Inlet

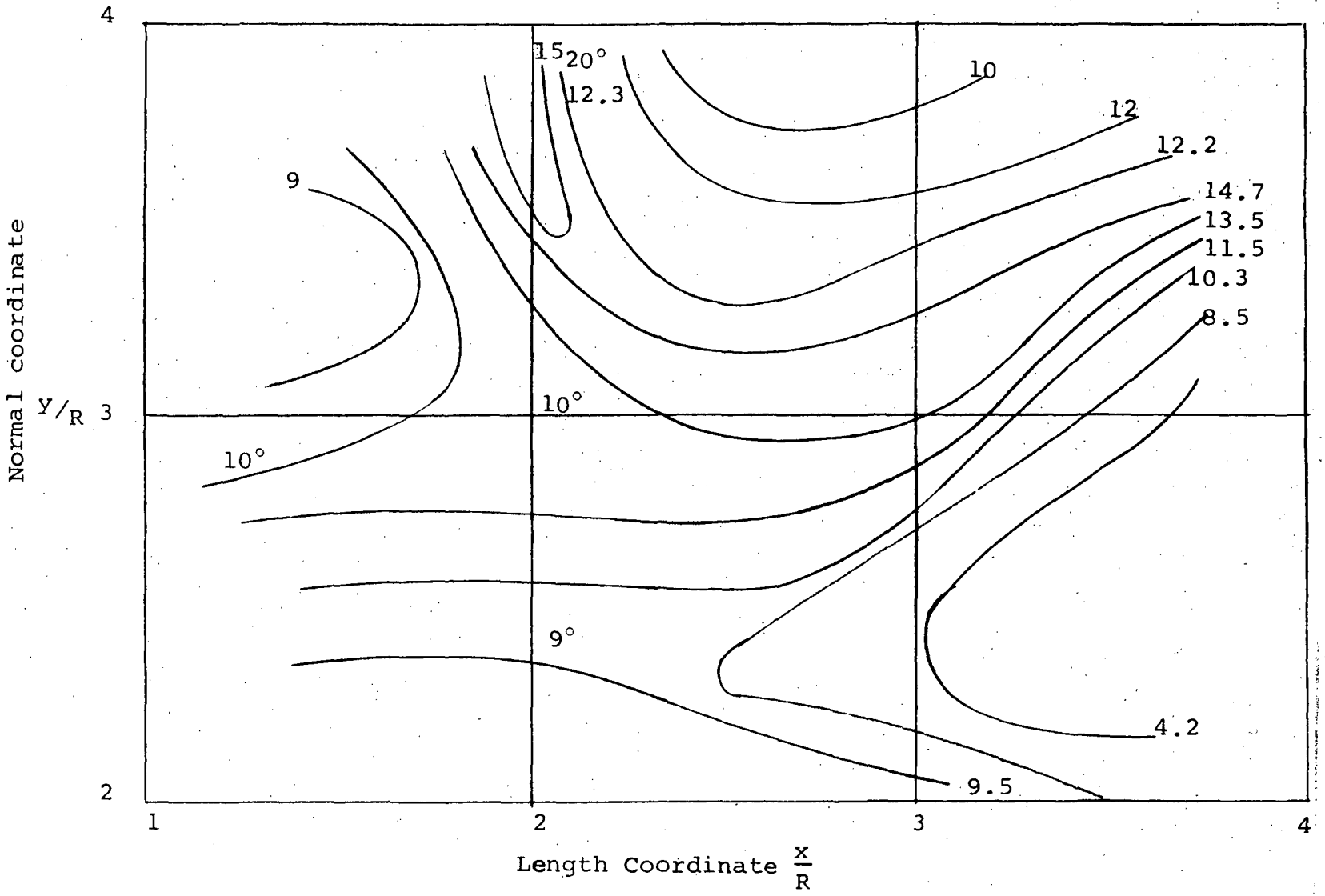

Figure 22. - Map of Flow Angle at Cascade Inlet

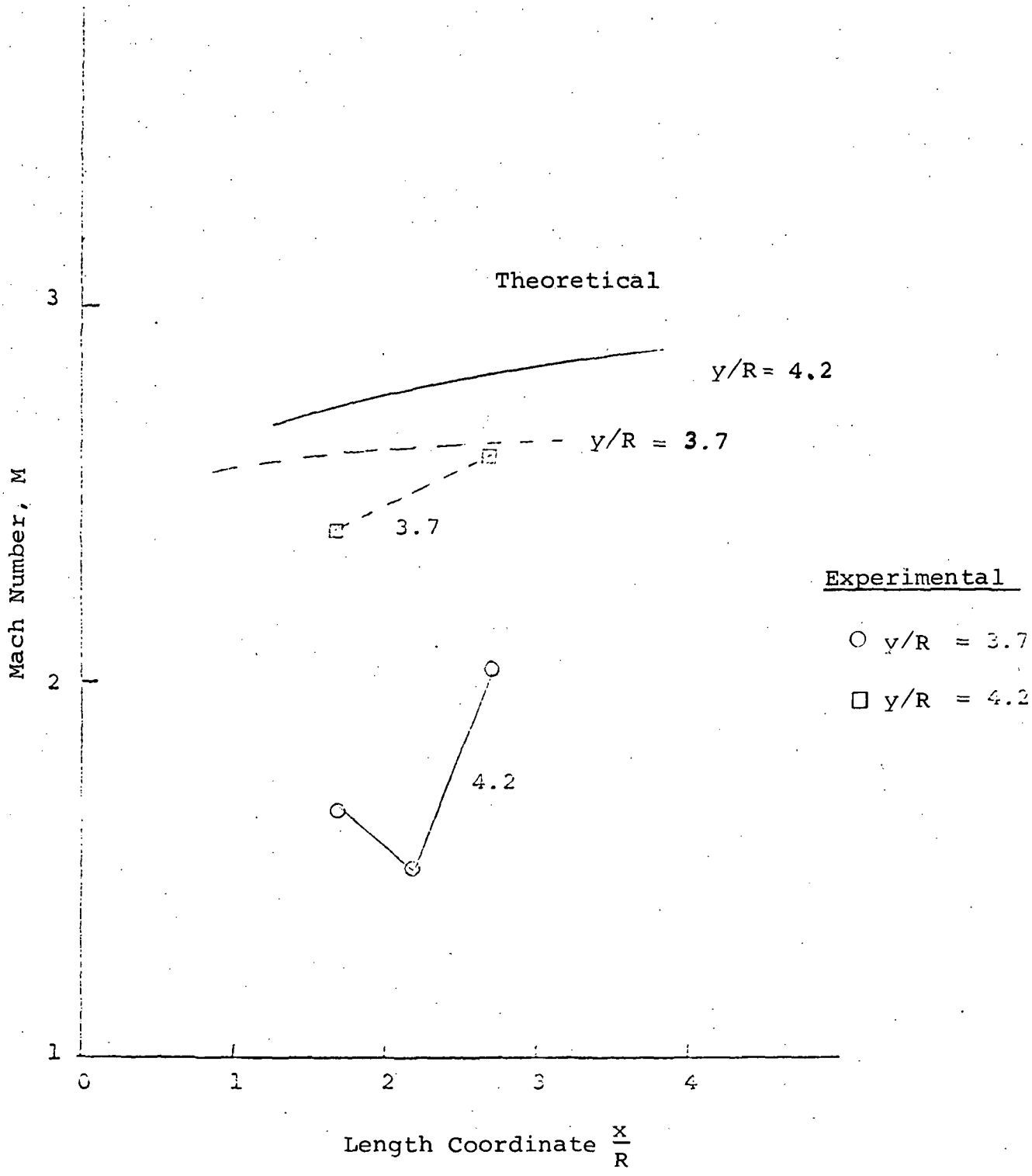

Figure 23. - Mach Number Distribution in Blunt Body Flow Field.

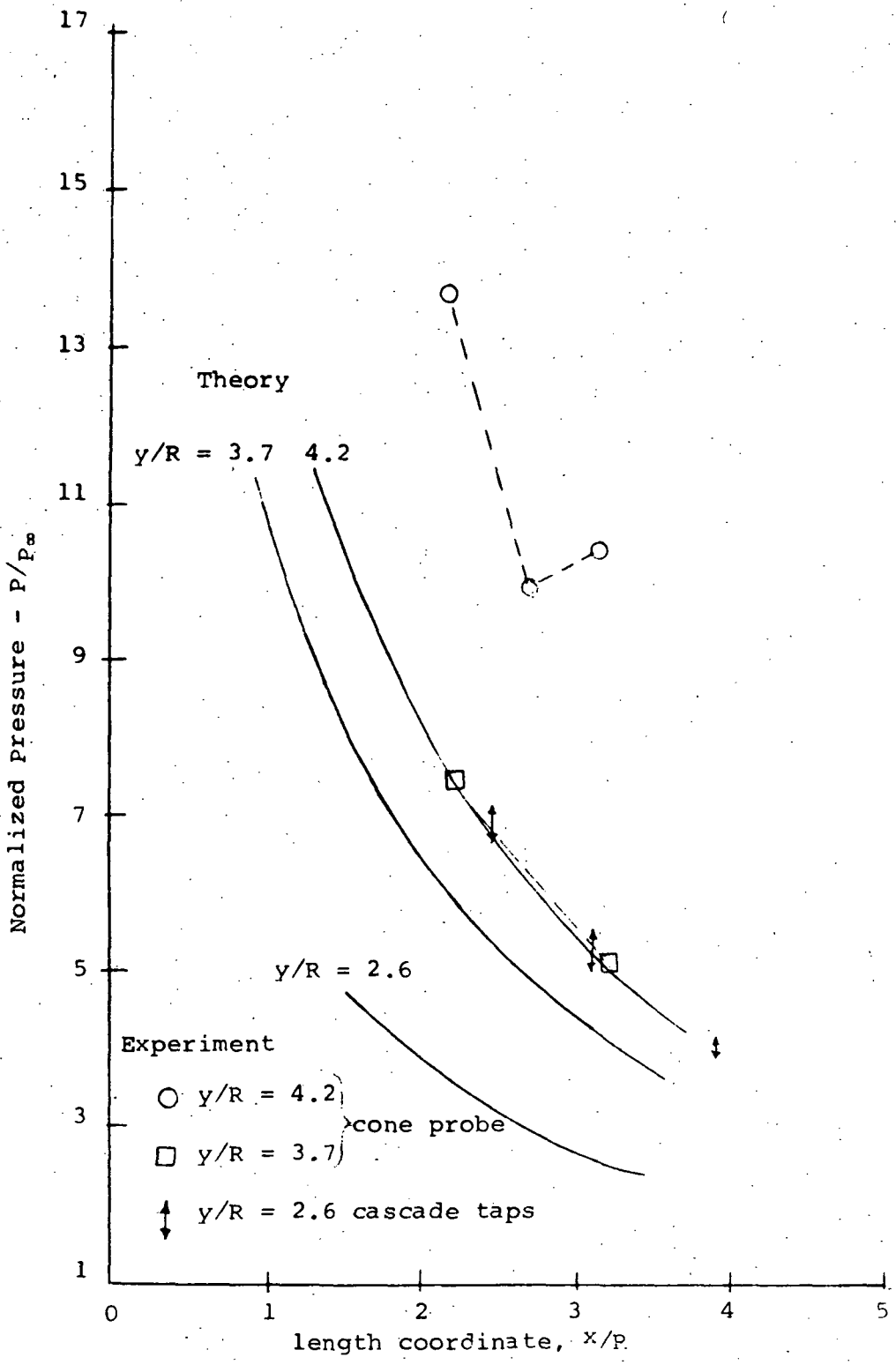

Figure 24. - Pressure Distribution in Blunt Body Flow Field

D. Cascade Test Results

1. Uniform flow results from Reference 1. - For reference purposes, some of the uniform flow results of Reference 1 are reported here (Figures 25-29) in order to contrast the effects of the nonuniform cascade entry flow of the present study.

The theoretical flow field is shown in Figure 25, accounting for the minor modifications that were made in that work to improve the flow. The blade surface pressure distribution (mid-span) before and after the modifications are shown in Figures 26 and 27, respectively. Note that the pressure surface has a relatively constant pressure region near mid-chord, but the suction surface expands to a very low pressure minimum followed by recompression to a nearly common exit pressure value for both sides. The experimental data also show some evidence of separation on the suction surface.

The exit flow field displays some of the classic finite-span cascade characteristics (Figure 28), in that the peak pitot pressure occurs at center span, but there is some evidence of secondary flow accumulation near the suction surface. A considerable asymmetry is also seen in comparing right and left side data, which may have been due to probe alignment.

It is also instructive to note from the uniform flow results that for small incidence angles, there is a zone of nearly 100% total pressure recovery at the exit near the pressure surface. This trend was used in reconstructing the (nonuniform) cascade inlet flow field.

2. Half blunt-body cascade results. The results with the half-thickness blunt body flow generator are shown in Figures 30-32. Two trends are apparent: First, the entrance conditions are fairly uniform from blade to blade. Secondly, the suction surfaces are seen to be completely separated, as indicated by the exit traverse results and the complete absence of an expansion-compression trend in the suction surface pressure distribution. Part of the explanation for this result lies in the ratio of cascade exhaust pressure to inlet pressure, which is quite high ($\sim$ 5:1) because of the low inlet pressure. There is also some indication (ratio of pressure to suction surface pressure at inlet) of a high cascade inlet Mach number which, of course,

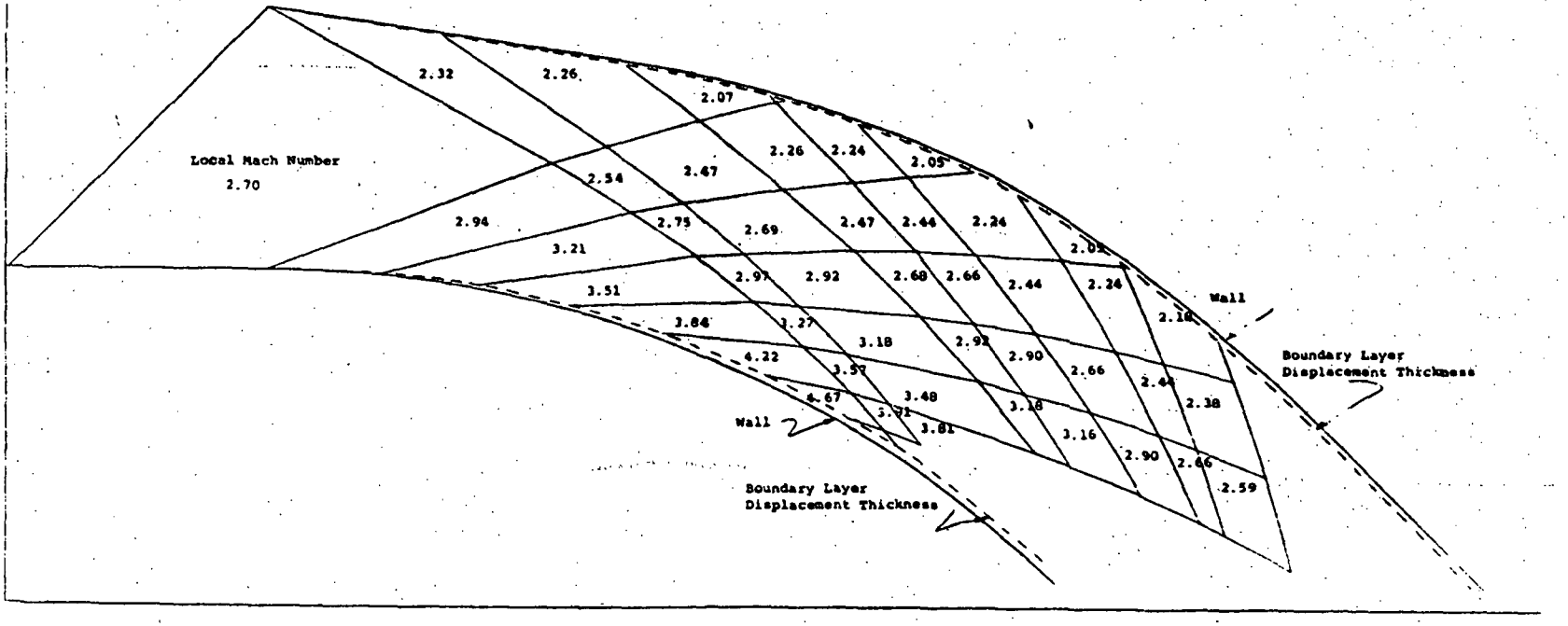

Figure 25. - Revised Cascade Blade Flow Field Network

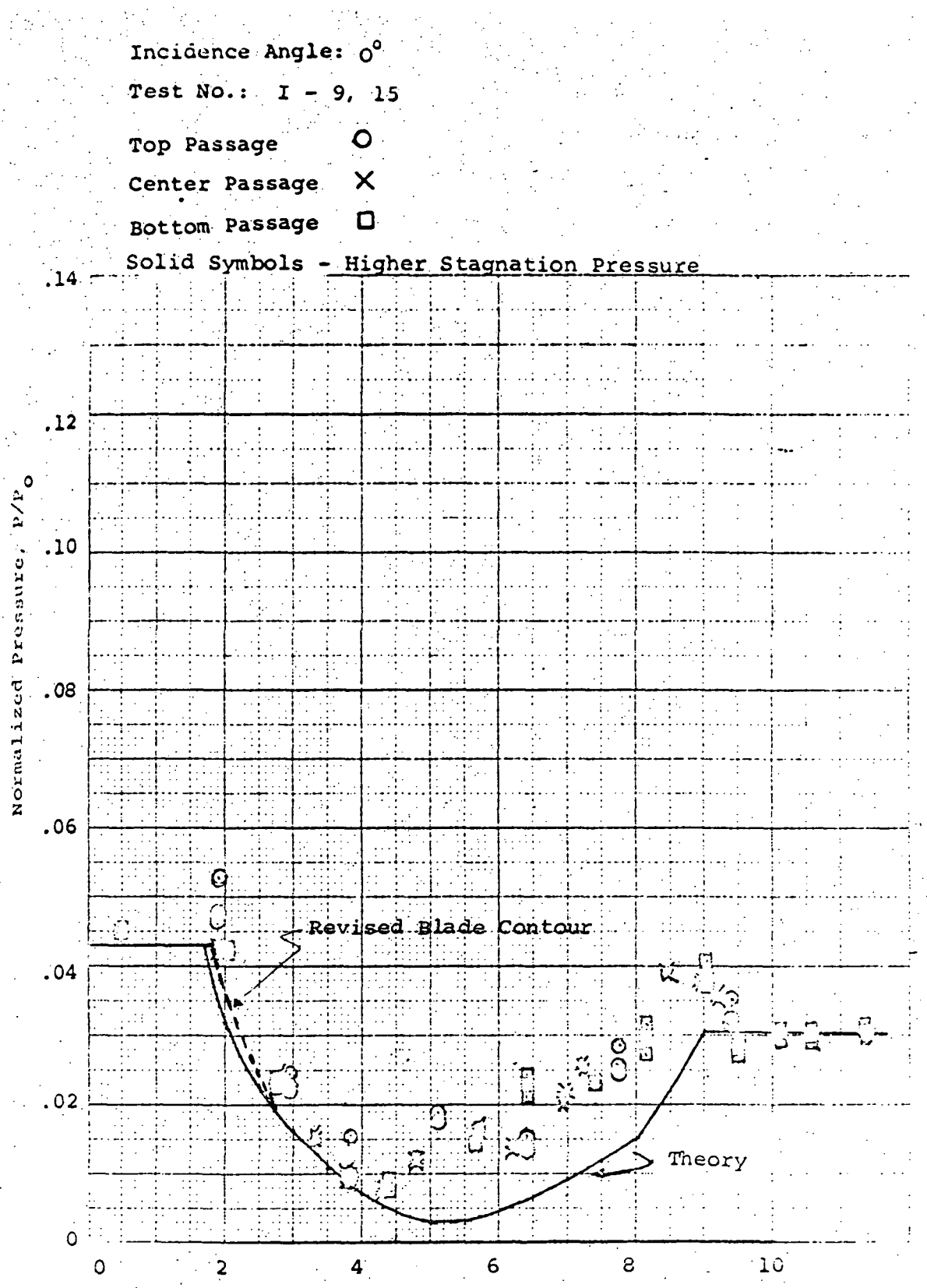

Figure 26. - Suction Surface Pressure Distribution (Reference 1), $\alpha = 0^{\circ}$

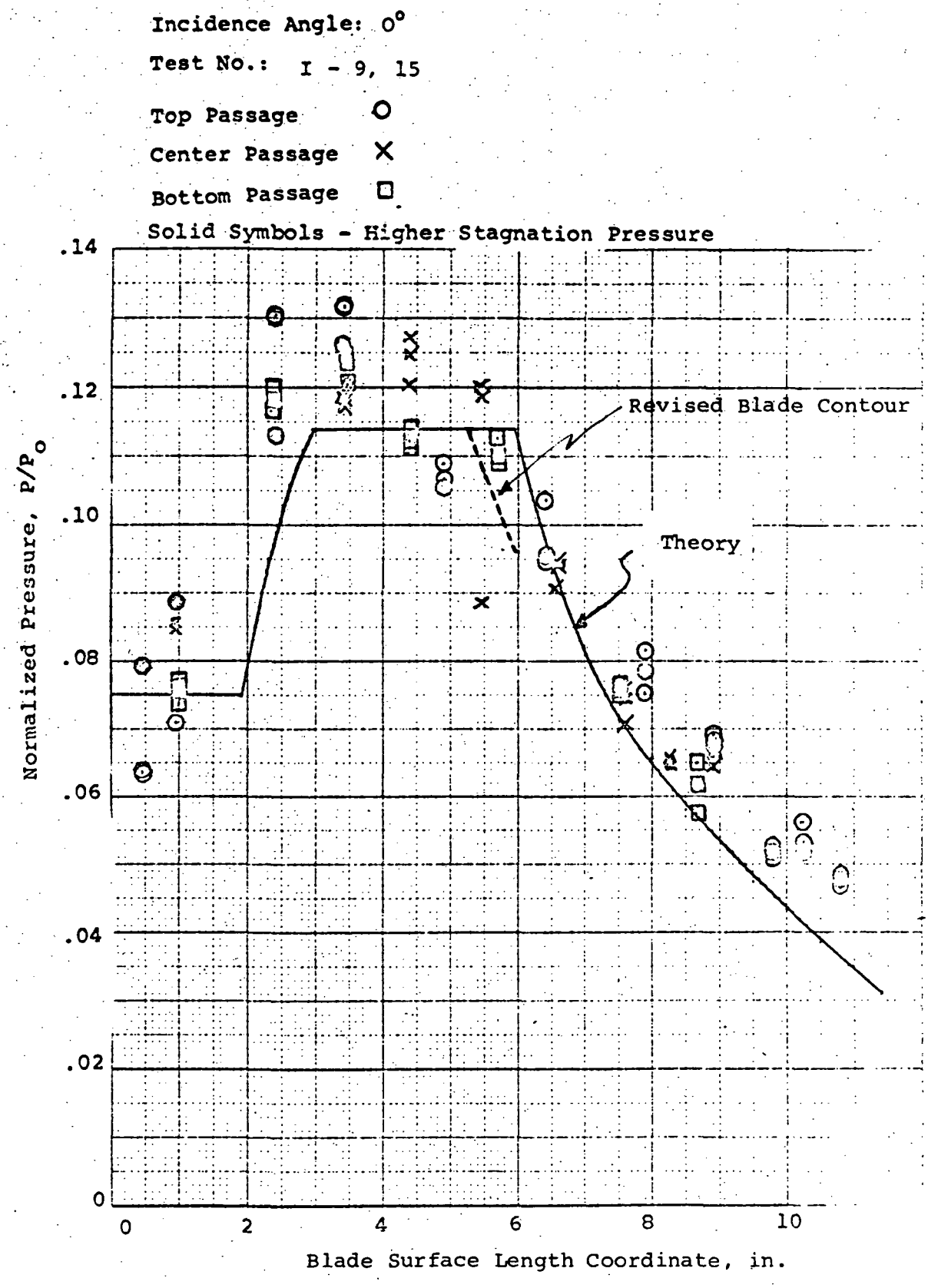

Figure 27. - Pressure Surface Pressure Distribution (Reference 1), $\alpha = 0^{\circ}$

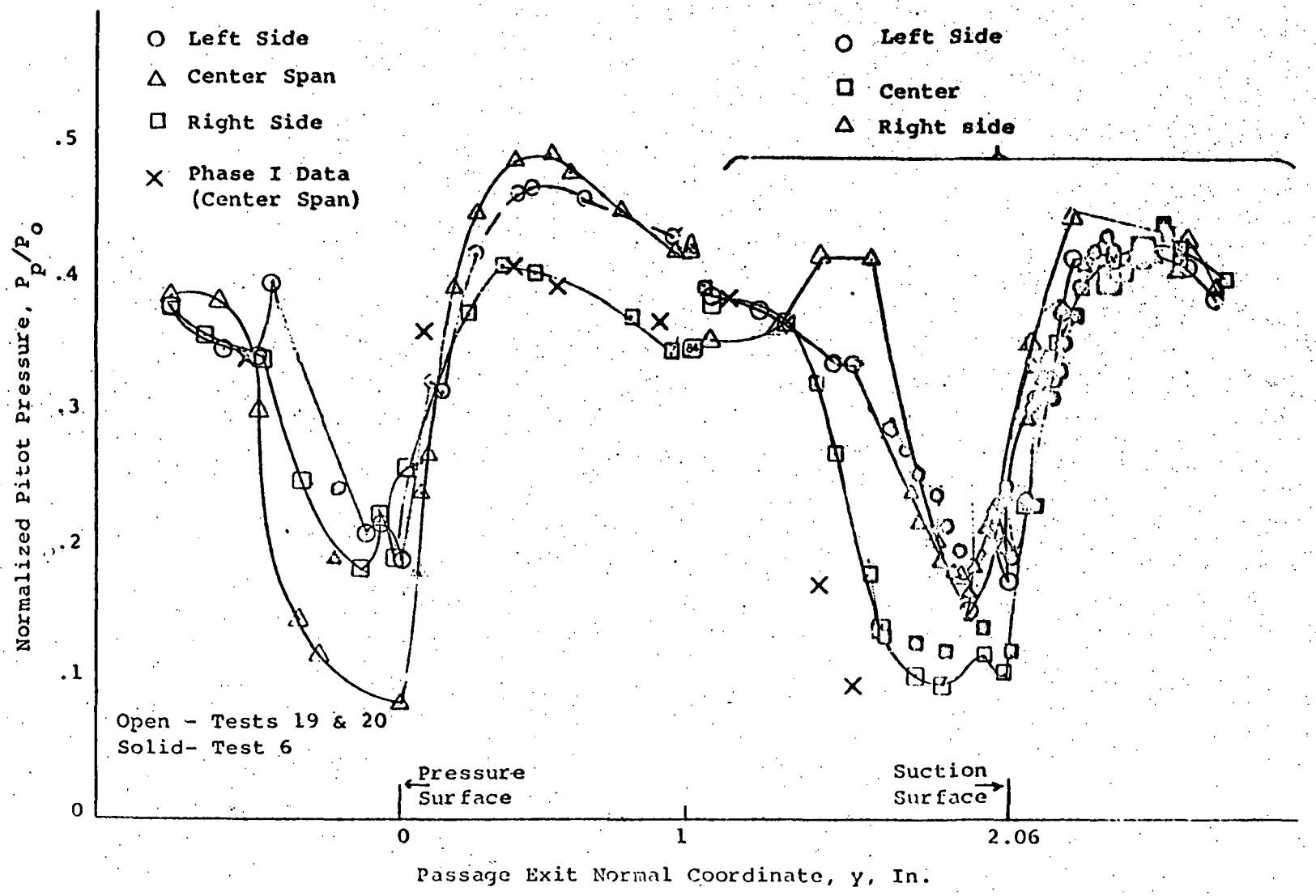

Figure 28. - Pitot Pressure Traverse Data,
$\alpha = 0^\circ$ (Reference 1)

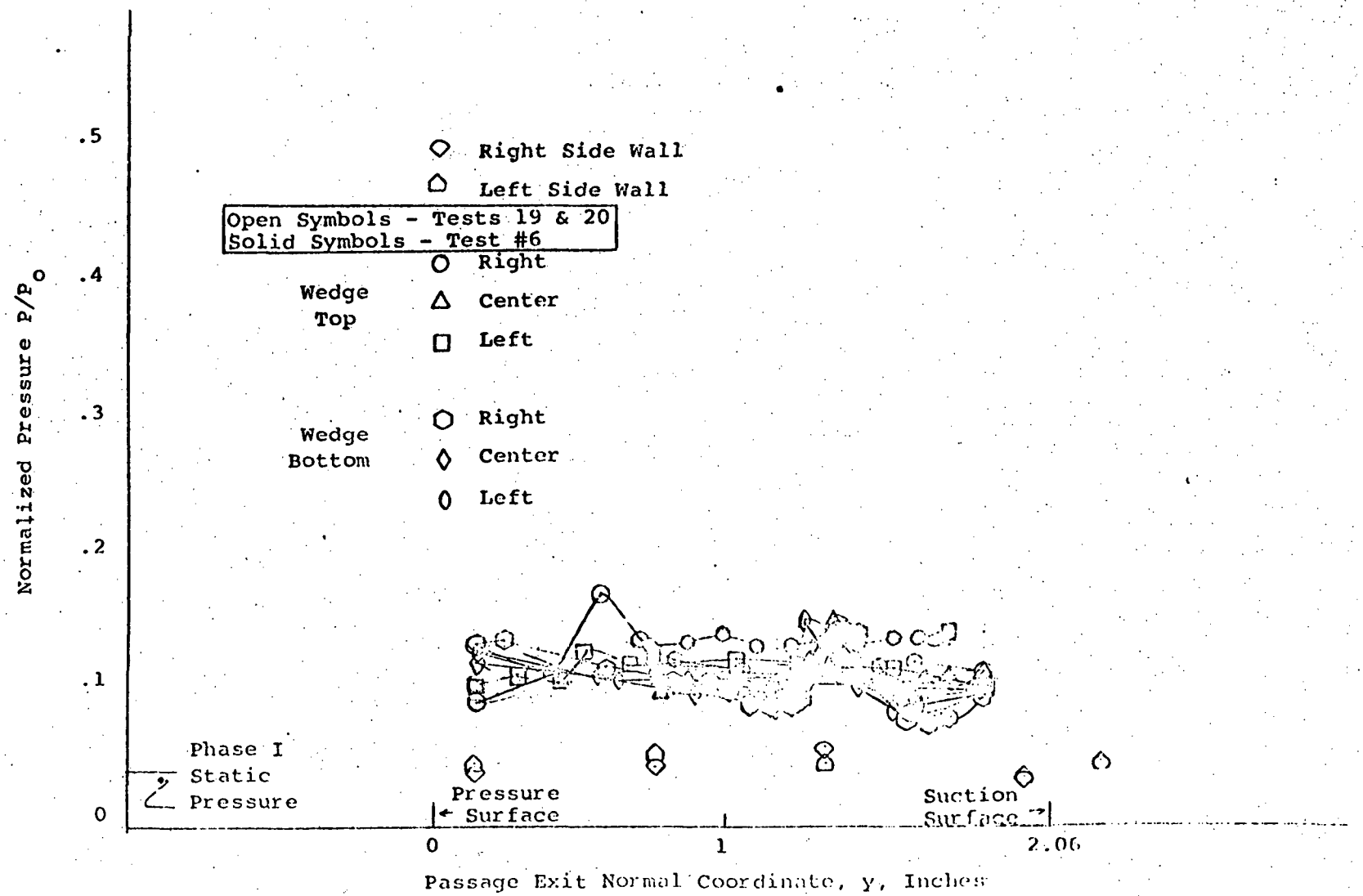

Figure 29. - Wedge Pressure Traverse, $\alpha = 0^{\circ}$ (Reference 1)

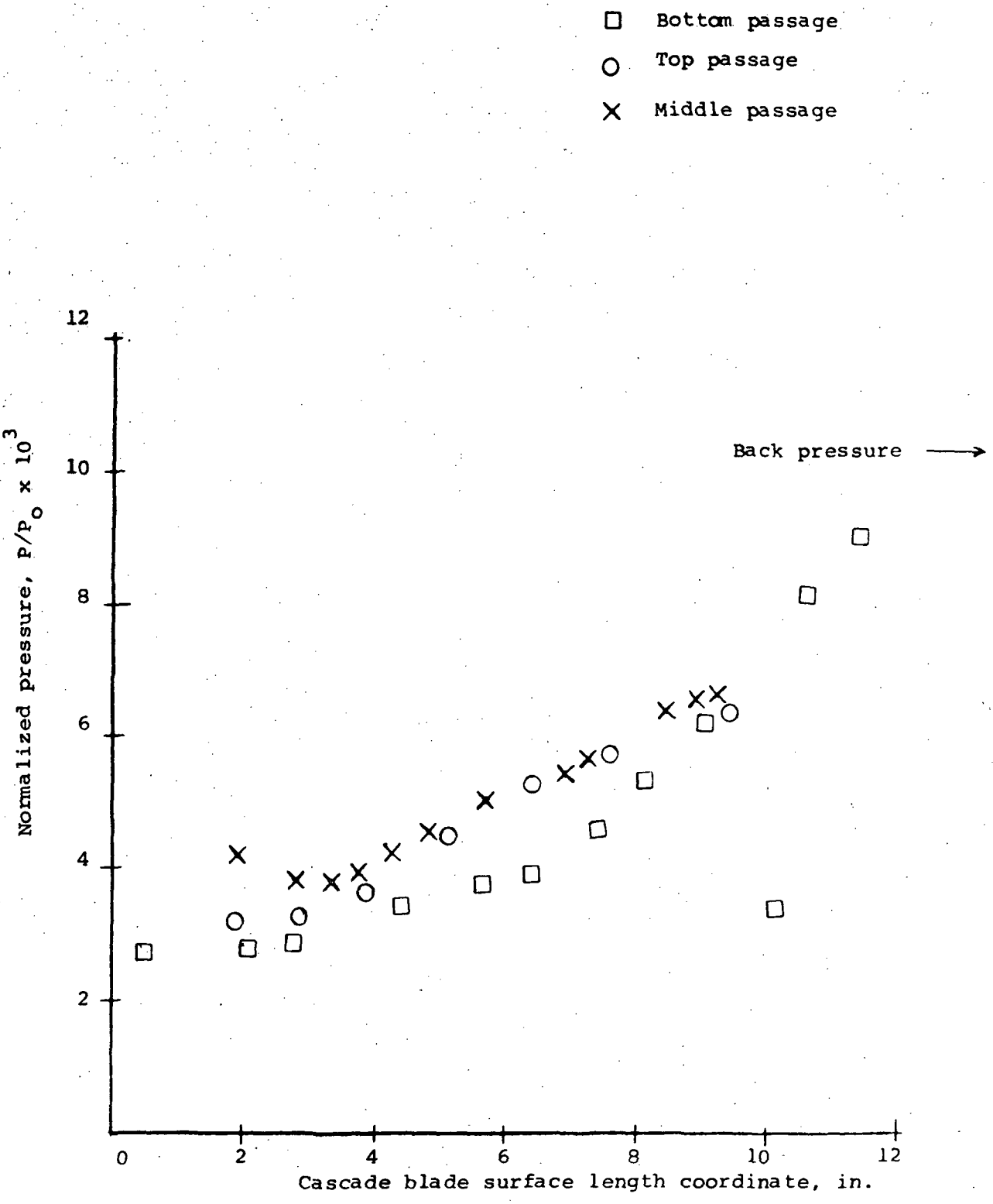

Figure 30a. - Cascade Suction Surface Pressure Distribution (Mid-Span): Half Body, No End Plates

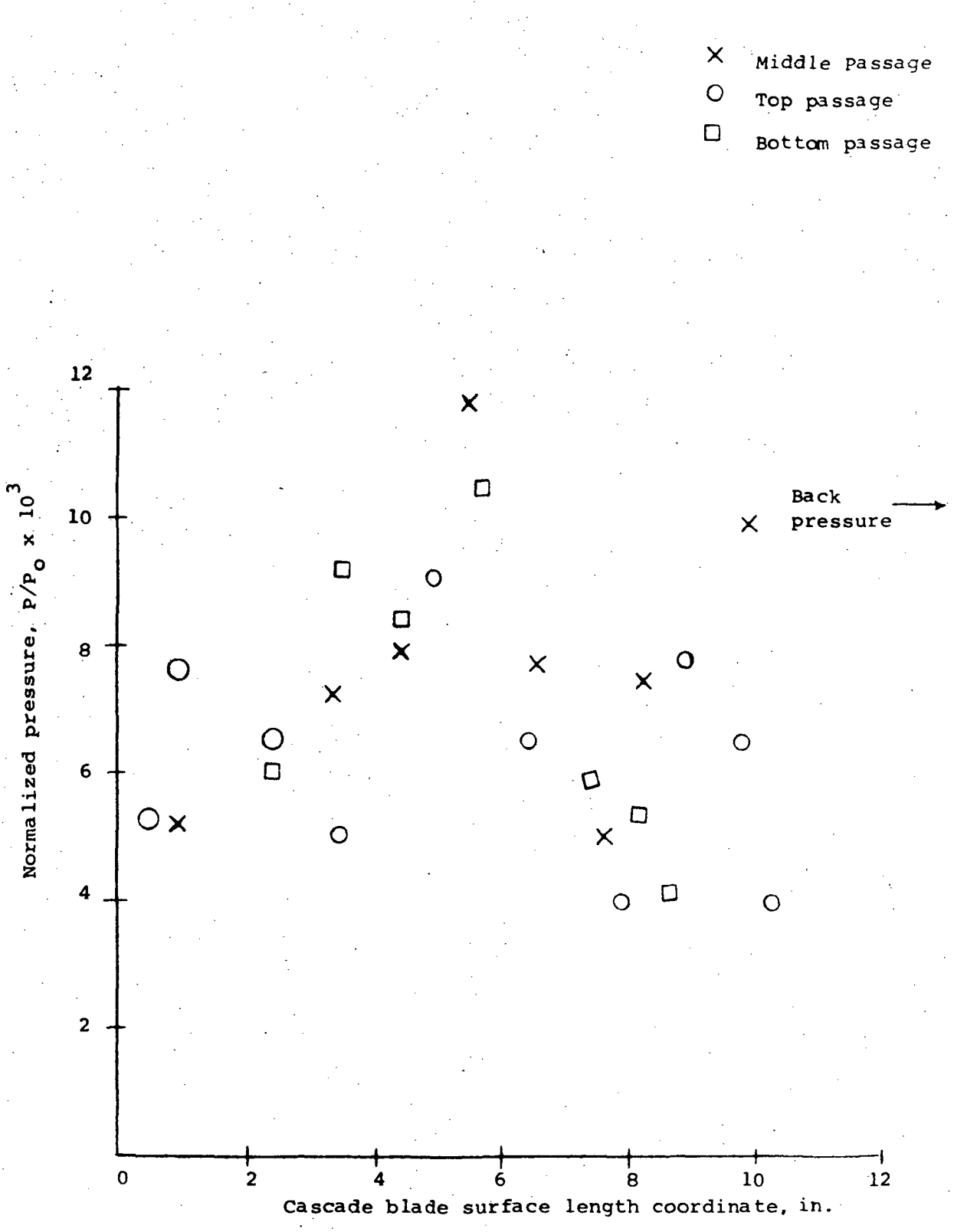

Figure 30b. - Cascade Pressure Surface Pressure Distribution (Mid-Span): Half Body, No End Plates

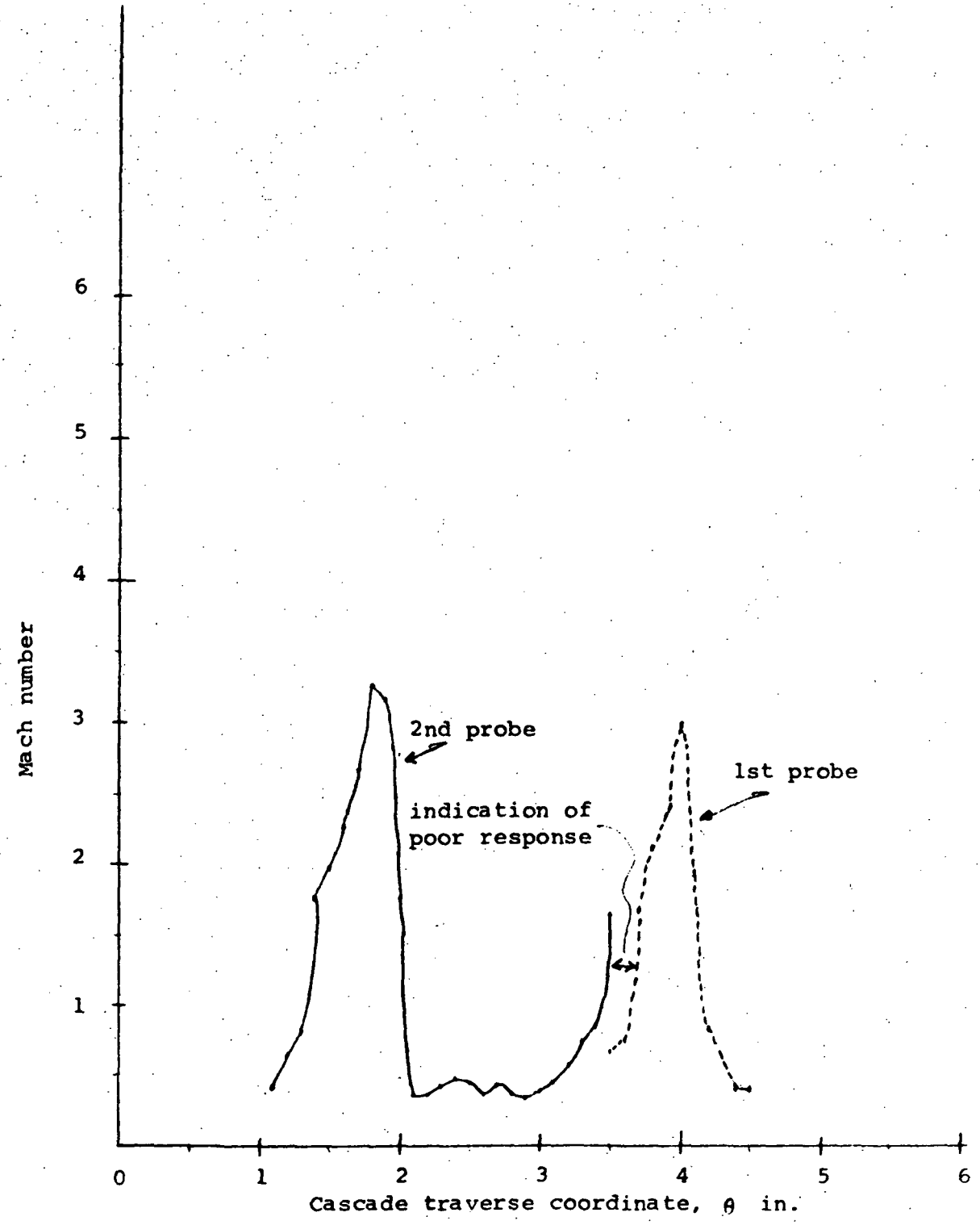

Figure 31. - Cascade Exit Mach Number Distribution, (Mid-Span); Half Body, No End Plates

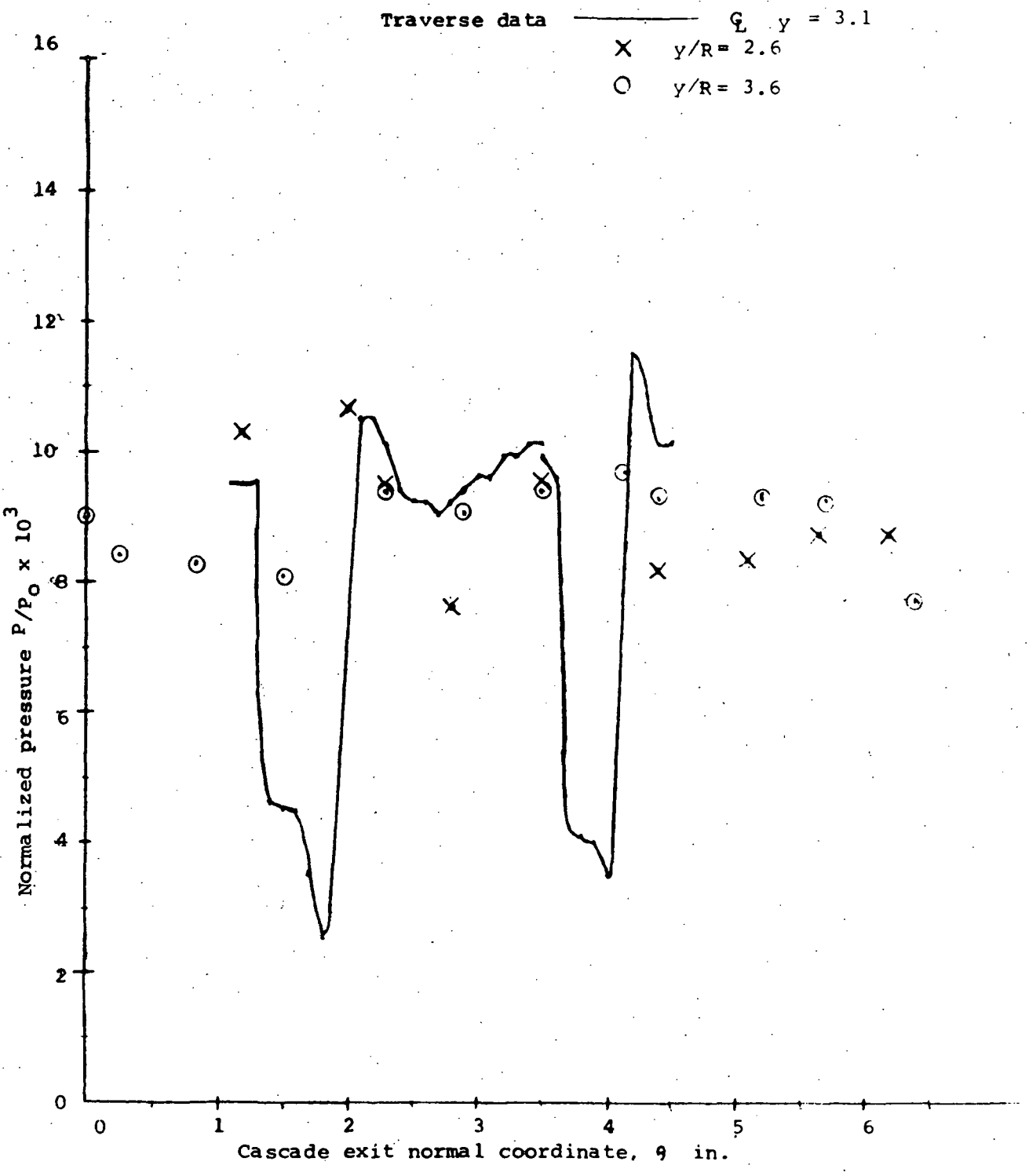

Figure 32. - Cascade Exit Pressure Distribution, Half Body, No End Plates

would worsen the situation because of the tendency for the first compression wave impingement point to move back along the suction surface. This extensive suction surface separation is thus not likely to be a result of the nonuniform inlet flow per se, and moreover, obscures any span-wise differences at the exit by promoting dissipative mixing within the blade passage.

3. Full-thickness blunt body cascade results. -

a) Data without end plates. - The initial results with the full thickness blunt body are shown in Figures 33 to 35. The blade surface pressure distributions, Figure 33, display considerable blade-blade nonuniformity, indicating a pressure gradient increasing in the axial direction, as also indicated previously on the blunt plate surface.

The cascade exit travers, however, indicated very little spanwise nonuniformity, but some passage-passage nonuniformity. The classic secondary flow phenomena were also apparent. Calculation of the total pressure entering the cascade (based on local 100% recovery) indicated values far below those expected from the theoretical blunt body calculation.

These measurements were thus taken to indicate strong wind tunnel effects influencing the cascade inlet flow and dominating any spanwise nonuniformity effects.

Data with end plates. - Installation of the blunt body end plates and extensions improved the uniformity somewhat, in that the first two blade passages exhibited nearly uniform entrance conditions (Figure 36); only the pressure side of the top passage appeared substantially different. However, there was some evidence of slight angle of attack with respect to the blade's suction surface entry, apparently also due to the side effects. Thus the blunt body end plates did not appear to be of sufficient extent.

The exit traverse data (Figures 37-38) for this configuration showed a small zone near the pressure surface of high Mach number and recovery, and a larger zone extending to the suction surface of lower performance. The isentropic stagnation pressure associated with the high zone was computed for the three total pressure measuring stations at the cascade exit, and compared

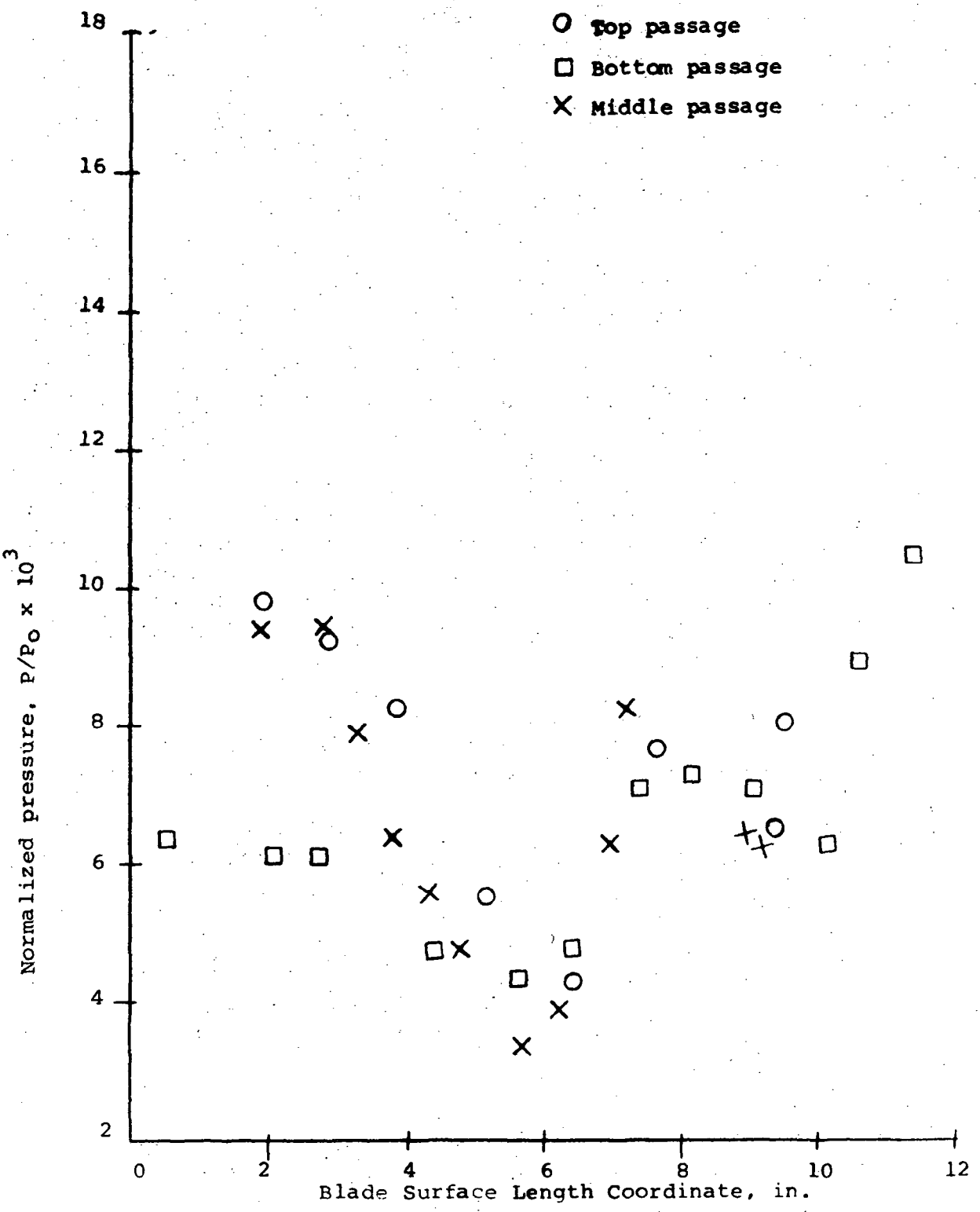

Figure 33a. - Cascade Suction Surface Pressure Distribution, Full Body, No End Plates, Original Position

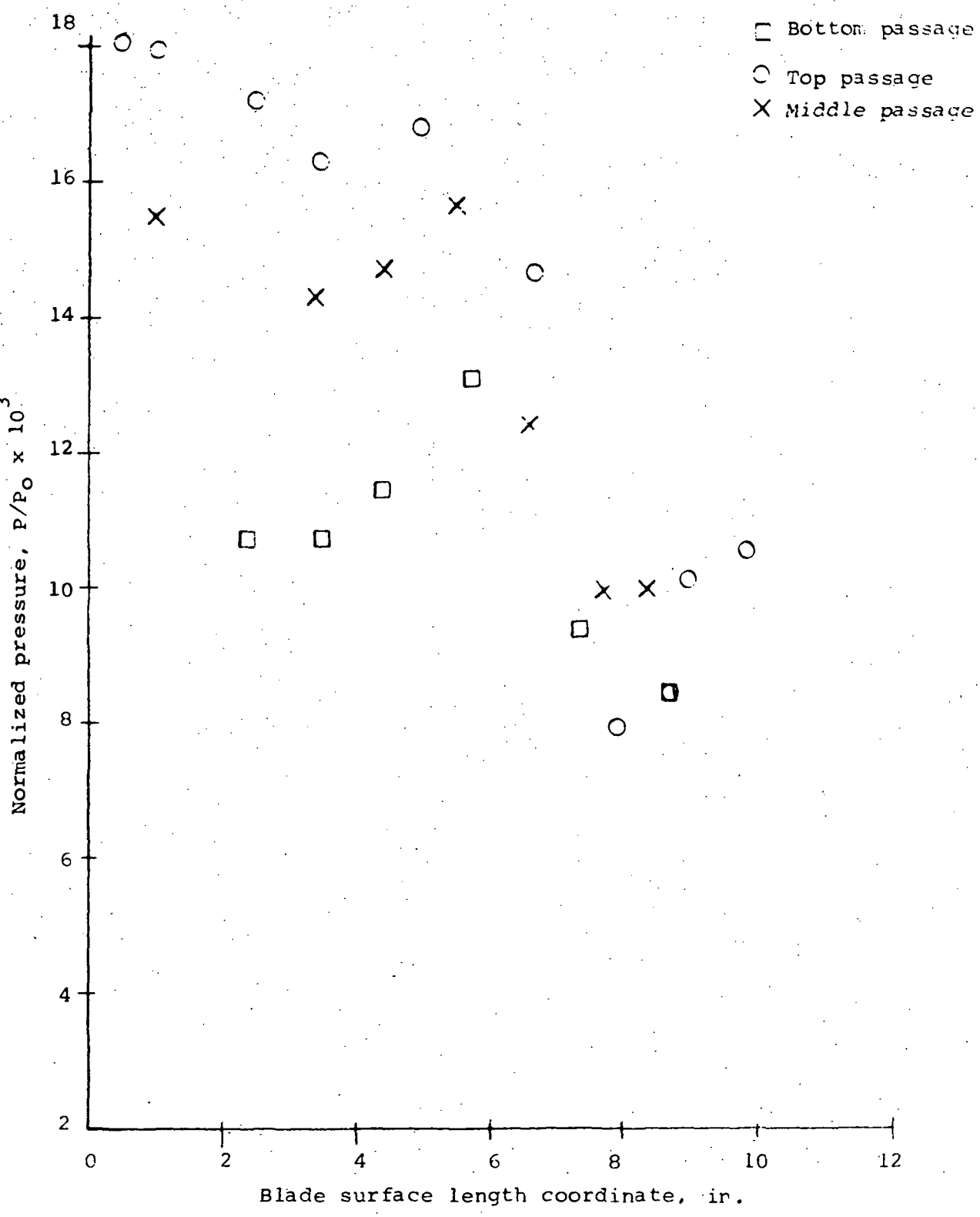

Figure 33b. - Cascade Pressure Surface Pressure Distribution Full Body, No End Plates, Original Position

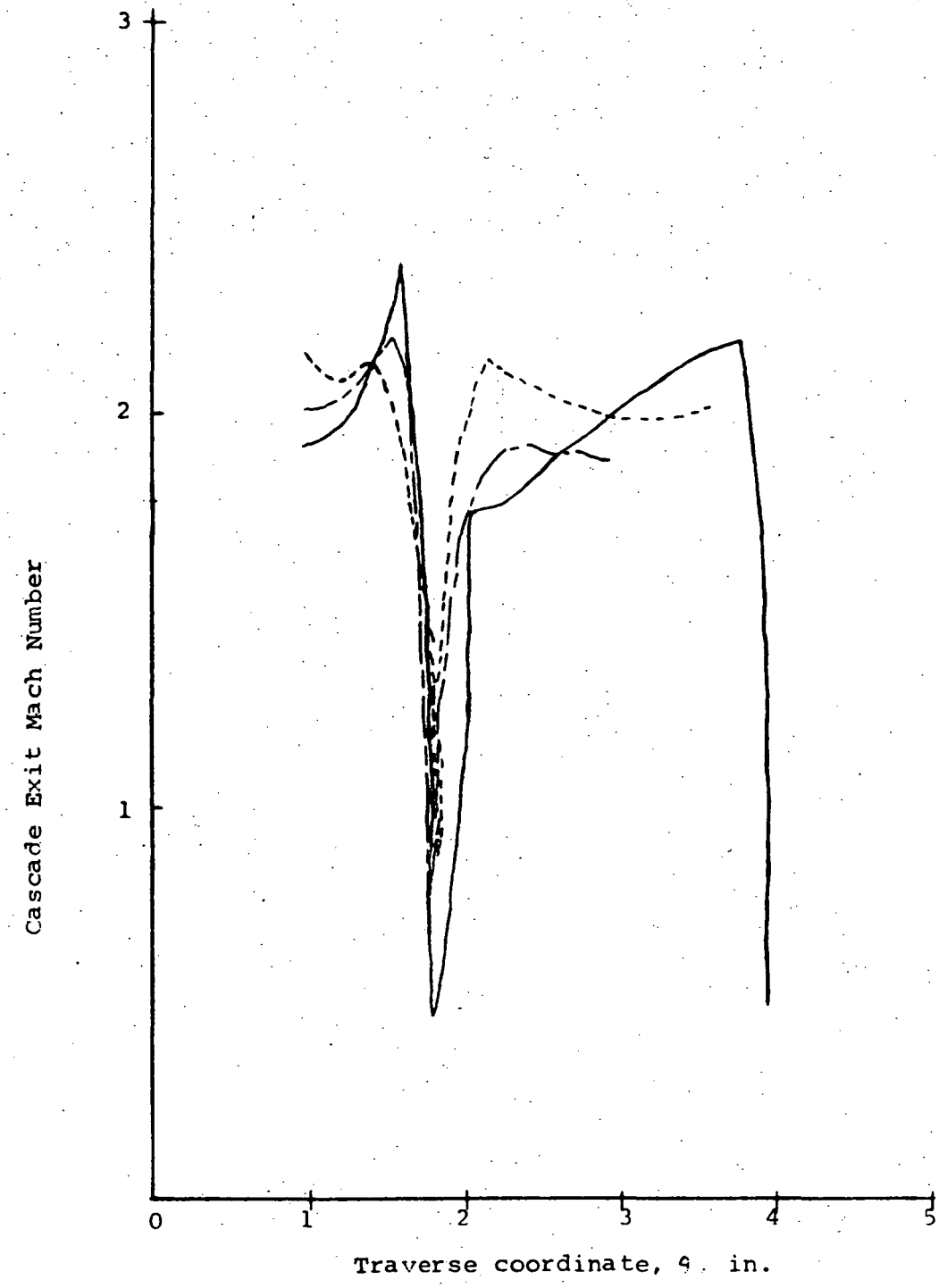

Figure 34. - Cascade Exit Mach Number Distribution, Full Thickness Blunt Body, No End Plates, Cascade in Original Position

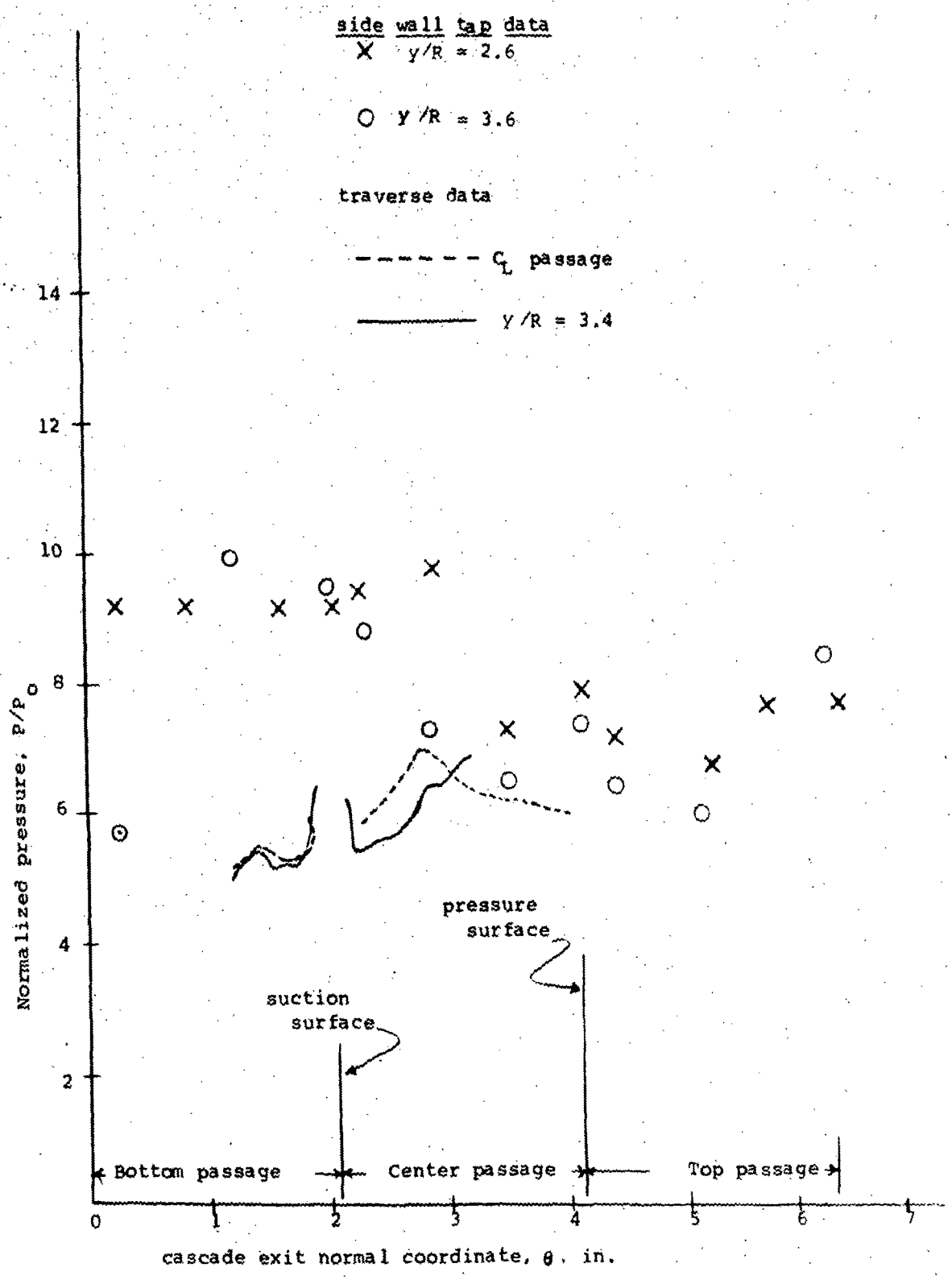

Figure 35. - Cascade Exit Pressure Data, Full Body, No End Plates Cascade in Original Position

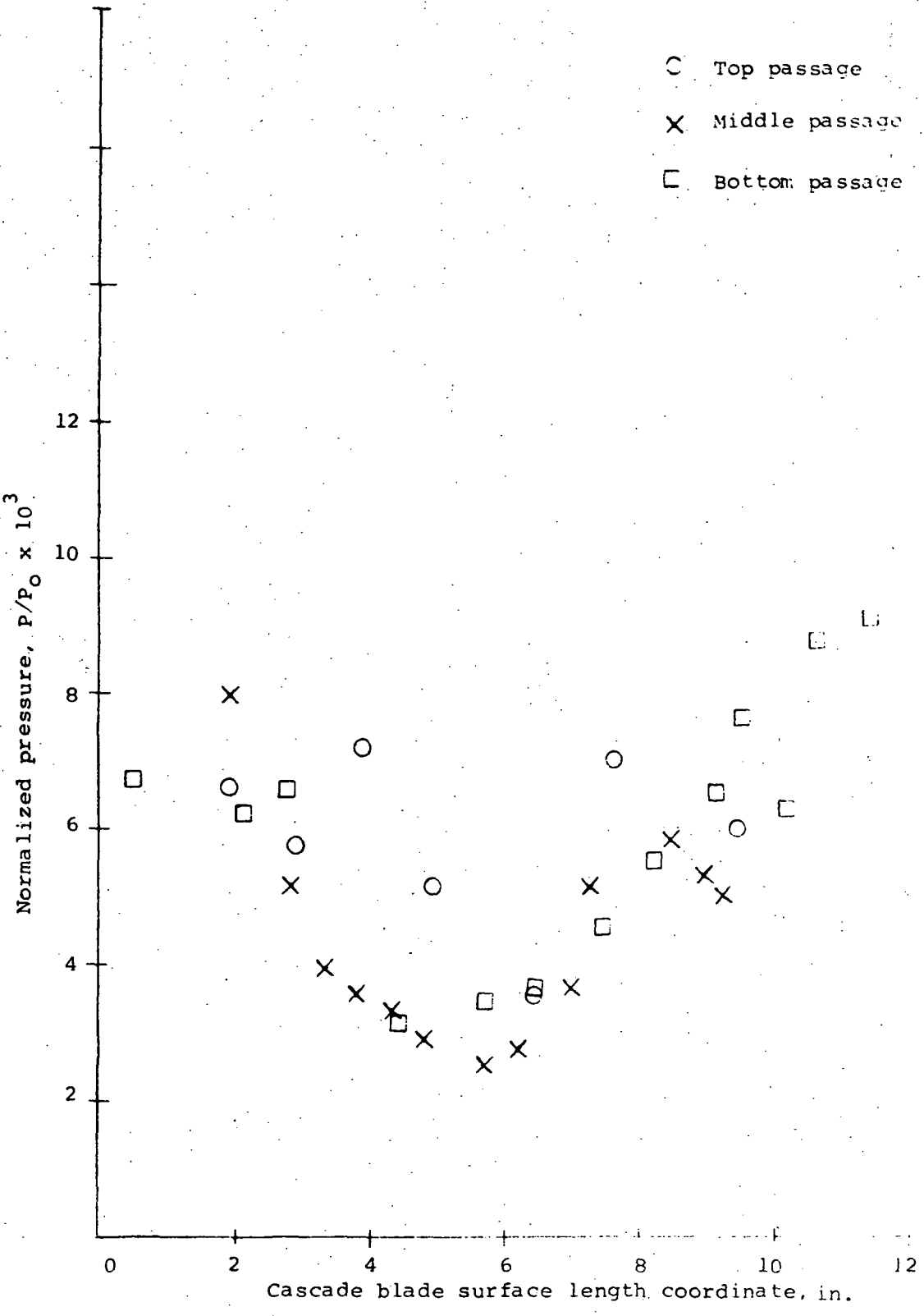

Figure 36a. - Cascade Suction Surface Pressure Distribution (Mid-Span) Full Body, with End Plates, Original Position

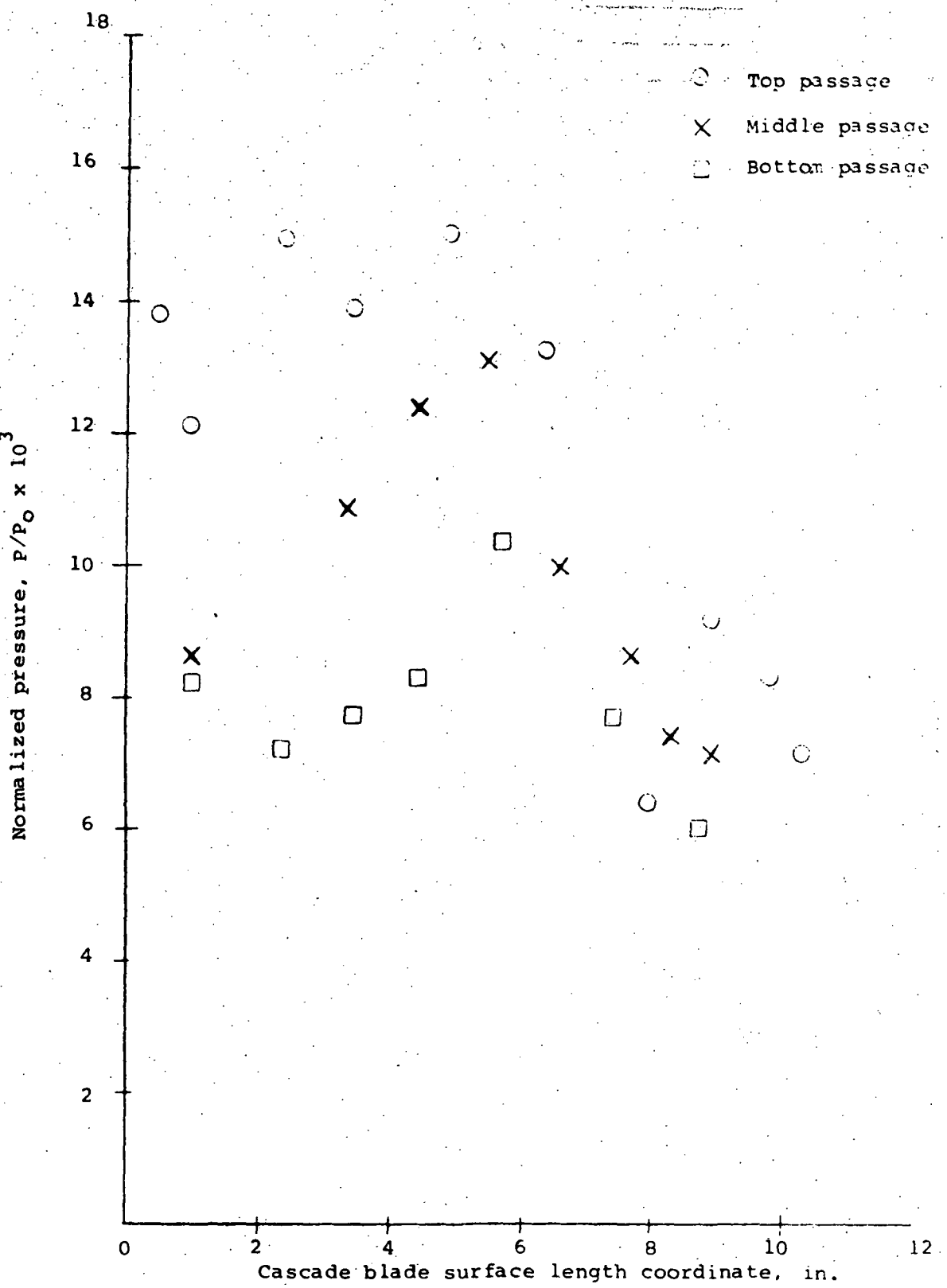

Figure 36b. - Cascade Pressure Surface Pressure Distribution (Mid-Span) Full Body, with End Plates, Original Position

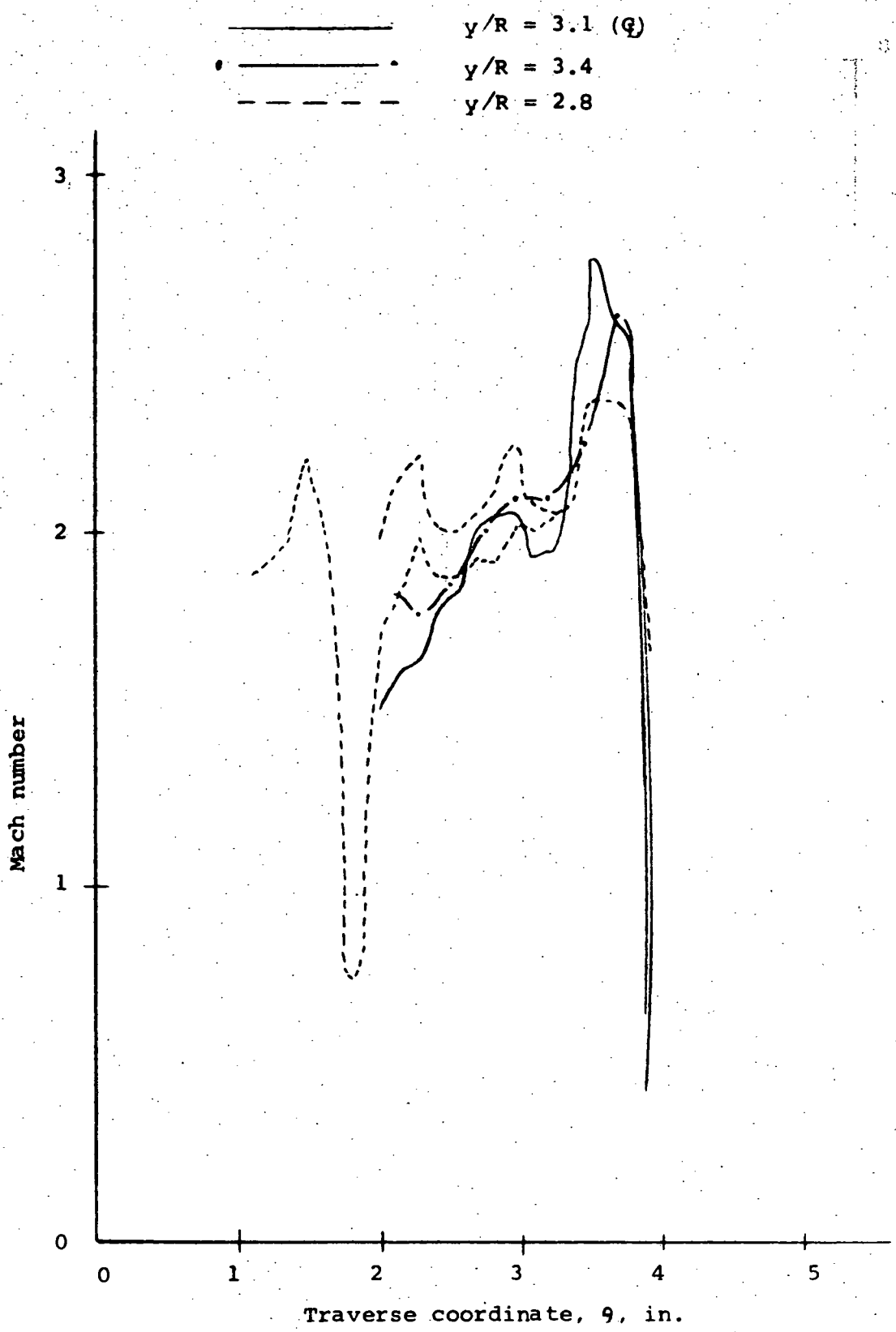

Figure 37. Cascade Exit Mach Number Distribution, Full Thickness Blunt Body, with End Plates, Cascade in Original Position

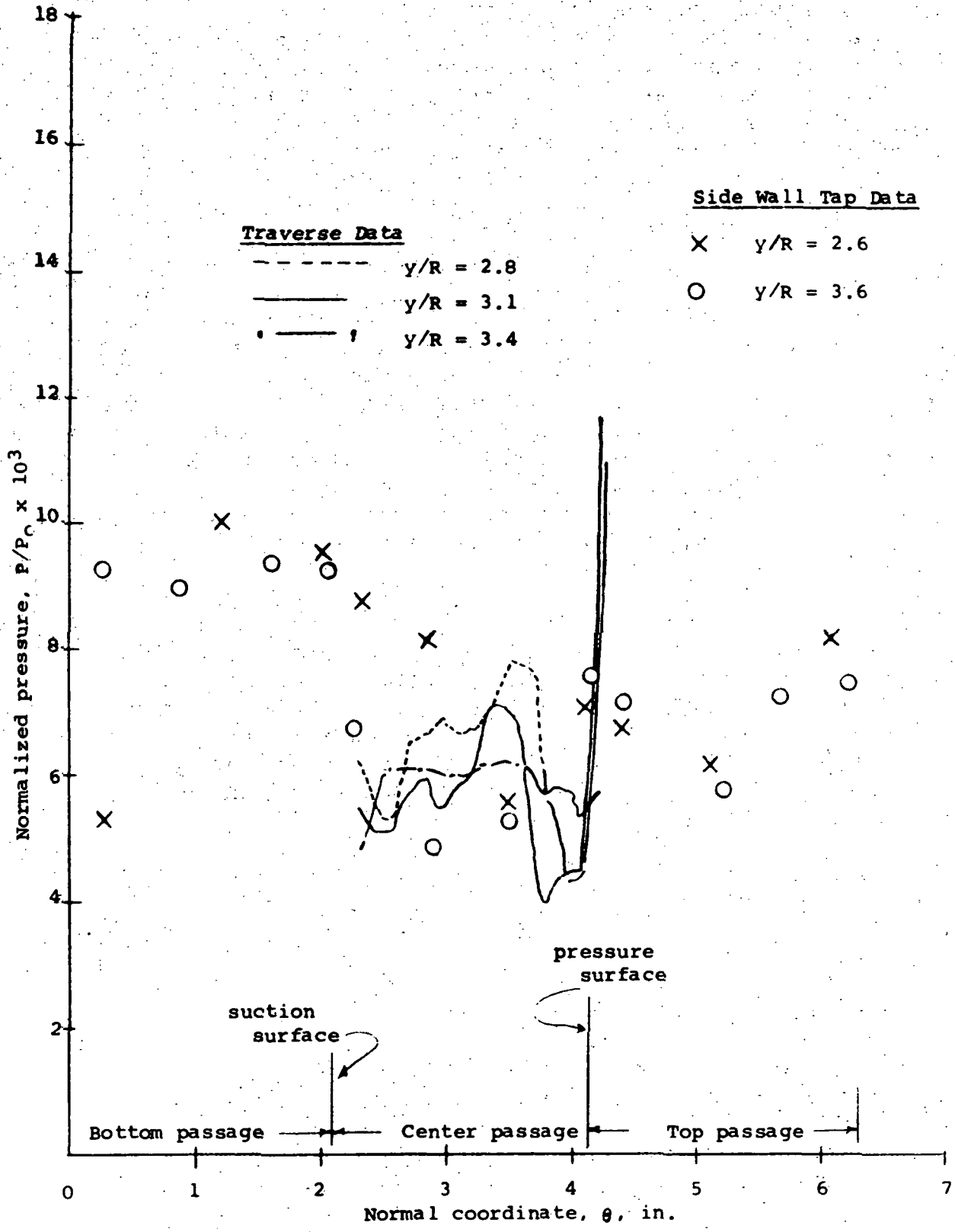

Figure 38. - Cascade Exit Pressure Data Full Thickness Body with End Plates, Cascade in Original Position

to the theoretical cascade inlet values for the center blade passage, as shown in Figure 39. The agreement is perhaps reasonable, but the cone probe measurement of flow conditions outside the cascade shows poor agreement. This could be interpreted as either a three-dimensional disturbance or as evidence of nearly constant stagnation pressure with respect to the normal coordinate. The latter interpretation would be consistent with an oblique shock pattern about (or upstream of) the blunt body, rather the predicted curved shock flow field.

b) Data with cascade and blunt body moved closer together. - As discussed above in Section B, on the basis of these results, it was theorized that the blunt body was interacting with the tunnel boundary layer, precluding establishment of the desired flow field. Accordingly, the blunt body was moved away from the tunnel wall one inch (closer to the cascade) as an attempt to reduce this interaction. Since our coordinate system for the blunt body-cascade system is fixed to the blunt body, this configuration is referred to as a change in the cascade position.

The results are shown om Figures 40 to 44. The cascade surface pressure distribution appears very much like the uniform flow (predicted) trends, suitably scaled to an arbitrary suction surface entrance pressure. This agreement would imply an entrance Mach number (mid-span) close to the desired value of 2.7. In addition, the pressures from passage-to-passage follow the predicted negative pressure gradient trend (Figure 24).

However, the exit traverse results were quite anomalous, in that high pitot pressures measured at all three stations and in all blade passages resulted in both exit Mach numbers and isentropic stagnation pressures much higher than predicted (Figures 42 to 43). These pressures were also significantly higher than on any of the previous tests. These results must be due at least in part to errors in determination of the local static pressure by means of wedge taps, which is quite difficult in a highly nonuniform flow because of the tendency of the wedge surface boundary layers to integrate. Figure 41 indicates very good repeatability of the two pitot probes in traversing the flow.

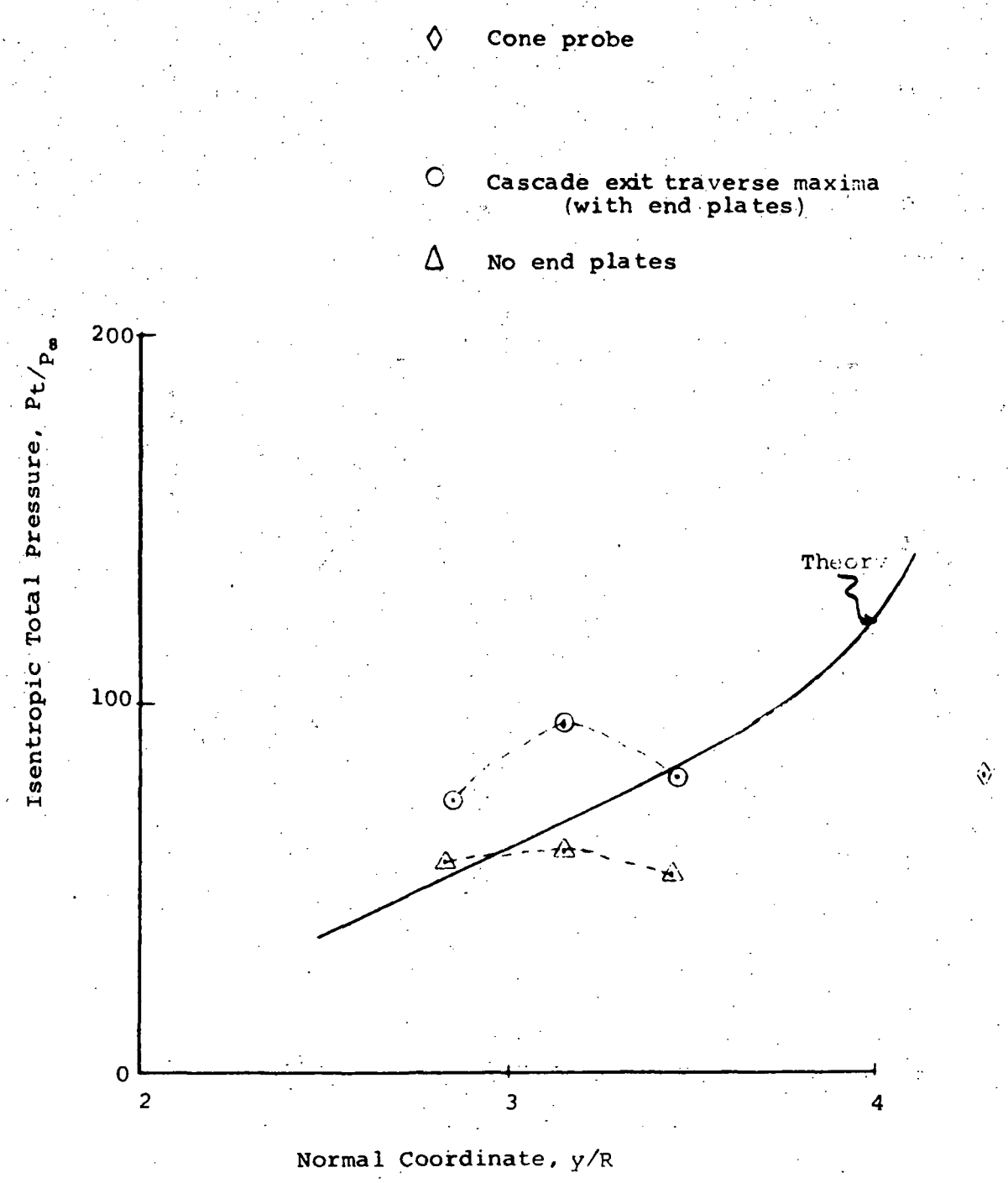

Figure 39. - Cascade Total Pressure Data in Original Position

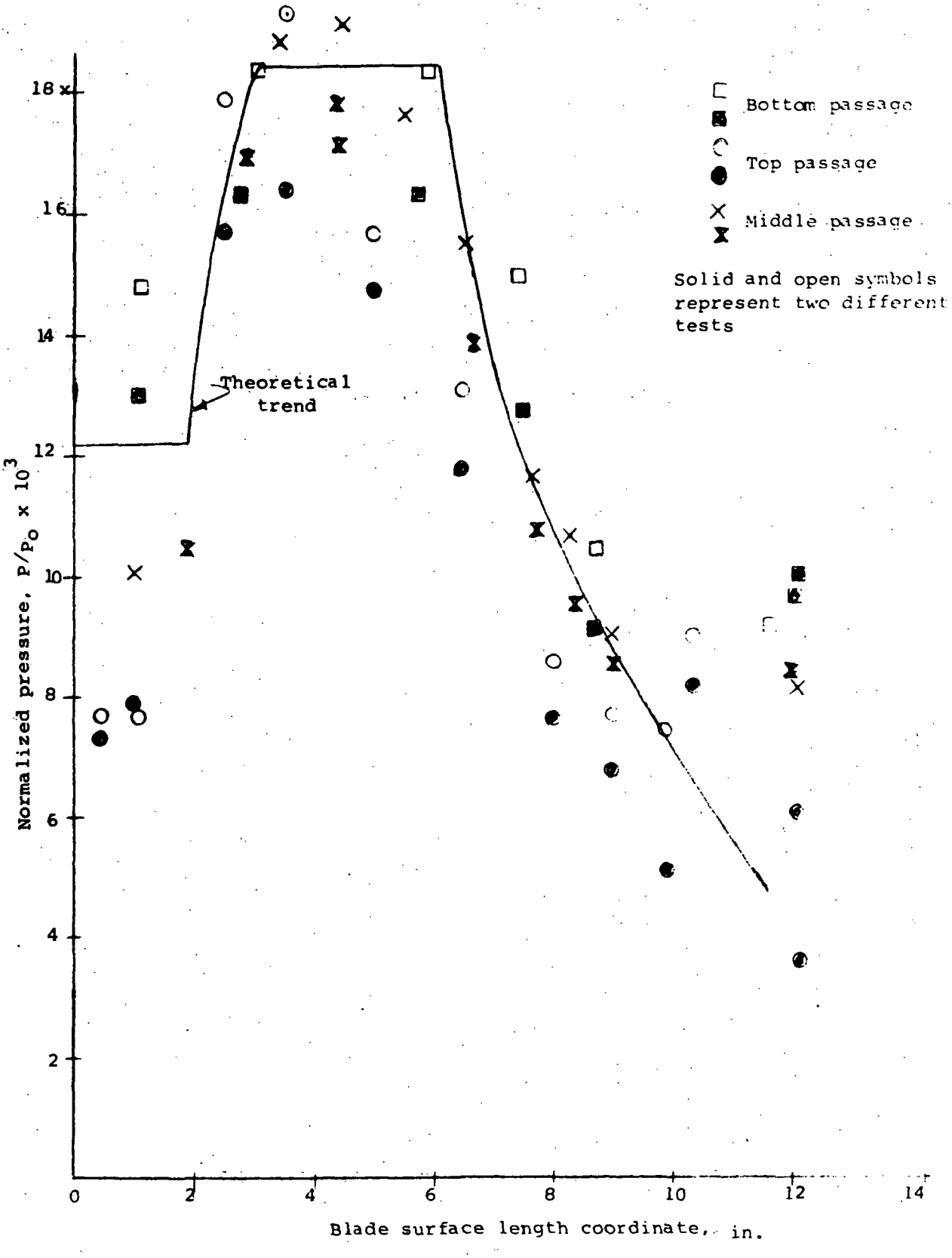

Figure 40a. - Cascade Blade Pressure Surface Pressure Distribution: Full Body with End Plates: Cascade Moved 1 in. Closer to Blunt Body

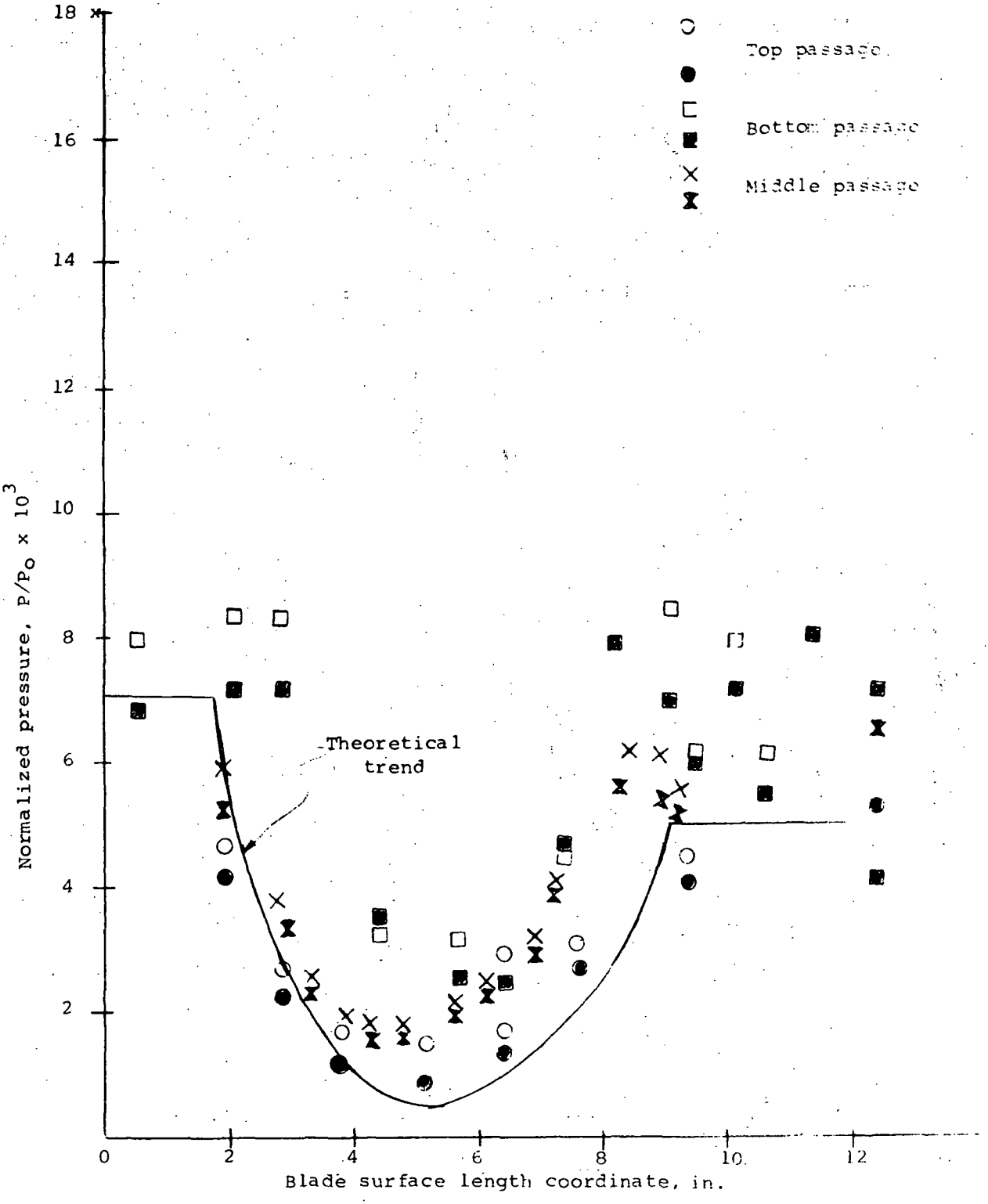

Figure 40b. - Cascade Blade Suction Pressure Distribution: Full Body with End Plates: Cascade Moved 1 in. Closer to Blunt Body

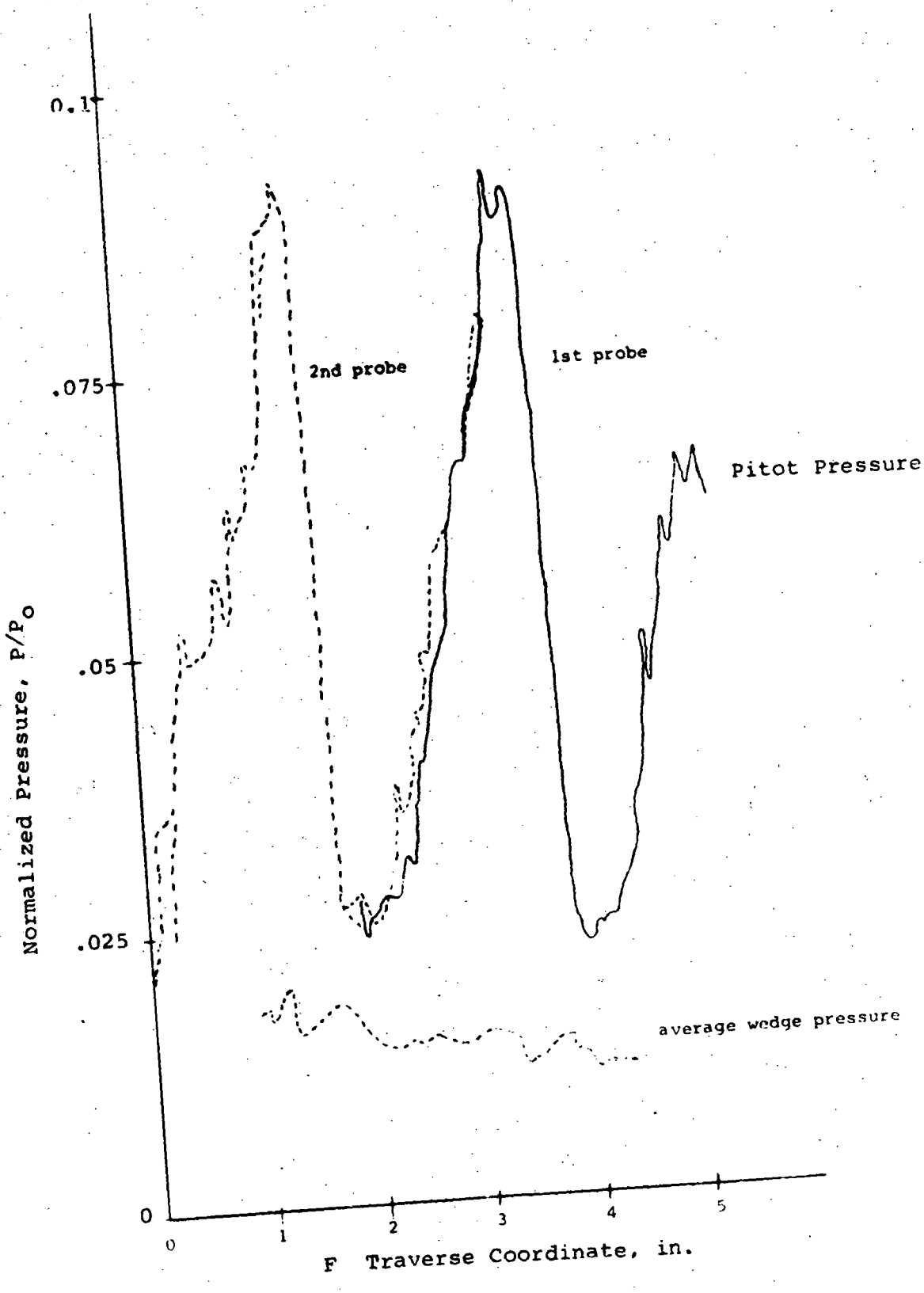

Figure 41. - Center Span Pitot Pressure Measurements - Full Body with End Plates: Cascade Moved 1 in. Closer to Blunt Body

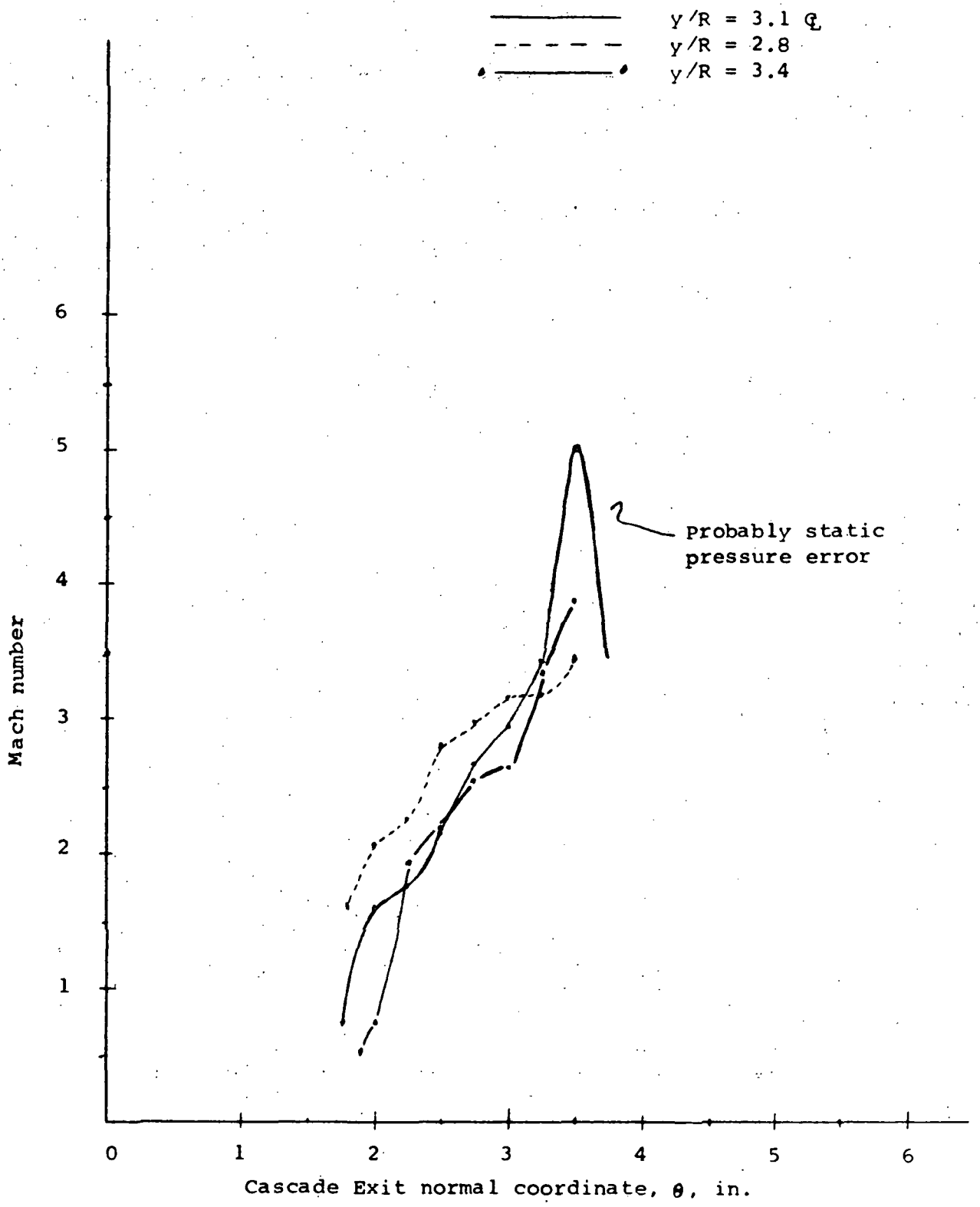

Figure 42. - Cascade Exit Mach Number Distribution (Center Passage) Full Body with End Plates: Cascade 1 in. Closer

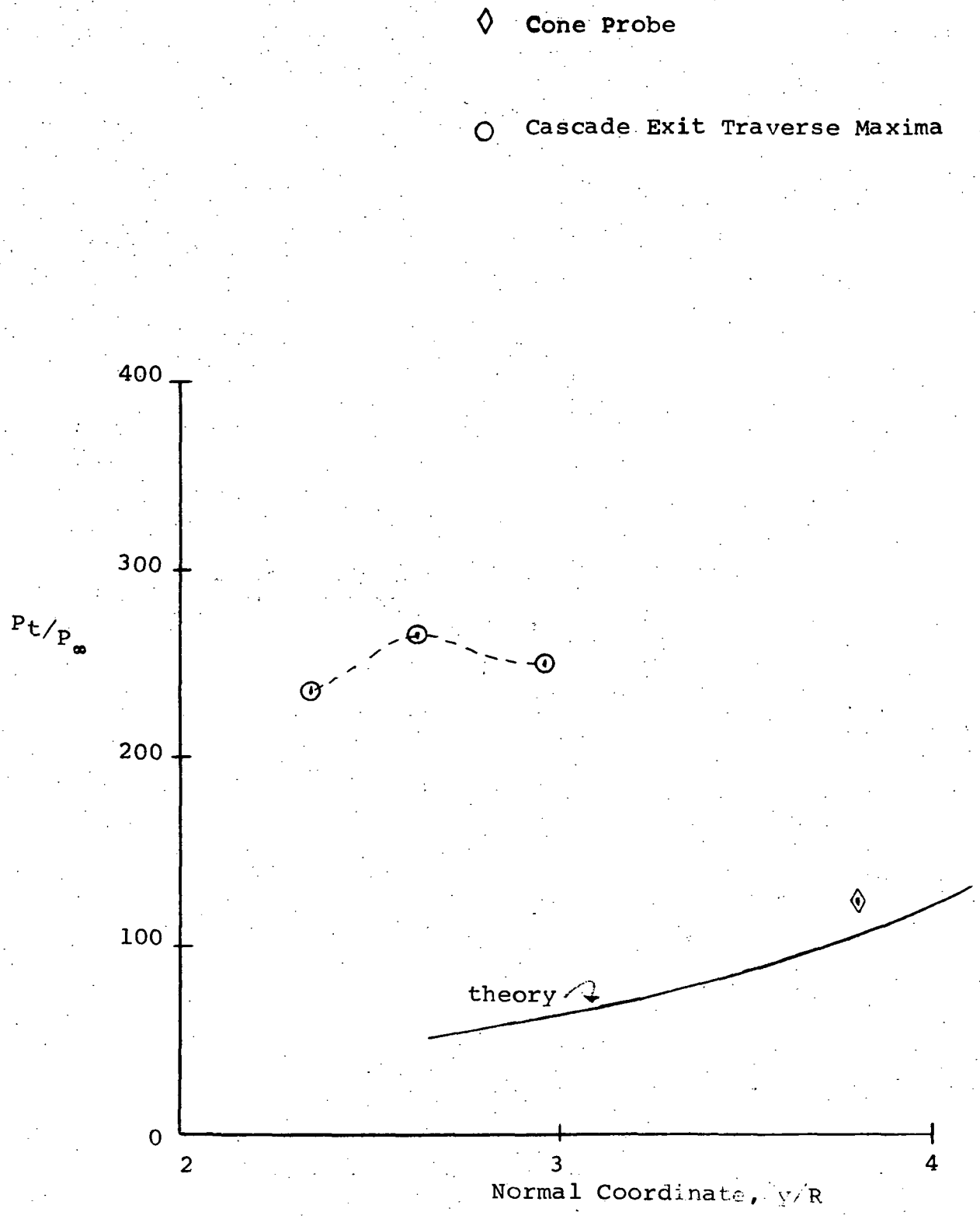

Figure 43. - Total Pressure Data, Cascade Moved 1 in. Closer to Blunt Plate

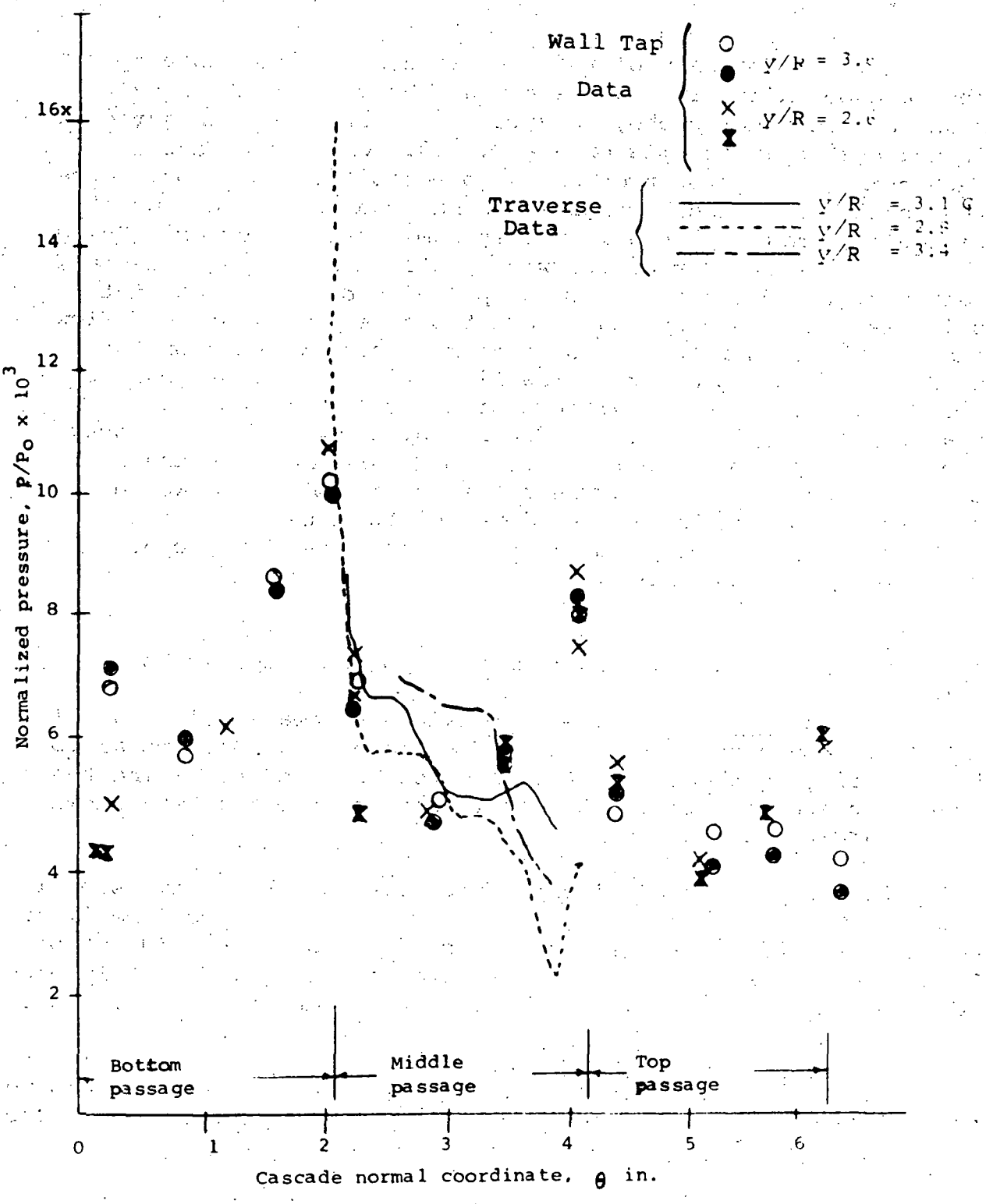

Figure 44. - Cascade Exit Pressure Distribution, Full Body with End Plates, Cascade 1 in. Closer

A comparison of the free stream static pressure at the cascade exit plane, as determined by wall taps and by means of the wedge probe, is given in Figure 44. The agreement is reasonable in the region y = 2. - 3., where the measured Mach numbers and pressures are also reasonable, but not in the previously mentioned high pressure-Mach number region, which, of course, implies a static pressure measurement error. Using the wall taps in lieu of the wedge data gives a more reasonable Mach number and isentropic total pressure distribution, but still far in excess of that predicted from the blunt body flow field. Thus, there seems to be no rational evidence of the existence of the predicted flow field with this test configuration; rather, there is evidence of a more efficient (from stagnation pressure loss standpoint) system of oblique shocks due to interaction with the tunnel boundary layer. Finally, the low cone pressure measurement shown in Figure 43 would correspond to the three-dimensional disturbance pattern shown in Figure 18; thus the end plates did not function properly for this configuration either.

E. Summary of Experimental Program - Conclusions

1. Tunnel blockage. - The maximum allowable blockage of 10% (based on nozzle exit area) of Reference 9 would appear to be justified by these results. The technique of providing test section geometries relief to accomodate the blockage was shown to be largely ineffective.

2. Blunt body model end effects. - The three-dimensional disturbance imposed on the tunnel flow by a blunt two-dimensional model is very important and must receive adequate consideration. It may be necessary to consider a porous surface end wall in order to have adequate shielding without undue boundary layer effects.

3. Cascade performance. -

a) The cascade performed very poorly under the combined conditions of high entrance Mach number (> 3) and high back pressure.

b) The exit profiles with high entrance Mach number and reasonable back pressure are very nonuniform and would imply large mixing losses downstream of the cascade.

c) With lower entrance Mach numbers and reasonable back pressure, the cascade exit profiles were uniform. There is an implication that the performance under these conditions was better (in terms of exit profile uniformity) than the uniform inlet profile case. This could be explained in terms of better suction surface boundary layer performance because of the high vorticity and turbulence levels present, although the effect of lower entrance Mach number (undetermined) cannot be ruled out.

Instrumentation

A need for a better means of determining cascade exit static pressure was shown. A high response technique was needed for this program because of the relatively short test times available.

VI. OVERALL PROGRAM CONCLUSIONS

The basic technique of evaluating cascade performance under simulated nonuniform rotor outflow conditions was demonstrated. However, it was also shown that much larger wind tunnels are required for this technique than for the testing of the given cascade alone. Consideration should also be given to use of a staggered (or swept) blunt body, in accordance with the cascade geometry.

REFERENCES

1. Lipfert, Frederick W.: Supersonic Axial Velocity Compressor Study. Vol. I: Summary and Aerodynamic Design Studies. Technical Report (AFAPL-TR-67-68), General Applied Science Laboratories, Inc., August 1967.

2. Goldberg, T. J.; and Erwin, J. R.: Performance of an Impulse-Type Supersonic Compressor Rotor Having a Mean Turning of 114°. NACA RML56J01, 1957.

3. Ferri, A.; and Nucci, L.: The Origin of Aerodynamic Instability of Supersonic Inlets at Subcritical Conditions. NACA RML50K30, 1951.

4. Ferri, A.: Three-Dimensional Effects in Supersonic Compressors. PIBAL Report 233, Polytechnic Institute of Brooklyn, October 1953.

5. Wilcox, W. W.: Investigation of Impulse-Type Supersonic Compressor with Hub-Tip Ratio of 0.6 and Turning to Axial Direction II - Stage Performance with Three Different Sets of Stators. NACA RML55F28, 1955.

6. Savage, M.; Boxer, E.; and Erwin, J. R.: Resume of Compressor Research at NACA Langley Laboratory. Transactions of ASME, vol. 83, Series A, no. 3., J. for Eng. for Power, 1961, pp. 269-285.

7. Squire, H. B.; and Winter, K. G.: The Secondary Flow in a Cascade of Airfoils in a Nonuniform Stream. J. Aero. Sci., vol. 18, 1951, p. 271.

8. Moretti, G.; and Abbett, M. J.: A Time Dependent Computational Method for Blunt Body Flows. AIAA J., vol. 4, no. 12, Dec. 1966, pp. 2136-2141.

9. Anon.: Test Facilities Handbook. Arnold Engineering Development Center, Arnold Air Force Station, Tenn., 1969.

NASA CR-112097

DISTRIBUTION LIST

NAS1-10004

	No. Copies
NASA Langley Research Center Hampton, VA 23365	
Attn: 122/Acquilla D. Saunders	1
110/Raymond L. Zavasky	1
402/Emanuel Boxer	5
NASA Ames Research Center Moffett Field, CA 94035	
Attn: 202-3/Library	3
NASA Flight Research Center P. O. Box 273 Edwards, CA 93523	
Attn: Library	1
NASA Goddard Space Flight Center Greenbelt, MD 20771	
Attn: Library	1
NASA Manned Spacecraft Center 2101 Webster Seabrook Road Houston, TX 77058	
Attn: JM6/Library	3
NASA Marshall Space Flight Center Huntsville, AL 35812	
Attn: Library	1
Jet Propulsion Laboratory 4800 Oak Grove Drive Pasadena, CA 111-113/Library	1
NASA Lewis Research Center 21000 Brookpark Road Cleveland, OH 44135	
Attn: 60-3/Library	3
5-9/Melvin J. Hartmann	1
NASA John F. Kennedy Space Center Kennedy Space Center, FL 32899	
Attn: IS-DOC-12L/Library	1
National Aeronautics and Space Administration Washington, DC 20546	
Attn: KSS-10/Library	1
RP/NASA Headquarters	3
NASA Scientific and Technical Information Facility P. O. Box 33 College Park, MD 20740	8 plus reproducible

NASA CR-112097

DISTRIBUTION LIST

NAS1-10004

	No. Copies
The General Electric Company Attn: John Blanton 1 Jimson Road Evendale, OH 45215	1
Pratt and Whitney Aircraft Company Attn: Dr. A. MiKolajczak E. Hartford, CT 06120	1
Detroit Diesel Allison Attn: George Pederson P.O. Box 894 Indianapolis, IN 46206	1
AiResearch Corporation Attn: Linwood C. Wright 2525 W 190st Torrance, CA 90509	1
AiResearch Corporation Attn: John R. Erwin Airport, Phoenix, AZ 85034	1
Wright-Patterson Air Force Base Attn: Don Campbell Air Force Aero Propulsion Laboratory Dayton, OH 45433	1